

AD-A080 711

OHIO STATE UNIV COLUMBUS DEPT OF MECHANICAL ENGINEERING
STUDY OF ROTOR WAKES AT VERY LOW ADVANCE RATIOS.(U)
DEC 79 H R VELKOFF

F/6 20/4

DAA629-76-6-0260

UNCLASSIFIED

ARO-14142.1-EX

NL

1 of 1
AD
3000711

END
DATE
FILMED
3-80
DDC

Unclassified

SECURITY CLASSIFICATION OF THIS PAGE (When Data Entered)

REPORT DOCUMENTATION PAGE

READ INSTRUCTIONS BEFORE COMPLETING FORM

1. REPORT NUMBER (19) 14142.1-EX (19) ARO	2. GOVT ACCESSION NO.	3. RECIPIENT'S CATALOG NUMBER
4. TITLE (and Subtitle) (8) Study of Rotor Wakes at Very Low Advance Ratios.		5. TYPE OF REPORT & PERIOD COVERED (9) Final Report. 30 Jun 76--30 Jun 79
7. AUTHOR(s) (10) Henry R. Velkoff		8. CONTRACT OR GRANT NUMBER(s) DAAG29-76-G-0260 (15)
9. PERFORMING ORGANIZATION NAME AND ADDRESS The Ohio State University Columbus, Ohio 43212		10. PROGRAM ELEMENT, PROJECT, TASK AREA & WORK UNIT NUMBERS (12) 97
11. CONTROLLING OFFICE NAME AND ADDRESS U. S. Army Research Office P. O. Box 12211 Research Triangle Park, NC 27709		12. REPORT DATE (11) 15 Dec 79
14. MONITORING AGENCY NAME & ADDRESS (if different from Controlling Office)		13. NUMBER OF PAGES 97
LEVEL 1		15. SECURITY CLASS. (of this report) Unclassified
		15a. DECLASSIFICATION/DOWNGRADING SCHEDULE

DISTRIBUTION STATEMENT (of this Report)

Approved for public release; distribution unlimited.

DISTRIBUTION STATEMENT (of the abstract entered in Block 20, if different from Report)

18. SUPPLEMENTARY NOTES

The view, opinions, and/or findings contained in this report are those of the author(s) and should not be construed as an official Department of the Army position, policy, or decision, unless so designated by other documentation.

19. KEY WORDS (Continue on reverse side if necessary and identify by block number)

helicopter rotors	helicopters
wake	flight
low altitude	flow fields
low velocity	hot wire anemometers
air flow	data acquisition

20. ABSTRACT (Continue on reverse side if necessary and identify by block number)

With the recognition of the importance of operation of military helicopters at very low altitudes and very low velocities, the need for data on airflow under these conditions became apparent. Work was initiated to obtain data at very low advance ratios typical of such low speed helicopter flight. The original goals of the research were to try to obtain a description of the flow field both time averaged and instantaneous. Because of prior experience with hot wire anemometry the effort was directed towards using a hot wire probe to get all three components

ADA 080711

FILE COPY

D D C
RECEIVED
FEB 11 1980
REGISTRY
E

20. ABSTRACT CONTINUED

of velocity. The effort resulted in an operational rotor drive and measuring system, a probe calibration and positioning system, frequency response determination, and acquisition of average value data. The low speed flow fields found demonstrated a squirting affect that could be seen on both sides of the rotor at very low advance ratios. Two non-steady data acquisition systems were considered, one developed to the point of use but was found awkward to use, and a second interactive system which progressed to the point that initial tests using it in a time average mode illustrated the interactive capability.

Accession For	
NTIS GRA&I	<input checked="" type="checkbox"/>
DDC TAB	<input type="checkbox"/>
Unannounced	<input type="checkbox"/>
Justification	
By _____	
Distribution/	
Availability Codes	
Dist	Avail and/or special
A	

RF Project 760431/784461 ✓
Summary Report

Ohio
State
University

research foundation

1314 Kinnear Road
Columbus, Ohio
43212

STUDY OF ROTOR WAKES AT VERY LOW ADVANCE RATIOS

Henry R. Velkoff
Department of Mechanical Engineering ✓

For the Period
June 30, 1976 - June 30, 1979

DEPARTMENT OF THE ARMY
U. S. Army Research Office
Research Triangle Park, North Carolina 27709

Grant No. DAAG29-76-G-0260

December 15, 1979

SUMMARY REPORT

Project DAA G-29-76-G-0260
U.S. Army Research Office Durham

December 15, 1979

Henry R. Velkoff
Principal Investigator

Department of Mechanical Engineering /
Ohio State University
Columbus, Ohio

Study of Rotor Wakes at Very Low Advance Ratios

Introduction

With the recognition of the importance of operation of military helicopters at very low altitudes and very low velocities, the need for data on airflow under these conditions became apparent. Work was initiated with Department of Army support to obtain data at very low advance ratios typical of such low speed helicopter flight. The original goals of the research were to try to obtain a description of the flow field both time averaged and instantaneous. Because of prior experience with hot wire anemometry, the effort was directed towards using a hot wire probe to get all three components of velocity.

Experimental Method

The studies of the rotor wake were accomplished using a 2.5 ft. (.762m) diameter two bladed teetering rotor. The rotor was driven by an electric motor mounted on a six component balance and placed in a 4 ft. by 8 ft. (1.22m x 2.44m) wind tunnel. Details of the installation may be found in appendix A. The actual studies of rotor flow began with the recognition that the task of obtaining and presenting accurate instantaneous data on the time and space varying velocity field would be most challenging. Two problems presented themselves, first the ability of the hot wire system to

accurately record the instantaneous velocity components, and secondly the large number of data points that would be needed. It was also anticipated that once the measurement system was developed, that the time-average flow field data could be obtained either concurrently or separately from the non-steady flow field data.

Probe Frequency Considerations

If one considers the probe and hot wire system first, it had been found that if the hot wires were used to get large amounts of data, considerable wire breakage could result. Such breakage would require extensive recalibration of repaired hot wires. After studying several possibilities a hot film probe, TSI 1294-60-18, was chosen. Although the probe was considered to be rugged enough to ensure long service, questions remained as to the frequency response characteristics of that probe and the DISA anemometers used. Since the anemometers had a frequency response of several kilohertz, attention was directed to the hot film sensors. To determine the response needed one must consider the frequency content that must be obtained in the input signal to the anemometers.

The frequency content of interest in the rotor wake is that which would be seen by an ideal probe at a point in the wake. Since the detailed wake structure consists of individual vortices, and vortex sheets moving past the point, as

well as interacting vortices and sheets an ideal probe would put out a signal that would contain a significant pulse at once per blade passage frequency. With a two bladed rotor this would mean two pulses per revolution. Since the rotor rpm used was approximately 2200 rpm, then the frequency would be 73 hertz. In order to analyze the data, it was decided that up to about twenty harmonics would be needed, and hence it would be desirable to try and achieve a useable probe response out to over 1 kilohertz.

Examination of the methods used in hot wire anemometry led to the realization that there were few if any useable means of determining the actual frequency response characteristics of a hot film probe. Most techniques in use involved an electrical simulation of the actual problem. Because of the need for good data at the high harmonics of blade passage frequency, a means was devised to measure the frequency response characteristics of a large hot film probe in a rather direct and simple fashion. This method is presented in appendix B.

Data Handling Considerations

To handle the data acquisition, reduction, storage and presentation of the non-steady data presented a unique problem. Fifteen hundred points in the wake were considered necessary for a representation of the wake. If data were

taken at five degree azimuth positions of the reference blade, then 72 points per revolution would be needed. To get a reasonable sample a minimum of 5 readings would be required at each azimuth position. For the three wires this meant about 1.5 million data points per test condition. If one were to strive for greater confidence, then 10 or more readings would be required, and would at least double the data points. Automated data handling became a necessity.

Because no suitable automated data handling system was available at the initiation of the project, a careful survey was made of available options at The Ohio State University. No suitable large data processing system was found to exist which could handle the mass of data. Work was initiated to utilize an existing analog to digital conversion system which existed at the Perkins Observatory some 30 miles north of the main campus. Programs were written and a tape system used to record test data. The tape was then taken to the Perkins Observatory for conversion and then to main frame computer on campus. All the system components were checked and made functional.

The massive amount of data being generated indicated that essentially millions of punched cards would be generated if several rotor test cases were run and processed.

Study was then initiated on the use of tape or floppy

disk data storage, and on other data handling systems. At this juncture, about 60% through the program, the possibility arose that the Department of Mechanical Engineering in the University would receive industrial and University grants to establish a computer aided design laboratory with a dedicated minicomputer and associated peripherals including A to D conversion. Since the installation of this new laboratory seemed imminent, the non-steady flow efforts were reduced in magnitude until such time as the new capability became available. It was anticipated that direct coupling of data output from sensors into the computer could be accomplished either through tape or real time. Enormously great savings could result. Effort on the study of rotor non-steady flows was reduced in magnitude and work directed at a reduced level towards obtaining time averaged data on rotor wakes at low advance ratios.

Time Averaged Data

The decision to delay the instantaneous data part of the program led to a concurrent decision to step up time averaged flow field data acquisition. Since the entire probe positioning equipment, the force balancing, rotor model, and hot film systems were operational it was readily possible to get average data. Many runs were made at advance ratios ranging from $\mu = 0.02$ to 0.10. At the very low value $\mu = 0.02$ the

data were considered too erratic to be useful. From close observations it appeared that the rotor was operating in the "flow breakdown" region reported by Rae of Washington. Data were obtained for various shaft angles and blade pitch angles for both untwisted and twisted two bladed rotors. The detailed description of the test procedures and the data that were obtained may be found in Appendices A and C. The data at $\mu = 0.10$ are similar in nature to that reported by Heyson and Katsoff in NACA 1319. The most unusual finding as discussed in Appendix A, is the rollup of the flow that passes near the rotor into two concentrated vortices similar to the action of a low aspect ratio wing, with concurrent high axial velocities in the rollup cores.

At the conclusion of the work reported in Appendix C, effort was once again moved towards the study of the non-steady flow field since a minicomputer dedicated to work within the department became operational. Effort was then directed towards developing a system which would couple the output from the hot film probes directly to the minicomputer so that the entire system could operate in an interactive mode. The next section summarizes the work on the interactive system which has been accomplished up to the end of the third year and end of initial funding of this study of rotor flows.

An Interactive Method of Measuring Average Instantaneous
Velocities of a Rotor in Very Low Advance Ratios

The new minicomputer installed in the department of Mechanical Engineering at The Ohio State University provided the means of improving the system of average data acquisition and extending the work to average instantaneous velocities measurement.

The minicomputer is a DEC PDP 11/60 and is well suited to the Fortran based calculations. It has a 250 KBYTES memory (RAM) and 64 KBYTES are available to the user. The PDP hosts graphics (Tektronix 4014-1) and alphanumeric (Infoton) terminals. The terminals are supported by a high speed Printronix Printer-plotter and a Tektronix hardcopy unit. Data and program storage are provided by a dual floppy disc drive and two RKO cartridge discs drives.

Two A/D converters are available for data acquisition:
1) DEC LPA system which can sample up to 40 KHz and can be multiplexed up to 16 channels, with a multichannel interval of 22 μ sec.; 2) GENRAD 4 channel A/D System (ADS) with a sampling frequency of 160 KHz and a multichannel interval of 6 μ sec.

For the present application the four channel GENRAD ADS will be used initially because of its higher sampling frequency and lower multichannel time interval. However, if

more channels may be needed (for a fully automated process, where the computer controls the RPM of the rotor and the X-Y-Z location of the probe) the DEC LPA system can be used and the 22 μ sec. error, between any sequent channels, can be compensated for by means of delay lines.

Data Acquisition System

The data acquisition system will consist of the following components (Figure 1): 1) Computer; 2) A/D converter; 3) Alphanumeric terminal; 4) Interface; 5) Velocity measurement system (hot-film anemometer). A 500 ft. cable (eight twisted pairs individually shielded) was extended from the computer room on the second floor of the Mechanical Engineering building to the first floor where the windtunnel is located. The connection with the computer is complete. The dynamic effect of the wires on the analog signals and particularly on the triggering signal is yet to be investigated.

The development of the software was initiated. At this early stage of design, it seems that two programs, for average data and for average instantaneous data will be needed, because of limited storage space. However the outline for both programs is similar:

1. As long as the data acquisition is not fully automated the process should be interactive.
2. The bookkeeping should be done by the computer, and the operator will be instructed by the

computer how to proceed.

3. The data collection procedure would be that continuity from previous days will proceed with a minimal information input needed from the operator.
4. The operator would be able to repeat the last data point without disturbing the normal flow of operation, to provide a check.
5. If more then the last point has to be repeated this would have to be done by interrupting the normal procedure.

Average Data Collection

Mean value data averaged over several rotor revolutions can provide average velocity, and that about $1\frac{1}{2}$ KHz contains the significant frequency content of the wake. For a correct reconstruction of the wave the sampling frequency must be at least 2000 Hz. An array, filled with the digitized values, having the dimension (2000,3) will be filled in one second, which corresponds to about 40 revolutions. At each location in the wake the data will be, averaged, the effective velocities calculated, and transformed to windtunnel coordinates. The three components of velocity (V_x , V_y , V_z) and the location of the probe (X-Y-Z) will be stored on the computer's hard discs. After the whole case will be finished the file will be transfered to the large ADMAHL 470 where the SPEAKASY language would be used for the vector plots.

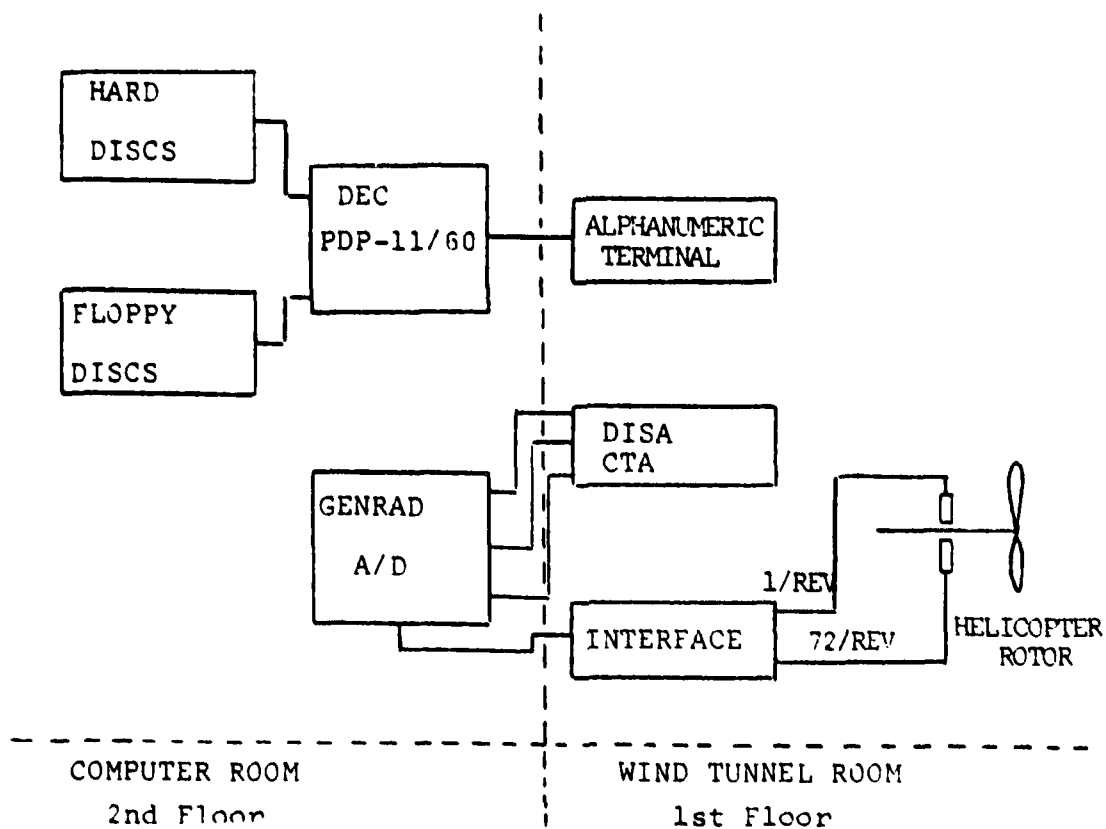


Figure 1. DATA ACQUISITION SYSTEM.

Instantaneous Data Collection

For the average instantaneous data collection two methods will be developed: 1) Computer on-the-line with the ADS; 2) The whole case will be recorded on a FM analog recorder (PI-6100) and then reproduced at the ADS. An interface should be designed and built. It's basic specifications and requirements were provided to the electronic lab in the M.E. department, and it is expected to have it operational at the beginning of October 1979.

Computer Mode Operation

The inputs to the interface are:

1. 1/REV pulse from a magnetic proximity pickup indicating $\psi = 0$.
2. 72/REV pulses from a second magnetic proximity pickup indicating 5 degrees increments in rotor rotation. The output from the interface will be one pulse at each 5 degrees increment for 10 revolutions (Figure 2).

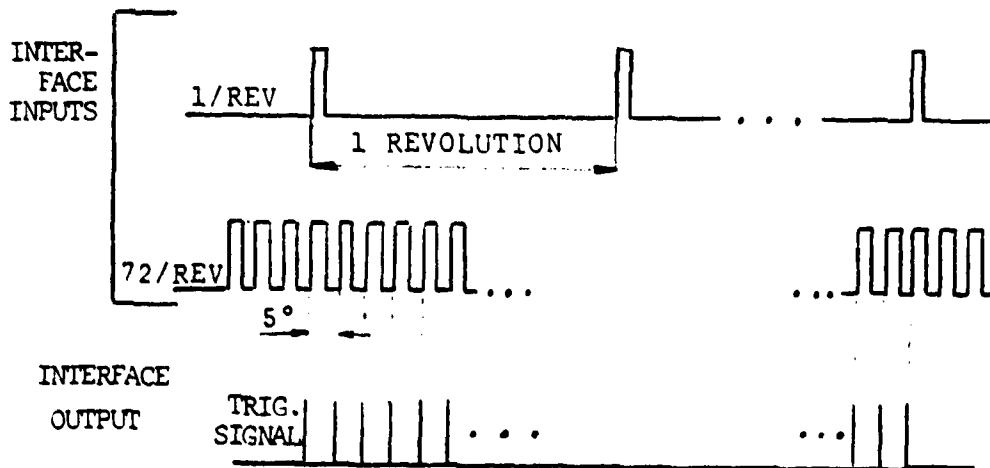


Figure 2.

The ADS will be initiated by the software, but the digitizing process will start when the operator will signal, from the interface, that the probe is at the correct location. Then, the ADS will be triggered every 5 degrees by the

triggering output from the interface. After the digitizing process has been completed, the computer will average the data for every 5 degrees increment for 10 revolutions. The three averaged voltages will be transformed then in the usual manner in wind tunnel coordinates. These velocities and the probe location will be stored, temporarily, on the computer's hard discs until the case is completed. Then the data will be stored, permanently, on floppy discs for further use and reference.

Tape Mode Operation

At this mode of operation, the interface has a dual purpose. When recording the data, it will produce the triggering signals for each 5 degrees increment and will also operate the FM tape recorder. The procedure is as follows: The operator will signal, from the interface, that the probe is at the correct location, then the device will start the tape recorder and after 0.5 second delay (to let the tape get to its steady state velocity) the analog data will be recorded on 3 channels. On the fourth channel the triggering signals will be recorded. After 10 cycles have been counted the interface will stop the recording. In the reproduction process the three analog channels will be connected directly to the ADS and the fourth channel with the triggering signals will be connected to the interface whose role now will be the same as in the computer mode.

Data Presentation

The numerical values of the velocities and their location will be stored on floppy discs and could be displayed on any terminal or printed out by the PRINTRONIX high speed printer. However, the vast amount of "numbers" (1188 points x (72 x 3 numbers per point) = 256608 "numbers") makes the use of data visualization a necessity.

For data visualization the TEKTRONIX 4014-1 graphics terminal will be used. This terminal has a refresh mode of operation and animated pictures of the wake as the rotor passes by, can be created. In addition, graphs of velocity vs. rotor position, or velocity vs. probe location can be obtained by using the PLOT-10 plotting routines available in the PDP's library.

Summary

The effort on the project resulted in an operational rotor drive and measuring system, a probe calibration and positioning system, frequency response determination, and acquisition of average value data. The low speed flow fields found demonstrated a squirting affect that could be seen on both sides of the rotor at very low advance rations. Two non-steady data acquisition systems were considered, one developed to the point of use but was found awkward to use, and a second interactive system which progressed to the point that initial tests using it in a time average mode illustrated the interactive capability.

The next phase of effort to be undertaken will be the completion of the mode control unit which will take the counter signals from the rotor azimuth position to trigger the automated acquisition system. When this is operational, then tunnel testing will resume and both non-steady and steady data will be taken. Emphasis will be placed upon the sequential pictorial presentation of the velocity data in a form that can be shown to groups interested in seeing the character of the rotor flow field.

Appendix A

ROTOR WAKE MEASUREMENTS AT VERY LOW

ADVANCE RATIOS

Henry R. Velkoff

Daniel Horak

The Department of Mechanical Engineering
The Ohio State University
Columbus, Ohio

PRESENTED AT THE 35th ANNUAL NATIONAL FORUM
OF THE
AMERICAN HELICOPTER SOCIETY
WASHINGTON, D.C.
MAY 1979

ALL PUBLISHING RIGHTS RESERVED BY THE
AMERICAN HELICOPTER SOCIETY
1325 18th STREET, N.W.
WASHINGTON, D.C. 20036



PREPRINT NO. 79-6

Rotor Wake Measurements At Very Low
Advance Ratios

Henry R. Velkoff
Daniel Horak

The Department of Mechanical Engineering
The Ohio State University
Columbus, Ohio

Abstract

The work revealed that even at very low advance ratios the rotor wake tends to roll up very quickly into two concentrated trailing vortices in a manner analogous to a low aspect ratio wing.

List of Symbols

A 3-D probe coordinate direction
B 3-D probe coordinate direction
C 3-D probe coordinate direction
E Anemometer output voltage, Volts
E_a Output of channel A of the 3-D anemometer, Volts
E_b Output of channel B of the 3-D anemometer, Volts
E_c Output of channel C of the 3-D anemometer, Volts
k Constant to express the deviation from Cosine
Law of cylindrical anemometer sensors, dimensionless
K₁ Constant of a cylindrical sensor calibration curve
K₂ Constant of a cylindrical sensor calibration curve
R Rotor radius, ft
U Magnitude of velocity vector, ft/sec
U_a Component of U along axis A, ft/sec
U_b Component of U along axis B, ft/sec

U_c Component of U along axis C, ft/sec
V Forward flight speed of helicopter, or wind tunnel free stream air velocity, ft/sec
V_a Effective cooling velocity of sensor A, ft/sec
V_b Effective cooling velocity of sensor B, ft/sec
V_c Effective cooling velocity of sensor C, ft/sec
V_{eff} Effective cooling velocity of a sensor, ft/sec
V_x Component of U along axis X, ft/sec
V_y Component of U along axis Y, ft/sec
V_z Component of U along axis Z, ft/sec
X Wind tunnel coordinate direction
Y Wind tunnel coordinate direction
Z Wind tunnel coordinate direction
α Angle between direction of U and axis A, degrees
β Angle between direction of U and axis B, degrees
γ Angle between direction of U and axis C, degrees
φ Angle between direction of U and a cylindrical anemometer sensor, degrees
Ω Rotor angular velocity, radians/sec

Presented at the 15th Annual National
Forum of the American Helicopter Society,
May 1979.
This work was sponsored by U.S. Army
Research Office - Durham.

Introduction

The knowledge of the flow field induced by the rotor is necessary in any detailed study of the characteristics of a helicopter. The induced flow is one of the most important factors involved in the overall performance, vibrations, structural reliability and acoustic noise problems of rotary-wing aircraft. For example, knowledge of the detailed flow characteristics results in a more accurate prediction of blade loads and thus a more rational design of the blade structure. Such knowledge could lead to better flight performance of the helicopter and reduction of the rotor induced vibrations. The knowledge of the wake geometry would be useful in determination of the interaction between rotors and the interference of the rotors with the fuselage and other non-lifting bodies.

The need for accurate experimental wake data has increased during the last ten years both because of the expanded use of helicopters and because of the development of computerized numerical methods for computation of rotor wake structures (Reference 1). These data are needed since the computerized methods used require a prior knowledge of the wake geometry. The data would be useful to determine the accuracy of the methods developed by comparison of the measured and the computed flow fields.

Rotor hover and forward flight performance and wake geometry have been studied by many authors, and the number of theoretical and experimental works is relatively large. However, little is known about the transition flight speed ($0 < V/QR < 0.1$) performance. Very large wake distortion and very severe vibratory loads occur at these speeds. The purpose of this work was to develop the instrumentation and the experimental methods and to measure the induced velocities in the vicinity of a small helicopter rotor placed in a wind tunnel and operated at transition flight speeds. The measurements were performed by a three-dimensional hot-film anemometer. A three-dimensional traverse system was used to traverse the anemometer probe throughout the rotor wake. The experimental study conducted concentrated on advance ratios of $\mu = 0.1$ and below and the data presented are time averaged values.

Prior Forward Flight Wake Studies

The rotor wake in forward flight is more complex than in hover, since here the spanwise variation of the bound vortex strength is a function of the azimuthal

position. In steady state forward flight the cycle of variation repeats itself for each and every rotor revolution. The wake in forward flight consists of a vortex sheet and a tip vortex, like in hover, but both components are more complex. The vortex sheet may be represented pictorially by a mesh of shed and trailing vortices, as shown in Figure 1 which is reproduced from Reference 2. The strength of the shed vortex elements is not constant along the span. The variation corresponds to the spanwise variation of the bound vortex which existed on the blade when the vortex was shed due to changes in circulation as the lift varies around the azimuth. In addition to the shed vortex elements there are trailing vortex elements, which are deposited to the wake because of the change of the bound vortex strength distribution as the blade changes its azimuthal position.

The rotor wake in forward flight does not look like a simple, helical sheet of vorticity as predicted by the momentum theory. The tip vortex is largely distorted and can become unstable and even disappear. Figure 2, reproduced from Reference 1, shows a computer simulated tip vortex trajectory in forward flight. Figure 3, reproduced from Reference 3, shows the rolling up of the wake in forward flight.

Most of the data on the rotor wake in forward flight come from flow visualization study. Some authors used Pitot-tubes to measure the velocity vectors, (3, 4, 5, 6). Data which describe the rotor wake velocity distribution in forward flight are limited (7, 8, 9). Especially rare are the data on transition speed forward flight of helicopters, which are needed by the helicopter designers because of the large wake distortion and severe rotor vibrations which occur at these speeds. This work was an attempt to develop the instrumentation the experimental methods needed to produce these data, and produce the data at low advance ratios.

Experimental Apparatus and Procedure

The Test Rig

The tests were carried out on a 2.5 ft. model, teetering, two-blade rotor in the test section of the 8 ft. x 4 ft. wind tunnel of The Department of Mechanical Engineering at The Ohio State University. The details of the rotor are shown below.

Details of the Rotor

Number of Blades 2

Rotor Radius, ft 2
 Blade Chord, ft 0.177
 Rotor Solidity 0.0894
 Root Cutout, %R 26.2
 Blade Taper Ratio 1
 Blade Aspect Ratio 7.1
 Blade Twist 0
 Airfoil Section
 NACA 0012
 $I = 0.0022 \text{ slug-ft}^2$

The collective pitch and the rotor shaft tilt angle are variable. The speed of the rotor is variable up to the maximum of 3000 RPM. This results in tip speeds up to 400 ft/sec. The wind tunnel air velocity is variable up to the maximum of 75 ft/sec. Figure 4 shows the test section and the location of the rotor in the wind tunnel.

The Hot-Film Anemometry

The Anemometer

The rotor induced velocities were measured by means of a three-dimensional hot-film probe connected to three DISA 55D05/102C constant temperature anemometer circuits. To improve the resolution of the three-dimensional anemometer and to achieve signal levels suitable for magnetic recording the outputs of the anemometer were reduced by the factor of 4 by means of voltage dividers and then amplified by 20 by means of three DANA 2210 DC differential amplifiers. The differential feature of the DANA amplifiers was also used to remove the DC parts of the anemometer outputs which correspond to zero velocity inputs. The result of this arrangement was that the anemometer output voltages for input velocities of 0 to 80 ft/sec were between 0 and 10 volts.

Directional Sensitivity of Cylindrical Sensors

The basic hot-wire or hot-film anemometer output is a voltage which is related to the fluid velocity approximately as

$$E^2 = K_1 + K_2 U^{1/2} \quad (1)$$

where U is the velocity input, E is the voltage output and K_1 , K_2 are constants determined by the anemometer, the sensor and the fluid properties.

If the fluid velocity is not perpendicular to the sensor Equation (1) does not hold, since the heat transfer from the sensor is reduced. It is convenient to define the "effective cooling velocity"

as the perpendicular velocity which produces the same cooling effect as the actual, non-perpendicular velocity. Several relationships have been proposed to relate the actual and the effective velocities. The simplest relationship defines the effective velocity as the component normal to the sensor of the actual velocity. This correlation neglects the contribution of the flow along the sensor to the total cooling effect, and is not accurate for deviations larger than 40° from the normal direction. More accurate correlations have been suggested in References 10, 11, and 12.

We used the relationship proposed in Reference 11, because it matched the experimental data accurately. It also enabled us to obtain a closed form solution for the magnitude of the velocity vector and its directional cosines. Figure 5 and Equation (2) define this relationship.

$$V_{\text{eff}}^2 = U^2 (\sin^2 \delta + k^2 \cos^2 \delta) \quad (2)$$

k is a dimensionless constant. Note that if the flow is normal to the sensor $\delta = 90^\circ$ and $V_{\text{eff}} = U$.

Data Reduction Method

The three-dimensional probe consists of three orthogonal, cylindrical sensors, as shown in Figure 6. The effective cooling velocities of the three sensors are

$$V_a^2 = U^2 (\sin^2 \alpha + k^2 \cos^2 \alpha) \quad (3a)$$

$$V_b^2 = U^2 (\sin^2 \beta + k^2 \cos^2 \beta) \quad (3b)$$

$$V_c^2 = U^2 (\sin^2 \gamma + k^2 \cos^2 \gamma) \quad (3c)$$

Adding the three above equations leads to

$$V_a^2 + V_b^2 + V_c^2 = U^2 \{ (\sin^2 \alpha + \sin^2 \beta + \sin^2 \gamma) + k^2 (\cos^2 \alpha + \cos^2 \beta + \cos^2 \gamma) \} \quad (4)$$

The following trigonometric relationships exist between the directional angles α , β , γ .

$$\sin^2 \alpha + \sin^2 \beta + \sin^2 \gamma = 2 \quad (5)$$

$$\cos^2 \alpha + \cos^2 \beta + \cos^2 \gamma = 1 \quad (6)$$

Substituting Equation (5) and Equation (6) into Equation (4) gives

$$V_a^2 + V_b^2 + V_c^2 = U^2 (2 + k^2) \quad (7)$$

and solving for the mean velocity

$$U = \sqrt{\frac{v_a^2 + v_b^2 + v_c^2}{2 + k^2}} \quad (8)$$

After substituting Equation (8) into Equation (3) and some algebraic manipulations one can write

$$\sin \alpha = \sqrt{\left(\frac{2 + k^2}{1 - k^2}\right) \left(\frac{v_a^2}{v_a^2 + v_b^2 + v_c^2}\right) - \left(\frac{k^2}{1 - k^2}\right)} \quad (9a)$$

$$\sin \beta = \sqrt{\left(\frac{2 + k^2}{1 - k^2}\right) \left(\frac{v_b^2}{v_a^2 + v_b^2 + v_c^2}\right) - \left(\frac{k^2}{1 - k^2}\right)} \quad (9b)$$

$$\sin \gamma = \sqrt{\left(\frac{2 + k^2}{1 - k^2}\right) \left(\frac{v_c^2}{v_a^2 + v_b^2 + v_c^2}\right) - \left(\frac{k^2}{1 - k^2}\right)} \quad (9c)$$

Equation (8) and Equation (9) define the total velocity vector in the probe system of coordinates, provided one knows by some other means whether the angles α , β , γ are smaller or larger than 90° . Since the cylindrical sensors do not distinguish between yaw angle δ and yaw angle ($180^\circ - \delta$), the set of the three output voltages of the three-dimensional anemometer can correspond to $2^3 = 8$ different spatial orientations.

Transformation of Velocities

The probe used was a TSI 1294-60-18 hot-film probe. The three mutually perpendicular sensors are inclined 54.74° to the probe axis. The probe was placed in the tunnel as shown in Figure 7. Experiments have shown that this was the optimal spatial orientation, since the average velocity vector in the tunnel stayed in one octant for most of the experiments. The above mentioned octant is the one determined by outward pointing vectors along sensors A and B, and an inward pointing vector along sensor C.

Since the velocity data was needed in the tunnel system of coordinates, a

transformation of coordinates was required. The two sets of axes are shown in Figure 8. The orientation of the probe is such that axis C lies in plane X-7 and plane ROAD is perpendicular to plane X-2. The geometry of the probe is such that

$$\angle FOC = 35.26^\circ$$

$$\angle EOD = 54.74^\circ$$

$$\angle AOD = \angle ROD = 45.0^\circ$$

Using basic trigonometry, we now can express the velocity vector U , given by means of its components U_a , U_b , and U_c in the tunnel system of coordinates by means of the components V_x , V_y , and V_z . Equations (10) through (13) define the transformation.

$$V_y = 0.5774 U_a + 0.5774 U_b - 0.5773 U_c \quad (10)$$

$$V_z = -(0.4082 U_a + 0.4082 U_b + 0.8165 U_c) \quad (11)$$

$$V_x = 0.7071 U_a - 0.7071 U_b \quad (12)$$

where

$$U_a = U \cos \alpha \quad U_a \text{ has direction of A} \quad (13a)$$

$$U_b = U \cos \beta \quad U_b \text{ has direction of B} \quad (13b)$$

$$U_c = U \cos \gamma \quad U_c \text{ has direction of C} \quad (13c)$$

Calibration of the Three-Dimensional Probe

The calibration of the three-dimensional probe consists of two stages. The first is to obtain the voltage versus velocity curve for each sensor. The second is to determine the yaw angle sensitivity constant k .

Velocity Calibration

A calibrator similar to TSI Model 1125 was modified to make the calibration of the 3-D probe possible. The calibration procedure is similar to that described in references [13, 14].

Using the calibration rig, curves were obtained of anemometer output volts at various velocities for all three probes. Since the subsequent calculation of the velocities was done by a digital computer, it was desirable to fit a polynomial to do

the calibration curve of each sensor. The first approximation to the calibration curve of a cylindrical sensor is Equation (1). To achieve better accuracy we used fourth order polynomials.

The polynomials used to reduce the data collected were

$$V_a = 0.01546 E_a^4 - 0.2395 E_a^3 + 1.986 E_a^2 - 3.03 E_a + 0.9 \quad (14a)$$

$$V_b = 0.01424 E_b^4 - 0.2111 E_b^3 + 1.677 E_b^2 - 1.65 E_b - 0.1 \quad (14b)$$

$$V_c = 0.00188 E_c^4 + 0.0152 E_c^3 + 0.410 E_c^2 + 1.01 E_c - 0.5 \quad (14c)$$

where the constants were obtained by a least squares fit of the data.

The probe was recalibrated periodically and only negligible changes were observed.

Directional Sensitivity Calibration

The purpose of this calibration was to determine the constant k from Equation (2). The angle of the flow to the wire was set to give angle, δ , between 90° and 0° . The calibrator velocity is set to a constant value U , and the output of the anemometer, E , is recorded for several values of δ . Then, using the calibration curve of the anemometer, the effective cooling velocities are computed. One can now rewrite Equation (2) as

$$\frac{V_{eff}}{U}^2 = \sin^2 \delta + k^2 \cos^2 \delta \quad (15)$$

and obtain the value of k^2 using the Method of Least Squares.

This calibration was performed three times during a period of six months, for the three sensors of the 3-D probe. Velocities of 30, 50 and 80 ft/sec were used. The values of k^2 were always in the range of 0.098 to 0.102. The data for $\delta < 10^\circ$ were not used in determination of k^2 , since the disturbance due to the probe prongs at these yaw angles was large and the data did not fit Equation (2). The fit for angles larger than 10° was considered to be good, and the fit for angles smaller than 10° was considered to be fair.

The value of $k^2 = 0.10$ was used in the calculations throughout this work. It is interesting to note that the value of U obtained via Equation (8) and the values of α , β and γ obtained via Equation (9) are only slightly effected by large changes of k^2 . The velocity changes only 0.24% when k^2 changes from 0.09 to 0.10. The angle α for example, changes only by 1.56° when k^2 changes from 0.09 to 0.10 for the nominal value of $\alpha = 10^\circ$, which is a large yaw angle.

Probe Traverse System

The purpose of the traverse system is to locate the hot-film probe accurately within the wind tunnel test section, while the tunnel and the rotor are running. The system is based on a X-Y positioner which was built for another project, several years ago. The X-Y positioner is capable of moving the probe support 16 inches horizontally and 10 inches vertically by means of power trains moved by two DC motors. The motion is controlled from a control panel, and location is measured by counting the revolutions of the power screws using electromechanical counters. The number of counts per inch of motion is 13, so that the resolution is 0.08 inches.

To move the traverse assembly along the tunnel in the flow direction the device was equipped with wheels. The moving traverse unit is equipped with four cam followers which slave it to a 12 ft long track made of standard steel angle fixed to the tunnel floor. The X-Y positioner can be shifted ± 6 inches perpendicularly to the track by relocating the cam followers, which is accomplished in seconds. The motion along the tunnel is controlled external to the tunnel. The vertical range of the X-Y positioner was extended as necessary by positioning the probe at four different vertical locations on the traverse. A continuous vertical travel of 40 inches was achieved. The space covered by the traverse system is 28 in. x 100 in. x 40 in., and it can be increased even further by relocating the track. This range allows flow beneath the rotor to be studied. By resetting the rotor pitch the same traverse system can be used to study flow above the rotor.

Velocities were measured at grid points located at 3 inch spacings vertically, 4 inch spacings across the rotor in the X-Y plane, and at 4 inch spacing along the tunnel axis. For the tests of rotor flow near to and below the rotor a total of 1188 grid points were available.

Evaluation of Errors

Velocity and Angle Errors

Since the results of this work are only as good as the data taken, and the methods of reducing the data, a brief discussion of the magnitude of the errors involved on the work will be presented. A more detailed analysis can be found in reference 10.

The velocity measurements are considered to have an average error of 0.93 ft/sec over the entire velocity calibration range of 10 to 70 ft/sec. Detailed study of the effect of tunnel and probe vibration revealed that vibration had a negligible effect on the accuracy of velocity measurement. The estimated error in the measurement of angles with the probe indicated that the maximum errors were within $\pm 2^\circ$ in the ranges of angles useful in this study for the entire range of velocities considered.

The errors in determining the velocities in the x, y, z coordinate systems depend upon the velocity and the angle errors of the probe data. If the worst errors occur simultaneously, an error of 1.9 ft/sec could occur. The average error was considered to be 1.0 ft/sec or less.

Other Sources of Error

The three sensors of the 3-D probe are not at the same point in the wake, because of their finite size. They fit within a 0.35 inches diameter sphere. The error due to this arrangement will be small, except for the case when a vortex core or a vortex sheet cross this sphere.

The error of the probe location in the tunnel (X,Y,Z) is a result of the deflection of the probe holder and the probe, imperfection of the tunnel floor on which the traverse mechanism moves, errors of coordinate measurements, etc. It was estimated to be less than ± 0.25 inches in each coordinate direction.

The angular error due to misalignment of the probe with respect to the tunnel walls was estimated to be $\pm 0.5^\circ$. However, this error is included in the analysis of Section 3.5.2, since the same problem arises when the probe is mounted on the velocity calibrator. The angular alignment was done with an accurate mercury balanced indicator.

The error of the tunnel velocity measurement due to the finite resolution of

the manometer which measure the Pitot pressure was estimated to be from 2.5% at 20 ft/sec down to 0.25% at 70 ft/sec.

Changes of the room temperature might cause errors in the tunnel velocity measurements (Pitot tube), and in the wake velocity measurements (anemometer). However, we attempted to minimize this source of error by keeping the temperature constant within $78^\circ \pm 2^\circ$. It was done by controlling the number of open windows in the room where the tunnel was located.

The RPM of the rotor was steady. It was measured by an electronic counter, by counting the number of revolutions over the period of 10 seconds. The accuracy of this measurement was better than 1%.

The error of the computed advance ratio, which results from the errors of the tunnel velocity and the rotor RPM was computed to be from 3.5% at tunnel velocity of 20 ft/sec down to 1.3% at tunnel velocity of 70 ft/sec.

The errors of the rotor shaft tilt angle and of the collective pitch angle were estimated to be within the limits of $\pm 0.5^\circ$.

Test Results

The parameters of the flight conditions tested in this sequence of tests were:

Blade Tip Speed, ft/sec	300
Advance Ratio	0.10; 0.08; 0.06; 0.04
Collective Pitch Angle, degrees	8
Rotor Shaft Tilt Angle, degrees	8
Coning Angle, degrees	2

The output of each anemometer was read as a time average using a Westinghouse PX 161 RMS voltmeter and using a Fluke 8000A digital voltmeter.

The grid used for measuring flow in the wake below the rotor consisted of 1188 points, 167 of which were not used, because they were too close to the rotor. Figure 9 shows the grid points in the Y-Z plane for the case of $u = 0$ at the centerline $X/R = .27$. Eighteen such planes were equally spaced between $X = 1.60$ and $X = 2.67$, although not all are presented.

Several types of plots were used to interpret the results. Components of U in the X-Y, Y-Z and Z-X planes were plotted. This was done on a CRT terminal. Downwash velocity plots were also made. The data

that follow are average or mean velocity data and are not instantaneous values.

Data are presented for advance ratios of 0.04, 0.06, 0.08, and 0.10. It should be noted that the rotor is not trimmed, but simply set at the collective pitch and shaft angle.

Figure 10 presents the data for $\mu = 0.10$ for the transverse Y-Z plane, which are planes similar to the reference diagram in figure 9. The expected rollup as the flow moves downstream, (as X/R gets increasingly negative) can be observed from the data. Figure 11, for $\mu = .10$ depicts the various longitudinal X-Z planes showing the downwash influence of the rotor. Figure 12, for $\mu = 0.10$ and X-Y planes shows the flow field when viewed from "above" the rotor and the lateral flow due to roll-up can be seen.

For $\mu = 0.08$ Figure 13 presents the transverse Y-Z planes, Figure 14 presents the longitudinal X-Z planes and Figure 15 presents the X-Y planes.

For $\mu = 0.06$ Figure 16 presents the transverse Y-Z planes, Figure 17 presents the longitudinal X-Z planes, and Figure 18 presents the X-Y planes.

For $\mu = 0.04$ Figure 19 presents the transverse Y-Z planes. Figure 20 presents the longitudinal X-Z planes and Figure 21 presents the X-Y planes.

Due to limitations on time data for the above the rotor are not included in this presentation. Data acquired in the region up to 0.6 Z/R above the rotor will be presented in the final report summarizing this work.

Discussion of Test Results

Advance Ratio of 0.10

If one examines the data presented in Figure 10 the expected vortex roll-up of the rotor wake can readily be seen. The picture of the wake velocities in the vertical cross section are similar to what one would expect from a low aspect ratio wing. The flow field when viewed from above, Figure 12, likewise show an expected inflow towards the rotor center above the rotor, changing to an outflow below the rotor. The side view of the rotor flow shown in Figure 11 likewise appears somewhat as one would anticipate, with up flow in the plane beyond the rotor tip and down flow under the rotor.

The results appear similar to those of Heyson and Katsoff (4).

At an advance ratio of $\mu = 0.10$, then, the picture that has been obtained appears similar to what had been expected.

Advance Ratio of 0.06

Examination of the data for $\mu = 0.06$ as shown in the vertical planes in Figure 16 reveals a vortex rollup pattern similar to what would expect behind a low aspect ratio wing. In this particular case the intensity of the vortex developing aft of the advancing side (on the right hand side of the figure) seems to be greater than the vortex developed aft of the retreating side.

The flow patterns when viewed from the side of the rotor, Figure 17 show an anticipated up flow in the plane outside the rotor tip on the advancing side, $X/R = -1.33$. Just inside the rotor tip at 80% radius, a strong downwash pattern develops, and also closer to the hub 27% radius the strong downwash pattern can be seen. When we reach the centerline, at 0% radius, the downwash pattern is evident, but it is not as strong. At the opposite side or retreating side at $X/R = 0.53$, a highly concentrated region of downwash is again evident. The flow beyond the tip at the retreating side, $X/R = 1.33$, is also upwards. The view from above the rotor reveals the anticipated inflows above the trailing vortex structure, $Z/R = -0.2$. In the plane of the rotor, $Z/R = 0.0$, and below the rotor one can see the outflow in the region of the trailing vortex.

The advance ratio data for $\mu = 0.08$ and $\mu = 0.04$ are somewhat similar in appearance to the $\mu = 0.10$ and $\mu = 0.06$ just discussed.

Interpretation

The data obtained at $\mu = 0.10$ reveal flow patterns similar to what was anticipated and has been seen in prior studies at similar advance ratios and higher advance ratios (4). The downwash is similar, and the vortex patterns shown when viewed from the rear of the rotor are expected. The side view does not reveal anything unexpected.

The advance ratio of $\mu = 0.06$ and other low advance ratios tested reveal a difference which is believed to be of considerable significance. If one examines various cuts of Figure 16 as well as other

vertical cuts through the flow in Figure 17, it becomes clear that the flow near the rotor tends to initiate roll up into two concentrated vortices in the rotor plane and not just downstream of the rotor. It appears that a significant portion of the total flow to the rotor is "encased" within these vortices as they develop. If we examine the magnitude of the longitudinal component in Figure 17 as well as the magnitude of the vertical velocity components it can be observed that the magnitudes are significantly increased, up to doubled in size. If one recalls from inviscid flow theory, if a vortex stretches out, a decrease in diameter results and an increase in tangential velocity follows. Now if the vortices shown in Figure 16 can be interpreted to be streamlines then the fluid once contained within the rolled up region will tend to stay there. Since continuity must be preserved, as the vortex rolls up and diameter contracts the axial (continuity component) velocity must increase. In a gross pictorial way, the flow coming to the rotor seems to wrap up and through a "porous" wing (actuator disk) and while whirling is squirted aft in concentrated streams almost like toothpaste squirted out of a toothpaste tube.

Study of data at $u = 0.04$ and 0.08 reveals similar behavior. By the time $u = 0.10$ is reached this pronounced squirting is no longer as evident.

The potential implications of these findings could be great if further data continue to verify their existence. It is well known that large changes in yaw control (tail rotor performance) occur with small changes in crossflow or forward flight at very low flight speeds. Likewise significant changes to horizontal stabilizers or stabilators operating characteristics occur during small changes in wind velocity, direction or magnitude when operating a helicopter at low flight speeds.

From the data obtained, the highly concentrated, high velocity flows generated could impinge upon the tail rotor, tail surfaces and the tail boom, and depending on the unique angle of yaw, pitch, wind heading, c.g. position, or side winds such interaction could result in sudden and significant changes to the forces generated by the aft located aerodynamic surfaces and tail rotors.

References

1. Landgrebe, Anton J.; Foelf, T. Alan: ROTOCRAFT WAKE ANALYSIS FOR THE PREDICTION OF INDUCED VELOCITIES. United Technologies Research Center; USAAMRLD Technical Report 75-45; Fustis Directorate, U. S. Army Air Mobility Research and Development Laboratory, Fort Fustis, Virginia, January 1976.
2. Trenka, A. R.: PREDICTION OF THE PERFORMANCE AND STRESS CHARACTERISTICS OF VTOL PROPELLERS. Proceedings CAL/USAAVLARS Symposium on Aerodynamic Problems Associated with V/STOL Aircraft. Vol. 1, June 1966.
3. Landgrebe, Anton J. and Bellinger, Elton D.: AN INVESTIGATION OF THE QUANTITATIVE APPLICABILITY OF MODEL HELICOPTER ROTOR WAKE PATTERNS OBTAINED FROM A WATER TUNNEL. United Aircraft Corporation; USAAMRDL Technical Report 71-69; Fustis Directorate, U. S. Army Air Mobility Research and Development Laboratory, Fort Fustis, Virginia, December 1971.
4. Heyson, Harry H.; and Katzoff, S.: INDUCED VELOCITIES NEAR A LIFTING ROTOR WITH NONUNIFORM DISC LOADING. NASA Rep. 1319, 1957.
5. Rowden, T. W.; and Shockey, G. A.: A WIND TUNNEL INVESTIGATION OF THE AERODYNAMIC ENVIRONMENT OF A FULL-SCALE HELICOPTER ROTOR IN FORWARD FLIGHT. Bell Helicopter Company; USAAVLARS Technical Report 70-35; U. S. Army Aviation Material Laboratories, Fort Fustis, Virginia, July 1970.
6. Boatwright, Donald W.: MEASUREMENTS OF VELOCITY COMPONENTS IN THE WAKE OF A FULL-SCALE HELICOPTER ROTOR IN HOVER. The Department of Aerophysics and Aerospace Engineering, Mississippi State University, USAAMRDL Technical Report 72-33; Fustis Directorate, U. S. Army Air Mobility Research and Development Laboratory, Fort Fustis, Virginia, August 1972.
7. Tararine, V. S.: EXPERIMENTAL AND THEORETICAL STUDY OF LOCAL INDUCED VELOCITIES OVER A ROTOR DISC. Proceedings CAL/TRFCON Symposium on Dynamic Load Problems Associated with Helicopters and V/STOL Aircraft. Vol. 1, June 1963.

8. Landgrebe, Anton J.: AN ANALYTICAL AND EXPERIMENTAL INVESTIGATION OF HELICOPTER ROTOR PERFORMANCE AND WAKE GEOMETRY CHARACTERISTICS. United Aircraft Corporation; USAAMRDL Technical Report 71-24; Eustis Directorate, U. S. Army Air Mobility Research and Development Laboratory, Fort Eustis, Virginia, June 1971.
9. Biggers, James G.; Lee, Albert; Orloff, Kenneth L.; and Lemmer, Opal G.: LASER VELOCIMETER MEASUREMENTS OF TWO-BLADED HELICOPTER ROTOR FLOW FIELDS. NASA TM 73,238, May 1977.
10. Fujita, Hajime; and Kovaszny, S. G.: MEASUREMENT OF REYNOLDS STRESS BY A SINGLE ROTATED HOT WIRE ANEMOMETER. The Review of Scientific Instruments, Vol. 39, No. 9, September 1968.
11. Champagne, F. H.; Slichter, C. A.; and Wehrmann, O. H.: TURBULENCE MEASUREMENT WITH INCLINED HOT-WIRES. Journal of Fluid Mechanics, 1967, Vol. 28, part 1, pp. 153-182.
12. Frishe, C. A.; and Schwartz, W. H.: DEVIATIONS FROM COSINE LAW FOR VANED CYLINDRICAL ANEMOMETER SENSORS. Journal of Applied Mechanics, Trans. OF ASME, December 1968, pp. 655-662.
13. Velkoff, H. R., Hoffman, J. D., Blaser, D. P.: INVESTIGATION OF BOUNDARY LAYERS AND TIP FLOWS OF HELICOPTER ROTOR BLADES. USAAMRDL TR 71-73. Eustis Directorate, U. S. Army AMRDL, Fort Eustis, Virginia, May 1972.
14. TSI Technical Bulletin No. 8: DATA REDUCTION METHOD FOR MODEL 1204 - 3-D PROBES - ORTHOGONAL SENSORS.

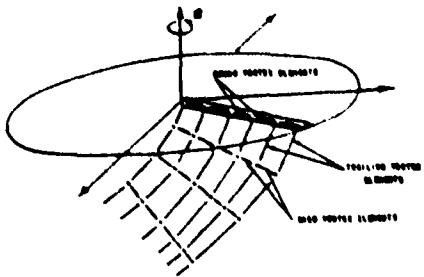


FIGURE 1 Planar Representation of the Rotor Wake in Forward Flight.

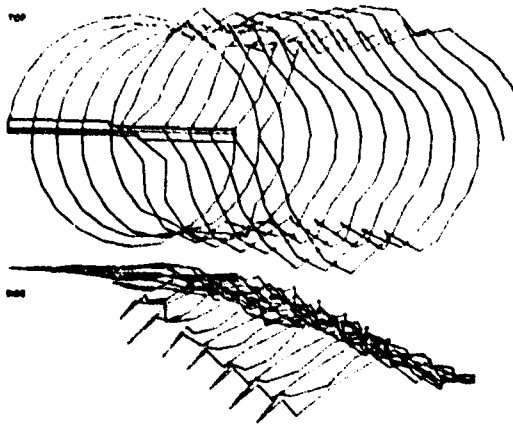


FIGURE 2 Computer Simulated Tip Vortex Trajectory in Forward Flight.

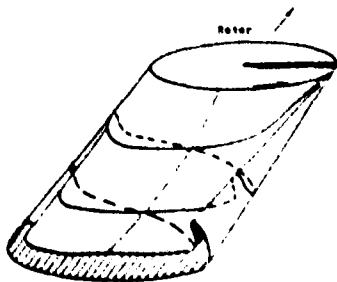


FIGURE 3 Rolling up of the Rotor Wake in Forward Flight.

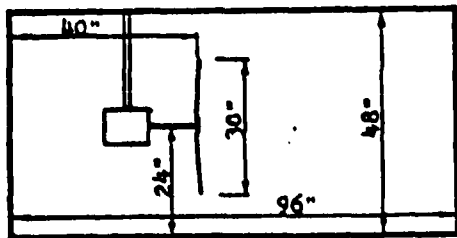
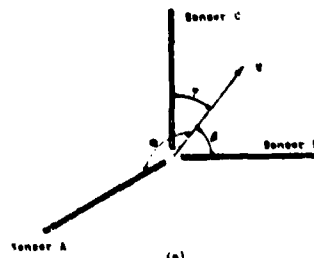


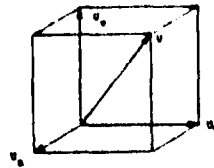
Figure A
Dimensions of the Test Section.



FIGURE 4 Inclined Cylindrical Sensor



(a)



(b)

FIGURE 5 Geometry of a 3-Dimensional Net-Wire (Net-Flu) Probe.
(a) Sensors (b) Velocities

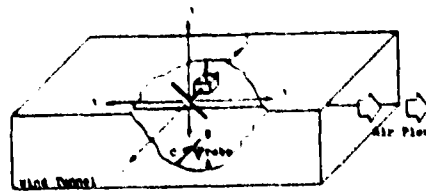


FIGURE 6 The Spatial Orientation of the Net-Flu Probe in the Wind Tunnel.

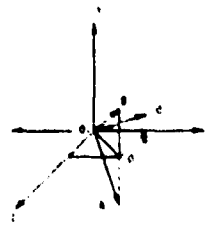


FIGURE 7 The Probe Axes A, B, C in the Tunnel System of Coordinates x, y, z.

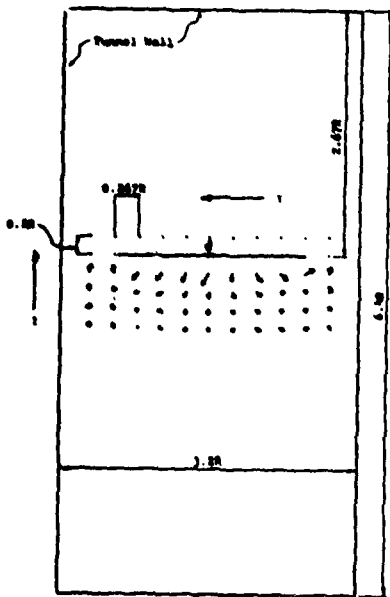


Figure 9. Dimensions of the Traversed Area in Plane Y-Z

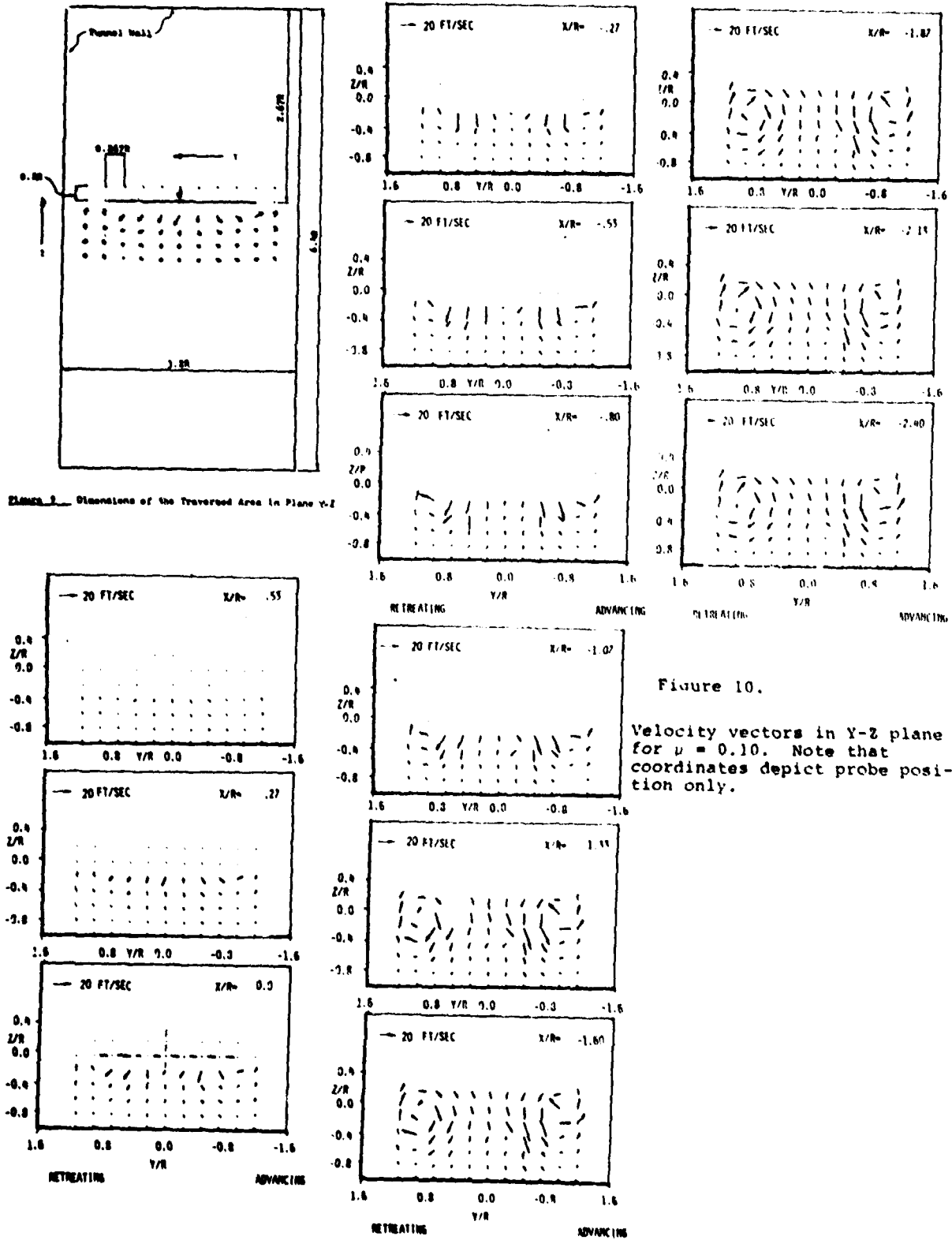


Figure 10.
Velocity vectors in Y-Z plane for $u = 0.10$. Note that coordinates depict probe position only.

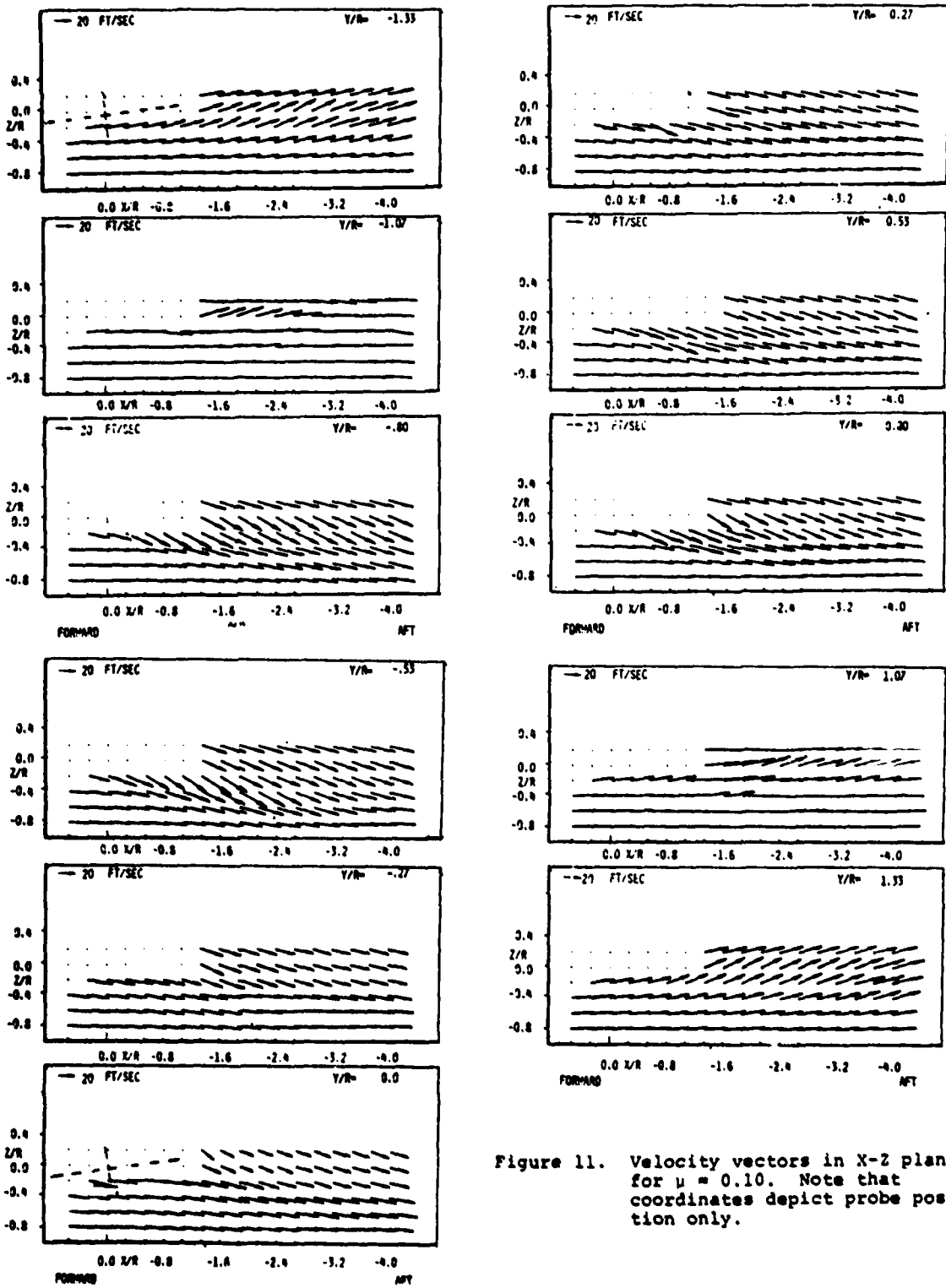


Figure 11. Velocity vectors in X-Z plane for $\mu = 0.10$. Note that coordinates depict probe position only.

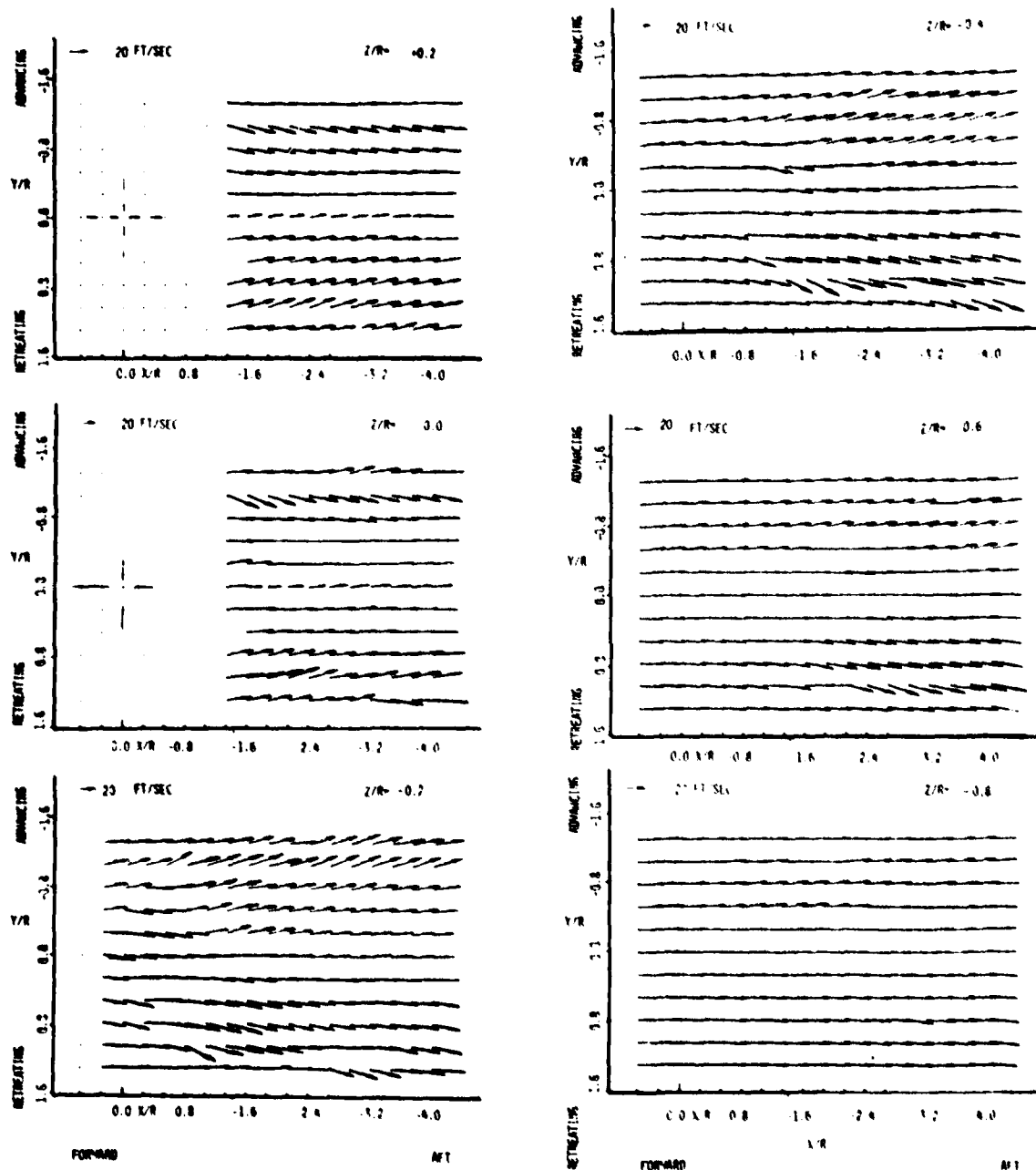


Figure 12. Velocity vectors in X-Y plane for $u = 0.10$. Note that coordinates depict probe position only.

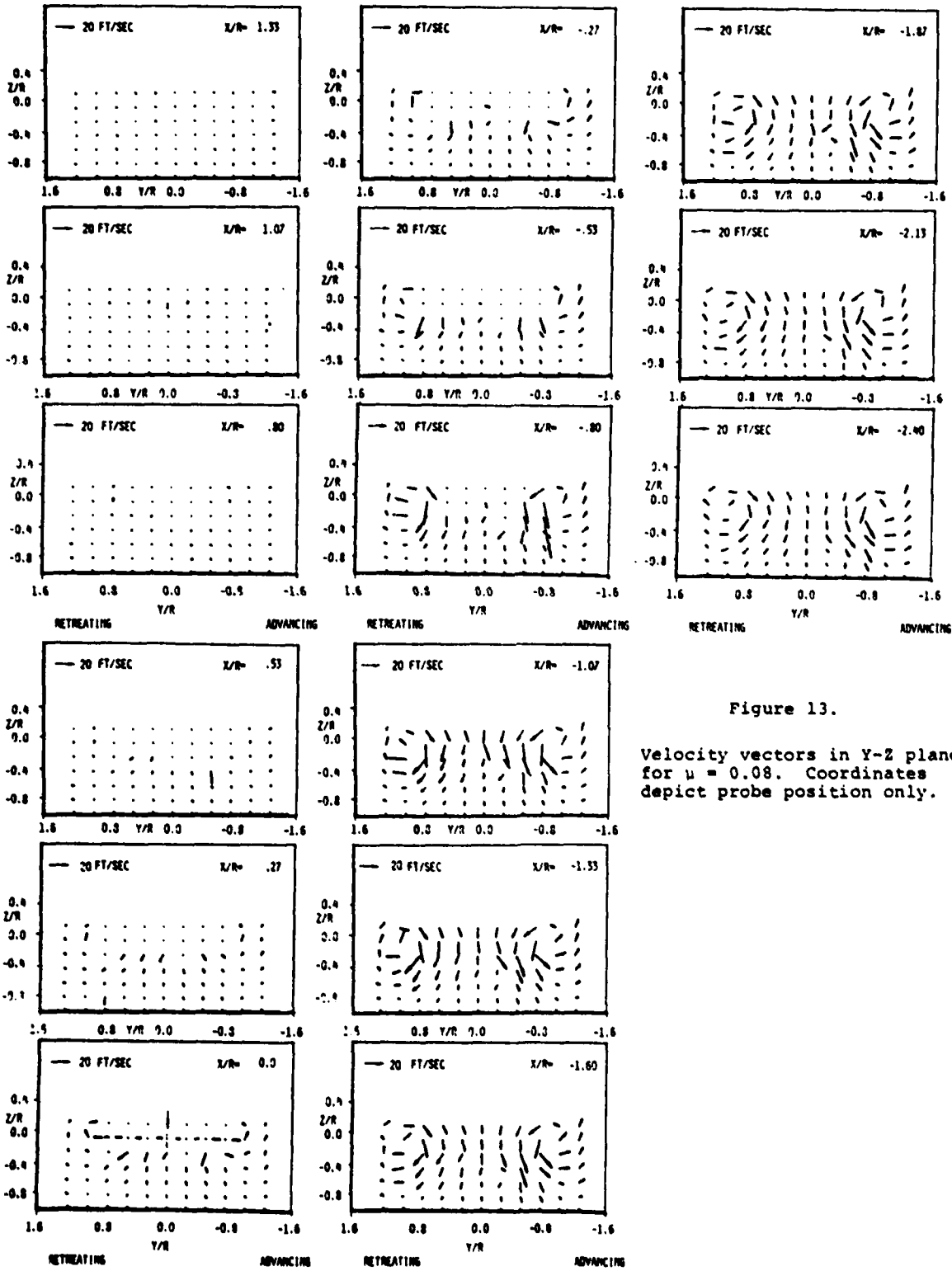


Figure 13.

Velocity vectors in Y-Z plane for $u = 0.08$. Coordinates depict probe position only.

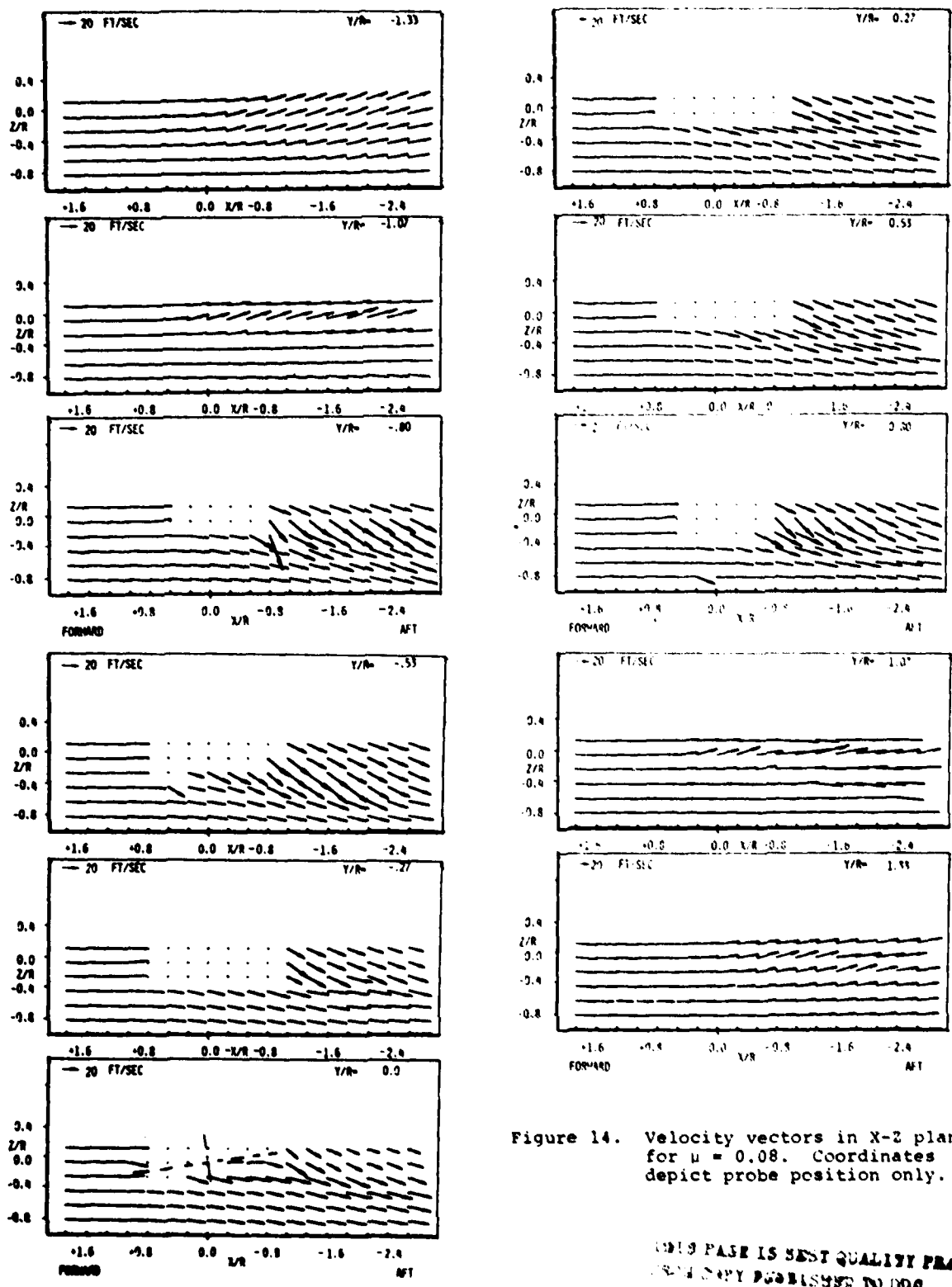


Figure 14. Velocity vectors in X-Z plane for $u = 0.08$. Coordinates depict probe position only.

THIS PAGE IS BEST QUALITY PRINTING
 ANY COPY REPRODUCED IN DDG

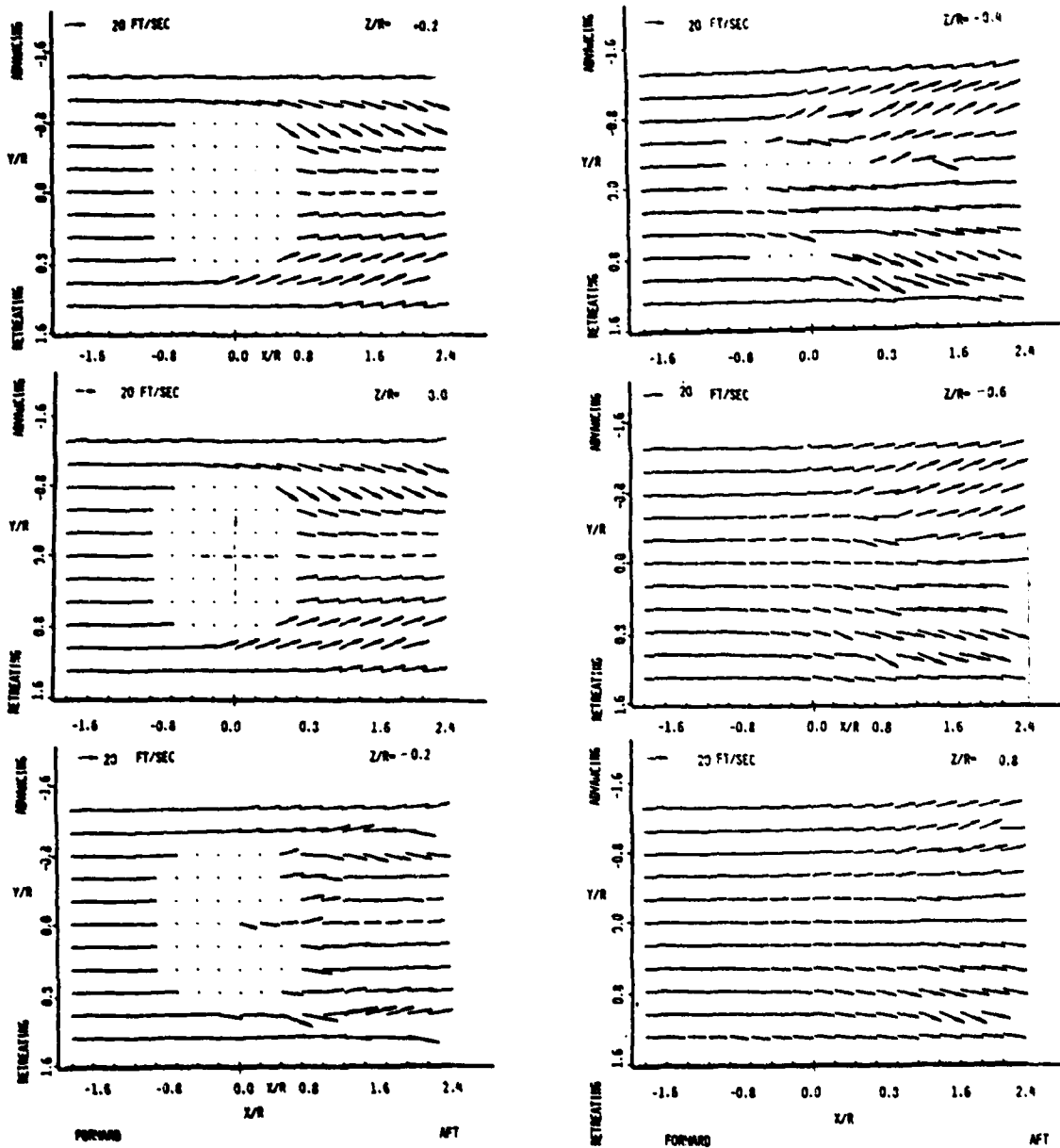


Figure 15. Velocity vectors in X-Y plane for $u = 0.08$. Coordinates depict probe position only.

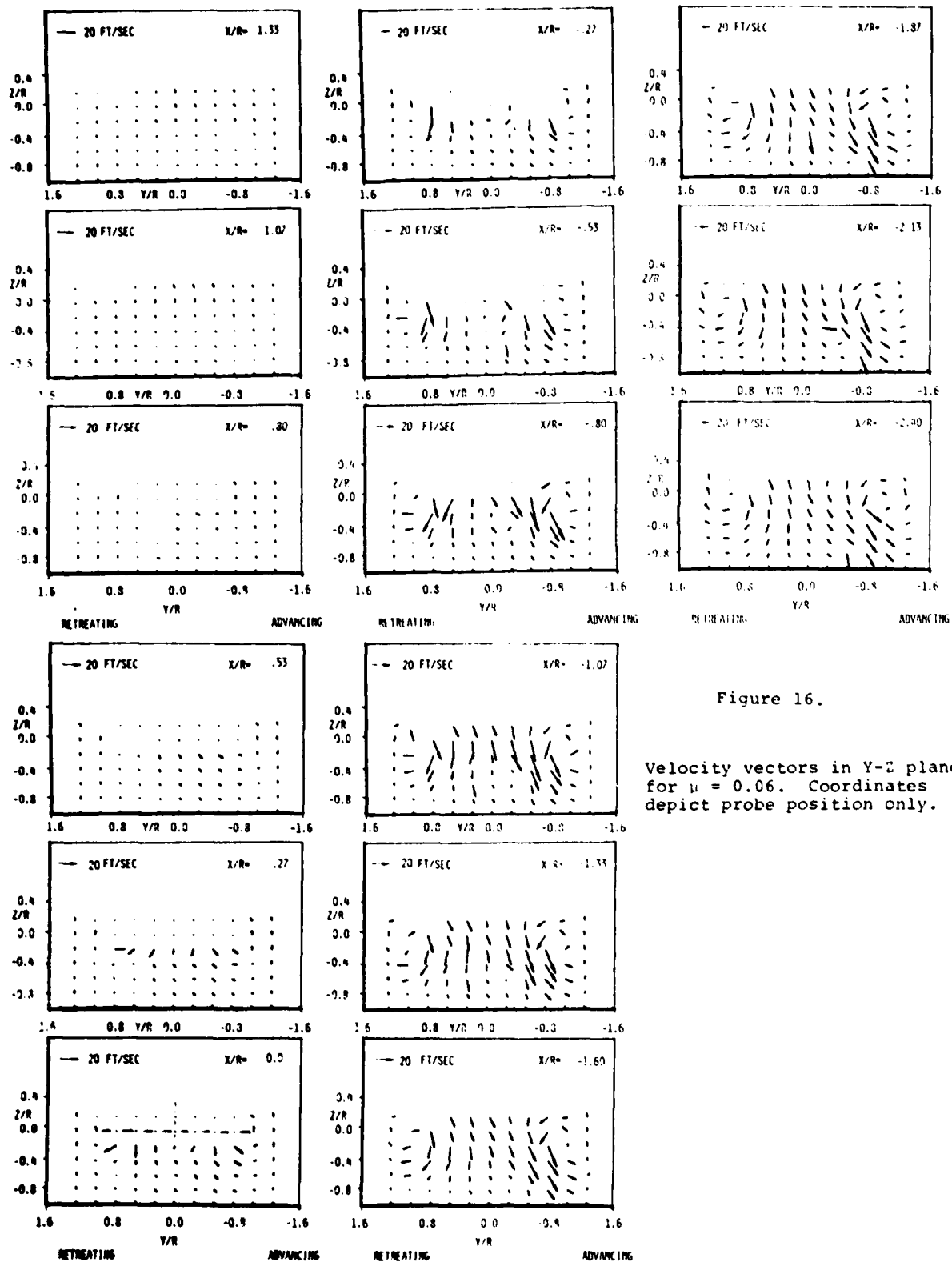


Figure 16.

Velocity vectors in Y-Z plane for $u = 0.06$. Coordinates depict probe position only.

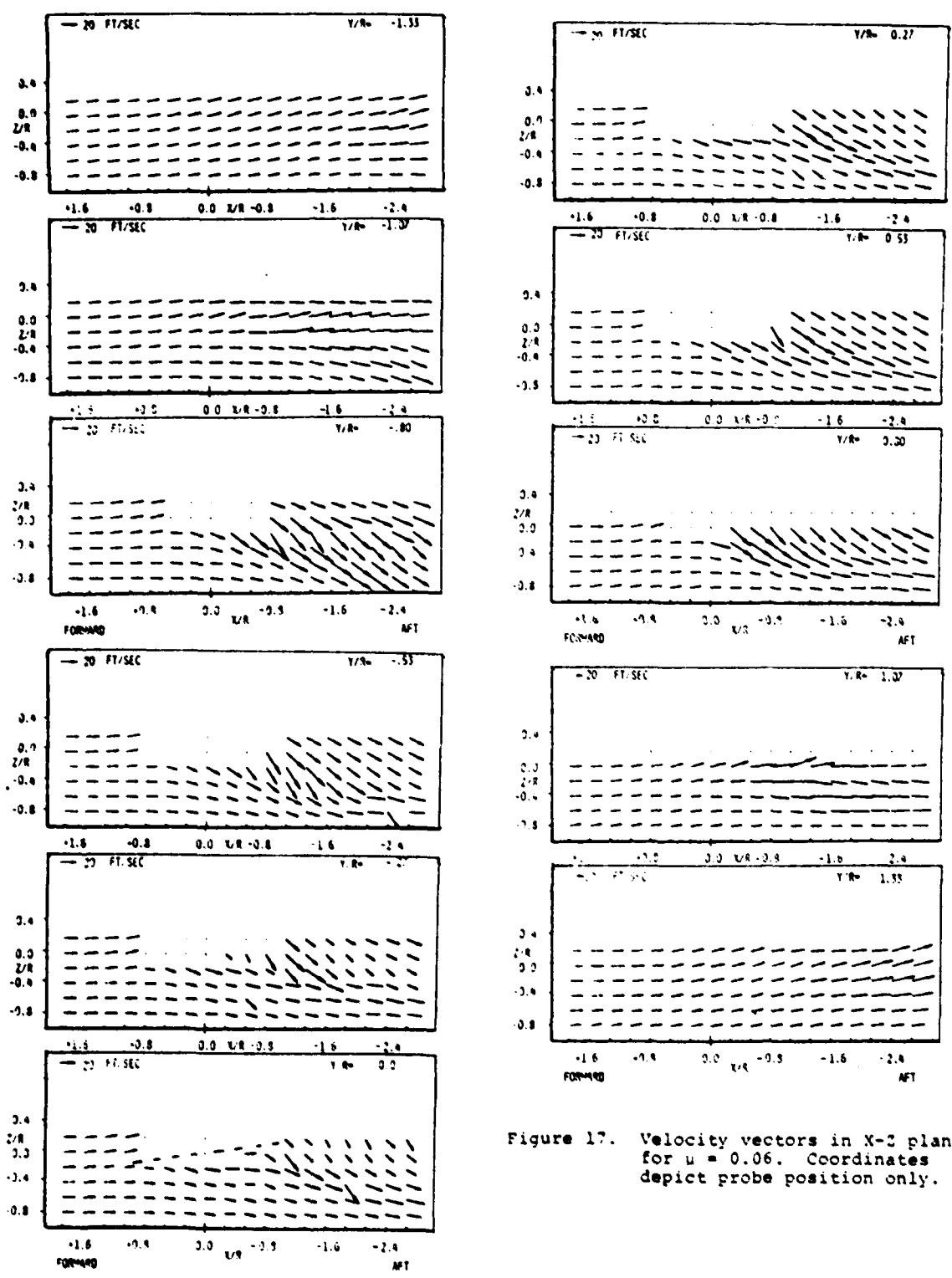


Figure 17. Velocity vectors in X-Z plane for $u = 0.06$. Coordinates depict probe position only.

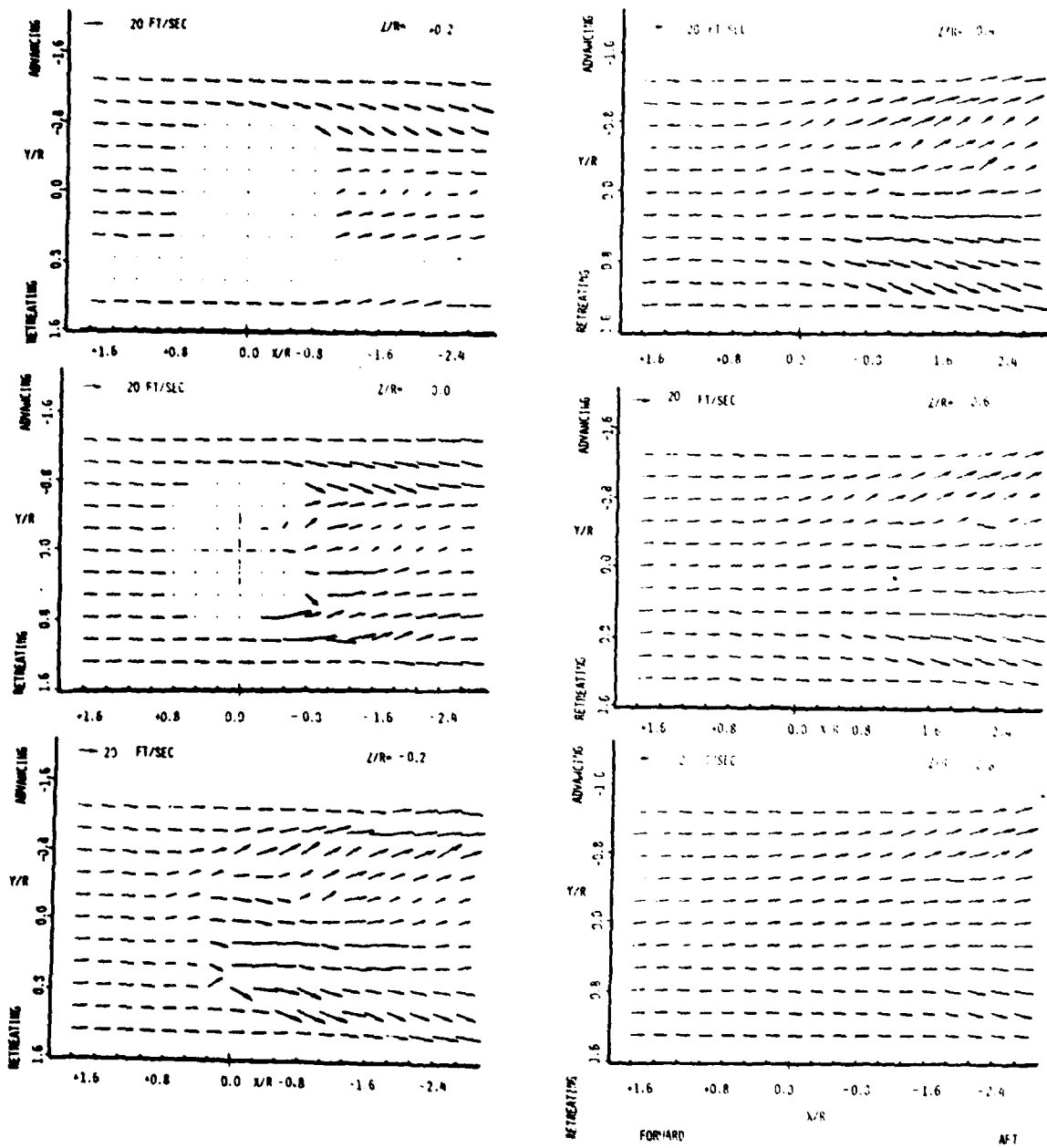


Figure 18. Velocity vectors in X-Y plane for $\mu = 0.06$. Coordinates depict probe position only.

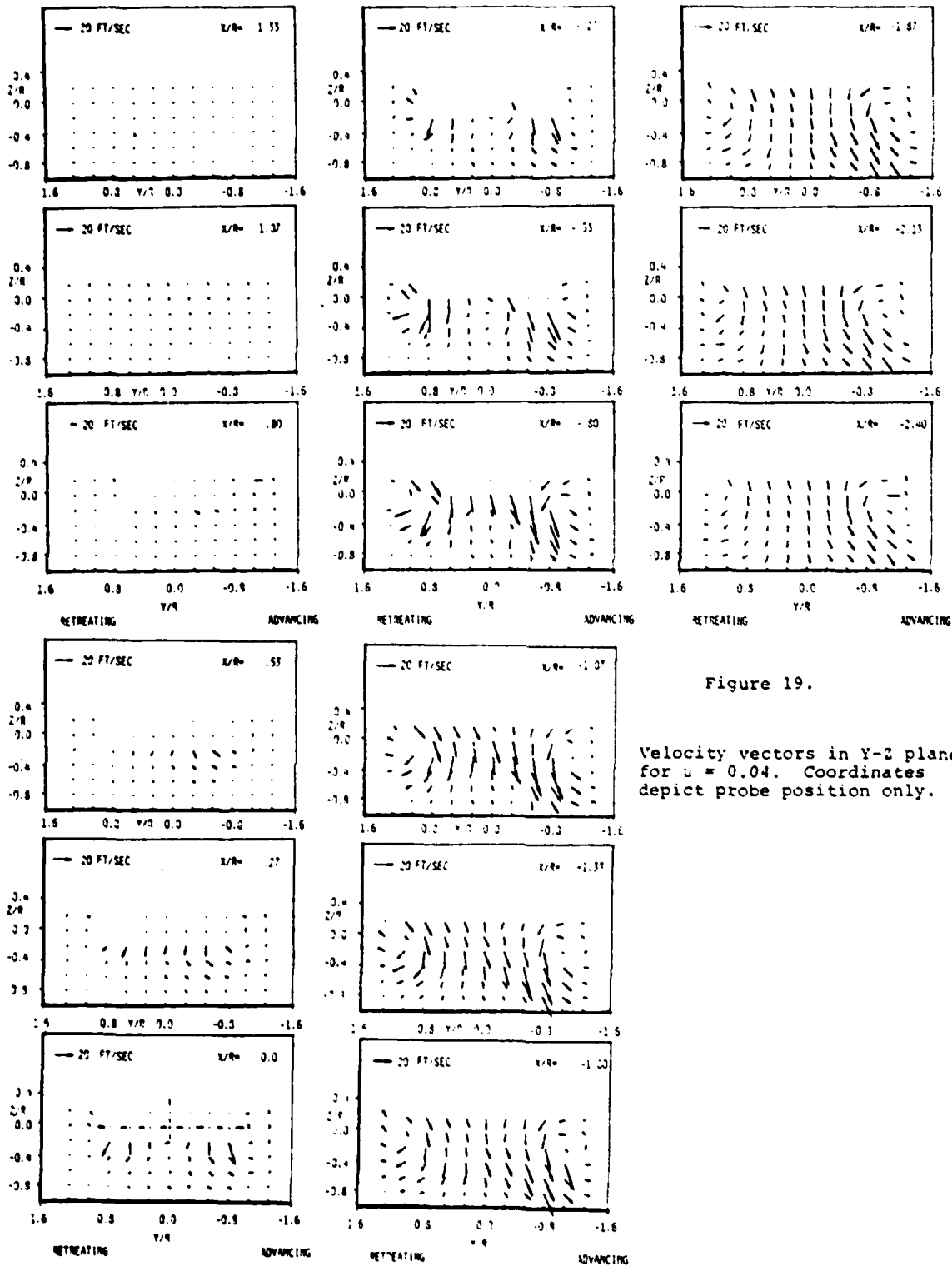


Figure 19.

Velocity vectors in Y-Z plane
for $u = 0.04$. Coordinates
depict probe position only.

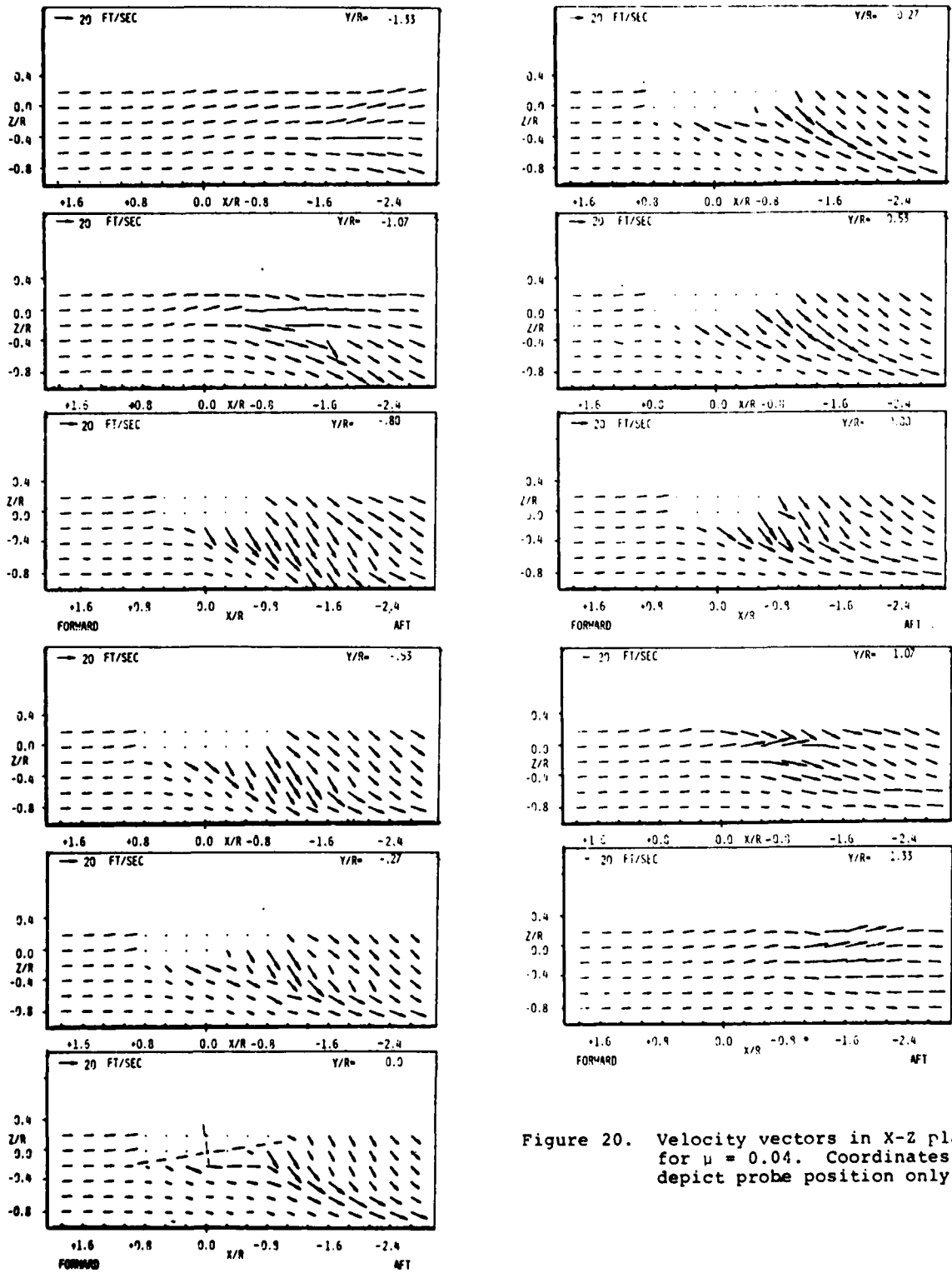


Figure 20. Velocity vectors in X-Z plane for $\mu = 0.04$. Coordinates depict probe position only.

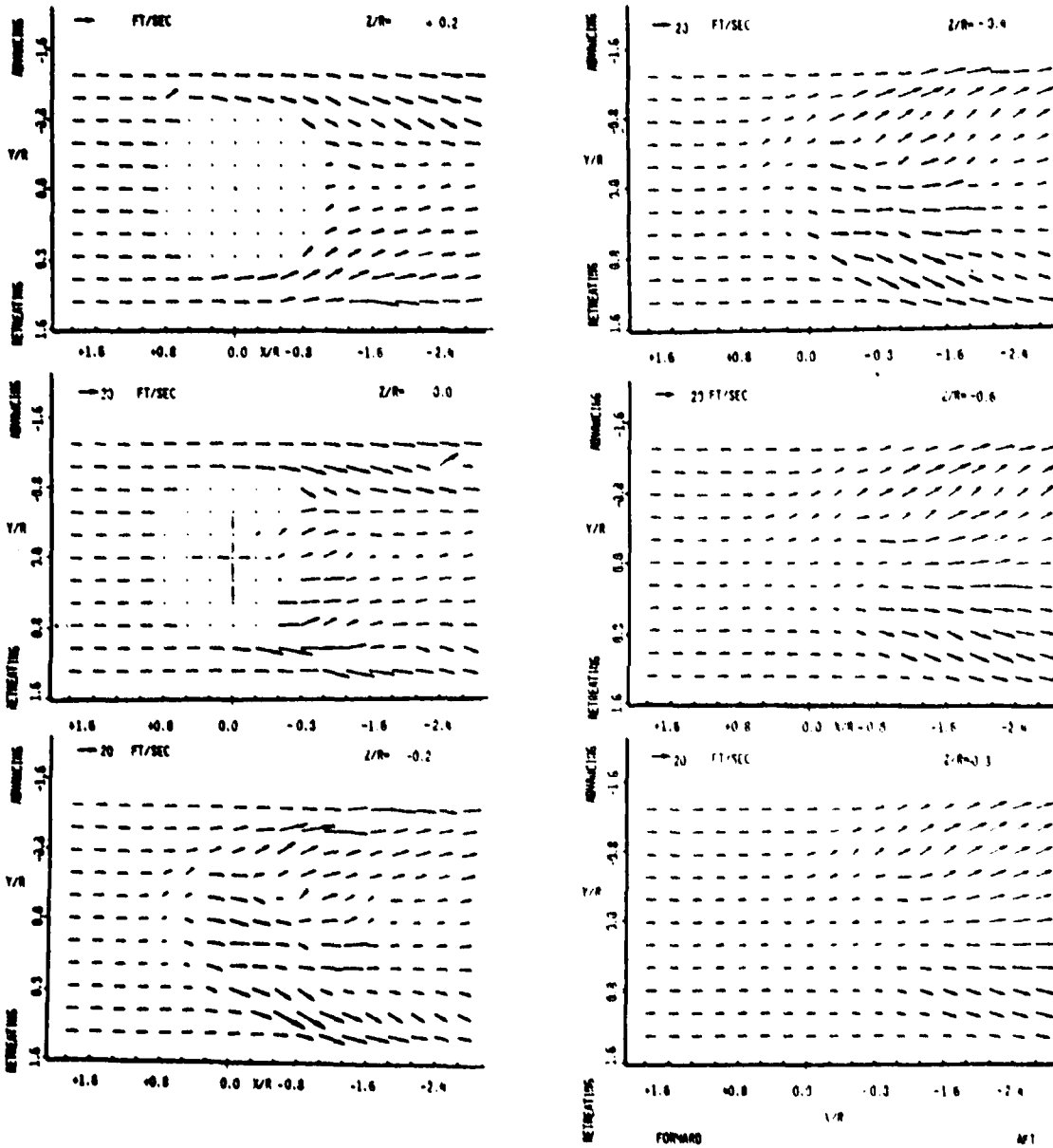


Figure 21. Velocity vectors in X-Y plane for $\mu = 0.04$. Coordinates depict probe position only.

Appendix B

DIRECT FREQUENCY RESPONSE OF
HOT-WIRE AND HOT-FILM ANEMOMETERS*

H. R. Velkoff and D. Horak

Department of Mechanical Engineering
The Ohio State University
Columbus, Ohio U.S.A.

*This work was supported by the U. S. Army Research
Office, Durham, North Carolina

Presented at the Winter Annual Meeting of the American
Society of Mechanical Engineers Winter Annual Meeting,
December 1978 at San Francisco, California

ABSTRACT

A method to measure the frequency response of hot-wire and hot-film anemometers directly was developed. It is based on the comparison of the input (velocity) frequency spectrum to the anemometer with the output (voltage) frequency spectrum it produces. The input spectrum was determined by a reference anemometer. The response of this anemometer was shown to be flat by an indirect, electrical test.

Very good agreement was observed between the results of the direct and the indirect tests for several sensors. Testing of an anemometer using the new method takes only few minutes and it determines the frequency response curve. The method can handle any type of anemometers or sensors, since it is independent of the electronic circuitry of the anemometers and the heat transfer mode of the sensors.

Since the frequency response curve of the tested anemometer is determined in a few minutes, the method developed is an efficient tool for frequency optimization of anemometers. This applies mainly for hot-film anemometers, for which the square wave testing method leads poor results as compared to hot-wire anemometers.

1. Introduction

The method to be described here was developed to facilitate the measurement of the three-dimensional velocity vector in the wake of a small helicopter rotor placed in a wind tunnel. To prevent mechanical failure of the expensive 3-D probe, it was decided to use large diameter hot-film sensors. Since the frequency response of a hot-film anemometer which uses large sensors is low, some of the high harmonics of the fluctuating flow were far beyond the flat range of the instrument. Accurate measurement of these harmonics required accurate measurement of the frequency response of the anemometer.

We first tried to use one of the known, indirect, methods of anemometer frequency response measurement. The most common method is the electronic square wave test, which is built into many modern anemometers. This method was described in detail by Freymuth (1967), Freymuth and Fingerson (1977) and others. It works well for constant temperature hot-wire anemometers, determines the cutoff frequency of the instrument and serves as a tool for frequency optimization. However, for hot-film anemometers the theory for square wave test has not been developed, and one cannot use it as an accurate tool neither for optimization nor for estimation of the cutoff frequency.

The second indirect method available is the sine wave

test, described by Weidman and Browand (1975), Freymuth (1977) and Freymuth and Fingerson (1977). We used this method to determine the accuracy of the direct method developed. This method, although quite simple if the techniques suggested in Section 3 of this paper are used, is not practical for frequency optimization.

Frequency optimization is a trial and error procedure, and several trials are required until the optimum is reached. Since the sine wave test is quite time consuming, performing it several times may take many hours. Another disadvantage of this method is its dependence on the knowledge of the form of the anemometer transfer function. If the assumed function is not accurate, the results will be poor.

Because of the above disadvantages of the indirect methods, we decided to use a direct method which would be independent of the electronics of the particular anemometer, will use a velocity signal as its input and will be fast enough to make "on-line" frequency optimization of anemometers possible.

Prior to developing our method we tried to adopt one of the known direct methods. However, we did not find one which would fulfill the above requirements. Measuring the response by placing the sensor in a vortex street shed from a cylinder (grant 1968, Perry and Morrison 1971)

was considered too complicated and time consuming, since a new combination of velocity and cylinder diameter is needed for every point of the frequency response curve. The method of vibrating the sensor on a high frequency vibrating table (Perry and Morrison 1971) is limited to low frequency and low perturbation velocity by the inertia forces. The problem of sensor resonance may also arise. The method of audio-frequency modulated microwaves directed at the sensor (Kidron 1966) was not actually a direct method since the input was not velocity.

2. Direct Determination of Hot-Wire or Hot-Film Anemometer Frequency Response

The method developed and presented here is based on the following equation known from signal theory (Doebelin 1975). Let $G(i\omega)$ be the sinusoidal transfer function of a dynamic system, $Q_i(i\omega)$ the input spectrum to that system and $Q_o(i\omega)$ its output spectrum. Then one can write:

$$G(i\omega) = \frac{Q_o(i\omega)}{Q_i(i\omega)} \quad (1)$$

Note that for a particular frequency the three above functions are just complex numbers. If one is not interested in the phase angles, he can write:

$$|G(i\omega)| = \frac{|Q_o(i\omega)|}{|Q_i(i\omega)|} \quad (2)$$

which relates the absolute values (amplitudes) of the functions. Note that the plot of $|G(i\omega)|$ versus the frequency ω is the frequency response curve of the dynamic system.

The logic behind the method is simply to excite the anemometer with a signal of known frequency spectrum, to measure its output spectrum and to obtain the frequency response curve by means of equation (2).

The fluctuating velocity signal was obtained using a small, radial, high speed fan taken out of a vacuum cleaner. It produced average velocities up to 25 m/s and fluctuations up to 5 m/s RMS. Different combinations of the average velocity and the RMS value were available

at different locations in the flow. The location we used is sketched in Figure 1. The average velocity at that point was 15 m/s and the fluctuations were 2 m/s RMS. The frequency spectrum produced by the fan is shown in Figure 2. It was measured by a DISA 55 D05/102C constant temperature anemometer with a TS1-1210-T1.5 hot-wire probe. The response of this system was found to be flat up to 3.5 kHz using an indirect, electric method to be described in section 3.1. The portion of the spectrum curve for frequencies above 3.5 kHz was corrected according to the frequency response curve of the anemometer, and smoothed to obtain Figure 2. Same frequency spectrum curve was obtained later using a TS1 1050 constant temperature anemometer with the same hot-wire probe. Note that the spectrum had significant content up to 10 kHz.

The fan was found to be a stable source of signal. The average velocity, the RMS value and the frequency spectrum curve did not change with time.

The measurement of the spectra was performed by a Nicolet UA-500 Ubiquitous Real Time Spectrum Analyzer Calculator. This very fast and accurate analyzer is linear to within $\pm 1/4$ db and is capable of spectrum averaging. The spectrum curve is displayed on a display scope and can be plotted using a X-Y plotter. Accurate measurement of amplitudes is achieved by a digital meter

with 0.1 db resolution. Two curves can be displayed on the display scope at once, since the instrument has a digital memory. Both linear and logarithmic coordinates are available.

The first step of the frequency response measurement procedure was to obtain the input spectrum and to store the curve in the memory of the spectrum analyzer, as described above.

The second step was to measure the output spectrum of the anemometer being tested. It was done by locating the probe at the same location in the flow where the reference probe was before. The accurate location was found using the output of the tested system which should read the average of 15 m/s. The output spectrum was then analyzed and displayed on the screen together with the input spectrum. The calculation of the frequency response was simplified using decibel coordinates for the amplitudes. Equation (2) expressed in decibels becomes:

$$\text{db} = 20 \log_{10}|G(i\omega)| = 20 \log_{10}|Q_o(i\omega)| - 20 \log_{10}|Q_i(i\omega)| \quad (3)$$

and the frequency response of the anemometer, in db, is simply the difference between the output and the input spectra, in db. Before the subtraction was performed, the two spectrum curves were shifted vertically so that their low-frequency regions coincided. (Note that every anemometer has flat response up to some frequency. If the curves appear vertically shifted, it is because the static gains of the two sensors are different.)

Figure 3 shows the spectra for the DISA 55 D05/1020

anemometer with a hot-wire sensor (sensor 2, see Table 1 for details). The upper curve is the input spectrum obtained with the T51 1210-T1.5 probe. The lower curve is the output spectrum of the tested system. Curve 2 in Figure 4 is the plot of the difference of the two curves. It is the directly determined frequency response for sensor 2.

Two hot-wire probes and two hot-film probes were tested using the above described method. The same anemometer and signal source were used for all the tests. Details on the sensors may be found in Table 1. The solid curves in Figure 4 are the directly determined frequency responses. The circles are data obtained by an electric, indirect test presented in section 3. The agreement between the two methods is considered very good.

Sensors 3 and 4 were two identical hot-films on a three dimensional probe. They were connected to two identically adjusted channels of the anemometer. However, the response of sensor 3 was about 2 db higher than that of sensor 4 for frequencies above 400 Hz. We then used the developed method to get equal responses from these two sensors. Figure 5 shows the output spectra of the two systems before the adjustments were made. Figure 6 shows the situation after the overheat of sensor 4

TABLE 1

Physical Constants for the test sensors.

Hot-Wires, all on TSI 1210 probe

<u>Parameter</u>	<u>Reference Sensor</u>	<u>Sensor 1</u>	<u>Sensor 2</u>
Material	Tungsten, Platinum coated	10% Platinum Rhodium	10% Platinum Rhodium
Diameter (mm)	0.0038	0.010	0.010
Length (mm)	1.25	1.37	1.77
Overheat	1.30	1.13	1.23

Hot-Films, all on TSI 1294 probe

<u>Material</u>	<u>Platinum Film on Quartz Substrate</u>
Diameter (mm)	0.152
Length (mm)	2.0
Overheat	1.39

was increased from 1.39 to 1.44. Now the response of sensor 4 was higher than the response of sensor 3 by 1 to 2 db. Next the overheat ratio was reduced to 1.42, and Figure 7 shows that the difference between the two sensors was less than 0.5 db. The whole procedure took less than 10 minutes.

3. Indirect Determination of Hot-Wire and Hot-Film Anemometer Frequency Response

An indirect method for determination of the hot-wire and hot-film anemometer frequency response utilizing the transfer functions of Weidman and Browand (1975) was evaluated and used extensively. This method was used for two purposes. First, it was used to determine the response of the reference anemometer by means of which the input spectrum was measured. Second purpose was to generate data for the four test sensors and to compare them with the results of the direct tests.

3.1 Hot-Wires

Weidman and Browand (1975) have shown that if the reactive elements are neglected, the frequency response of a constant temperature hot-wire anemometer was:

$$\frac{e}{u}(i\omega) = \frac{K_w}{\left(1 - \frac{\omega^2}{\omega_n^2}\right) + 2\zeta \frac{i\omega}{\omega_n}} \quad (4)$$

where u is the perturbation velocity input, e is the voltage output, and K_w , ω_n , ζ are system constants.

If a sinusoidal voltage e_t is applied across the wire, the frequency response becomes:

$$\frac{e}{e_t}(i\omega) = \frac{K_w^* (1+i\omega\tau)}{\left(1 - \frac{\omega^2}{\omega_n^2}\right) + 2\zeta \frac{i\omega}{\omega_n}} \quad (5)$$

where K_w^* is a system constant.

Note that equation (5) differs from (4) by a constant and a first order numerator term $(1+i\omega\tau)$ which is precisely defined by the time constant τ . Therefore, if one can determine the response described by equation (5) and determine τ , equation (4) can be obtained by simple division. If the frequency responses are in db and are normalized to their flat, low frequency portion, the constants K_w and K_w^* are not important.

The curve in Figure 8 is a db plot of equation (5) for the reference sensor. It was obtained by applying electrical white noise from a Hewlett-Packard HO1-3722 A Noise Generator across the wire and measuring the output spectrum. (The same results could be obtained using a sine wave generator and a scope). During the test the wire was exposed to a low turbulence flow of 15 m/s. The dashed line in Figure 8 has the slope of 20 db/decade, characteristic of a first order term. Note that the accuracy is very good. The effect of the second order denominator term on the slope of the curve is negligible, because $\omega_n \gg 1/\tau$ and the damping is nearly optimal ($\zeta \approx 0.7$).

The curve obtained by subtracting the db plot of a first order system which has the above described asymptote from the experimental curve of Figure 8 is the indirectly determined frequency response. It is shown as the dashed curve in Figure 4.

3.2 Hot-Films

Weidman and Broward (1975) have also shown that for hot-film sensors the following two equations apply:

$$\frac{e}{u}(i\omega) = \frac{K_f}{\left[1 + \beta x \operatorname{kel}(x)\right] (1+i\omega\mu) + A-i\omega B} \quad (6)$$

$$\frac{e}{et}(i\omega) = \frac{K_f^* [1 + \beta x \operatorname{kel}(x)]}{\left[1 + \beta x \operatorname{kel}(x)\right] (1+i\omega\mu) + A-i\omega B} \quad (7)$$

where

$$\operatorname{kel}(x) = \frac{\operatorname{ber}'_0(x) + i \operatorname{bei}'_0(x)}{\operatorname{ber}_0(x) + i \operatorname{bei}_0(x)} \quad x = a \left(\frac{\omega}{K_s} \right)^{1/2}$$

Here a is the film substrate radius, K_s is the thermal diffusivity of the substrate and K_f , K_f^* , β , μ , A , B are system constants. The Kelvin (Thomson) functions ber_0 and bei_0 and their first derivatives are extensively tabulated by Nosova (1961), and are also available in the Fortran Libraries of numerous computer centers.

The procedure for determining the frequency response for hot-films is similar to the one used for hot-wires. The only difference is that the numerator term here is $\left[1 + \beta x \operatorname{kel}(x)\right]$. A family of these curves for $a = 0.0762$ mm and $K_s = 0.84$ mm²/s is plotted in Figure 3. For better accuracy the indirect test was performed using a Weston-Boonshaft and Fuchs 711A Frequency Response Analyzer which measures both the amplitudes ratio and the phase

angle. As in the case of hot-wires, the accuracy was very good, and the $\beta=15$ curve from Figure 9, when subtracted from the experimental curves, leads to the data represented by circles on curves 3 and 4 in Figure 4. The value of β was determined by comparing the low frequency portions of the experimental curves with the low frequency portions of the curves from Figure 9. The $\beta=15$ curves matched the experimental curves very closely up to 80 Hz, for both amplitude ratios and phase angles.

4. Conclusions

The developed method was found to be a useful tool for determining the frequency response characteristics of anemometers. Once the experimental set up was ready, determination of an amplitude ratio curve for an anemometer was accomplished in few minutes.

Very good agreement between the direct tests of section 2 and the indirect tests of section 3 was observed, as shown in Figure 4. The solid curves (direct test) and the circles (indirect test) almost coincide. Thus the method developed gives strong substantiation for the validity for the analytical method of Weidman and Browand.

The direct method can be extended to higher frequencies, if an appropriate source of signal is used. Our source had significant frequency content up to 10kHz. (We were not interested in frequencies beyond 2KHz).

Although we used a rather expensive spectrum analyzer, a much simpler instrument can be used for the direct test. A general purpose analog spectrum analyzer used in the fields of sound or vibrations would be adequate, however, the procedure would be more time consuming (but still faster compared to other methods).

A particularly important application of the method presented here is for the measurement of the frequency

response of hot-film anemometers with sensors of complex shape. Even if the heat transfer model for the sensor is not known, one still can determine the frequency response curve, and use the sensor for measurements of fluctuating velocities. The experimentally determined response curve can also help in determining the heat transfer model for the sensor.

We also found that the indirect method described in section 3 was simple, accurate and required only a sine wave generator and a oscilloscope. When the technique of subtracting db curves is used, no knowledge of the system parameters is required (except a and K_g for the hot-film case). More time and effort, however, are required when compared to the direct method.

References

Doebelin, E. O., 1975, Measurement Systems (New York: McGraw Hill) 150-1

Grant, H. P., 1968, Advances in Hot-Wire Anemometry eds W. L. Melnik and J. R. Weske, (College Park, Maryland: University of Maryland) 251-7

Kidron, I., 1966, IEEE Trans. Instrum. Meas., IM-15 76-81

Nosova, L. N., 1961, Tables of Thomson Functions and Their First Derivatives (New York: Pergamon Press)

Perry, A. E. and Morrison, G. L., 1971, J. Fluid Mech. 47 765-77

Weidman, P. D. and Browand, F. K., 1975, J. Phys. E: Sci. Instrum. 8 553-60

Freythuth, P., 1967, The Review of Sci - Instrum, 38 5 677-81

Freythuth, P., 1977, J. Phys. E: Sci. Instrum., 10 705-10

Freythuth, P. and Fingerson, L. M., 1977, TSI Quarterly No./Dec.

APPENDIX

A. A Different Look at the Direct Method.

We have used the system dynamics approach throughout the paper. For those unfamiliar with this approach, the following may be useful in understanding the direct method.

Let the anemometer tested be represented by $G(i\omega)$, the Fourier transform of its impulse response (its transfer function) and the reference anemometer be similarly represented by $R(i\omega)$. Let the input signal to both anemometers be $Q_i(i\omega)$, the output of G be $Q_G(i\omega)$ and the output of R be $Q_R(i\omega)$.

Since G , R , Q_i , Q_G , and Q_R are Fourier transforms, one can write:

$$Q_G(i\omega) = G(i\omega) Q_i(i\omega)$$

and

$$Q_R(i\omega) = R(i\omega) Q_i(i\omega)$$

from which follows =

$$Q(i\omega) = \frac{Q_G(i\omega)}{Q_R(i\omega)} R(i\omega)$$

If $R(i\omega)$ is flat up to the highest frequency used, $R(i\omega) = R_1$ = constant and

$$Q(i\omega) = R_1 \frac{Q_G(i\omega)}{Q_R(i\omega)} = R_1 \frac{\text{SYSTEM'S OUTPUT SPECTRUM}}{\text{REFERENCE OUTPUT SPECTRUM}}$$

The presence of the frequency independent constant R_1 explains why the spectrum curves appear shifted on the screen.

B. Order of the Anemometer Transfer Function

Since we were not interested in frequencies above 2KHz, a second order denominator term was adequate to model the anemometer. (See equations 4,5,6,7) For higher frequencies a third order model is necessary, as explained by Freymuth (1977). However, neither the direct method nor the indirect method would change if the third order model was assumed, since they both are independent of the denominator of the transfer function. (The direct method is actually totally independent of the model.)

Legends for Illustrations

- Figure 1 Relative position of the radial fan and the hot-wire probe.
- Figure 2 The frequency spectrum produced by the radial fan. (Smoothed Curve)
- Figure 3 Frequency spectra for sensor 2. The upper curve is the input spectrum and the lower the output spectrum of sensor 2.
- Figure 4 The results of the direct and the indirect tests of frequency response. The dashed curve is the indirectly determined response of the reference sensor. Solid curves 1-4 are the results of the direct tests for sensors 1-4. The circles are the results of the indirect tests for sensors 1-4.
- Figure 5 Output spectra of sensor 3 (overheat 1.39) and sensor 4 (overheat 1.39).
- Figure 6 Output spectra of sensor 3 (overheat 1.39) and sensor 4 (overheat 1.44).
- Figure 7 Output spectra of sensor 3 (overheat 1.39) and sensor 4 (overheat 1.42).
- Figure 8 Response of the anemometer with the reference sensor to electrical input (solid line); 20 db/decade asymptote (dashed line).
- Figure 9 Plot of $[1 + \beta x \text{kel}(x)]$ for $a = 0.0762 \text{ mm}$ and $K_g = 0.84 \text{ mm}^2/\text{s}$.

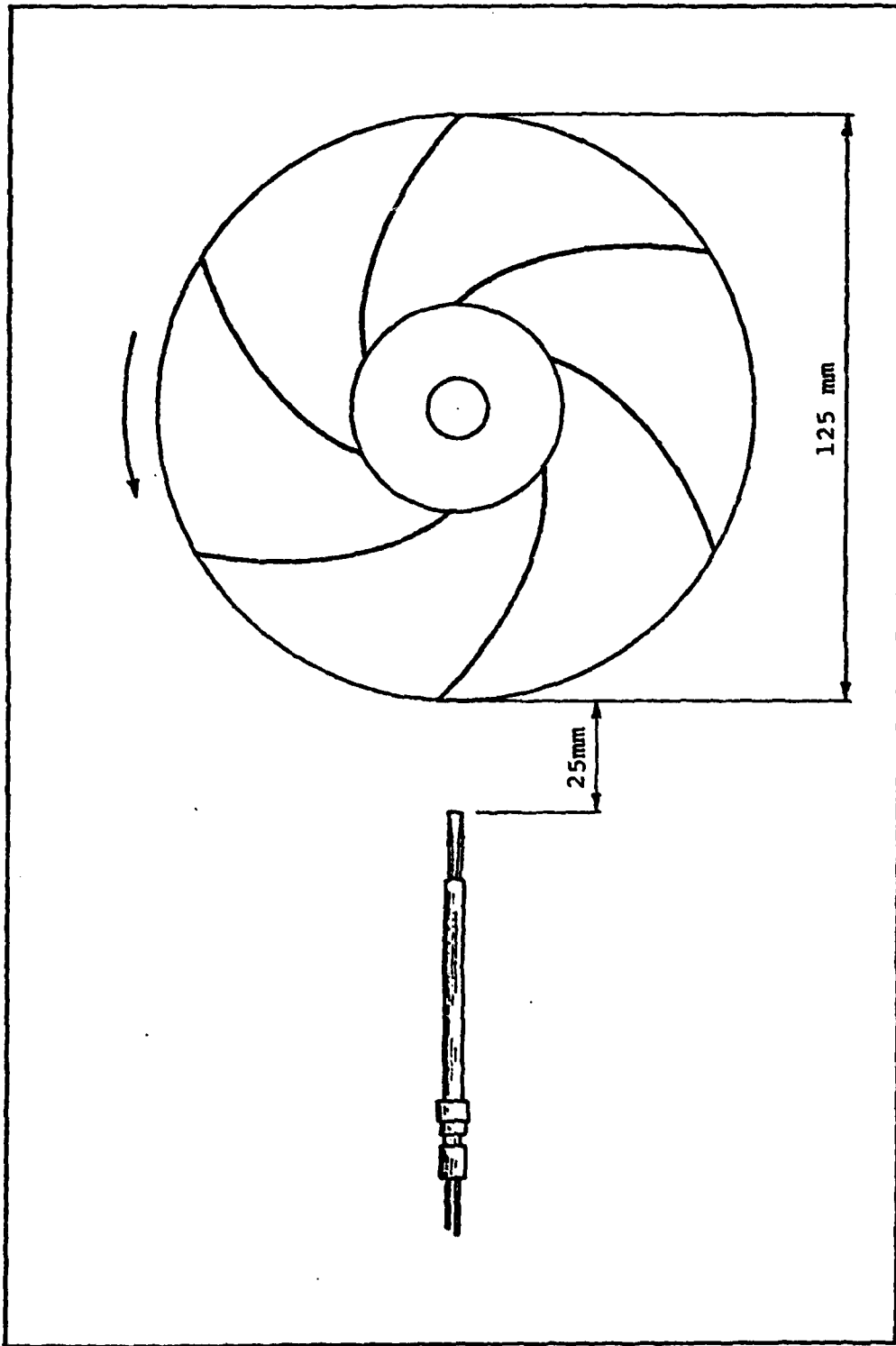


Figure 1: Relative position of the radial fan and the hot-wire probe.

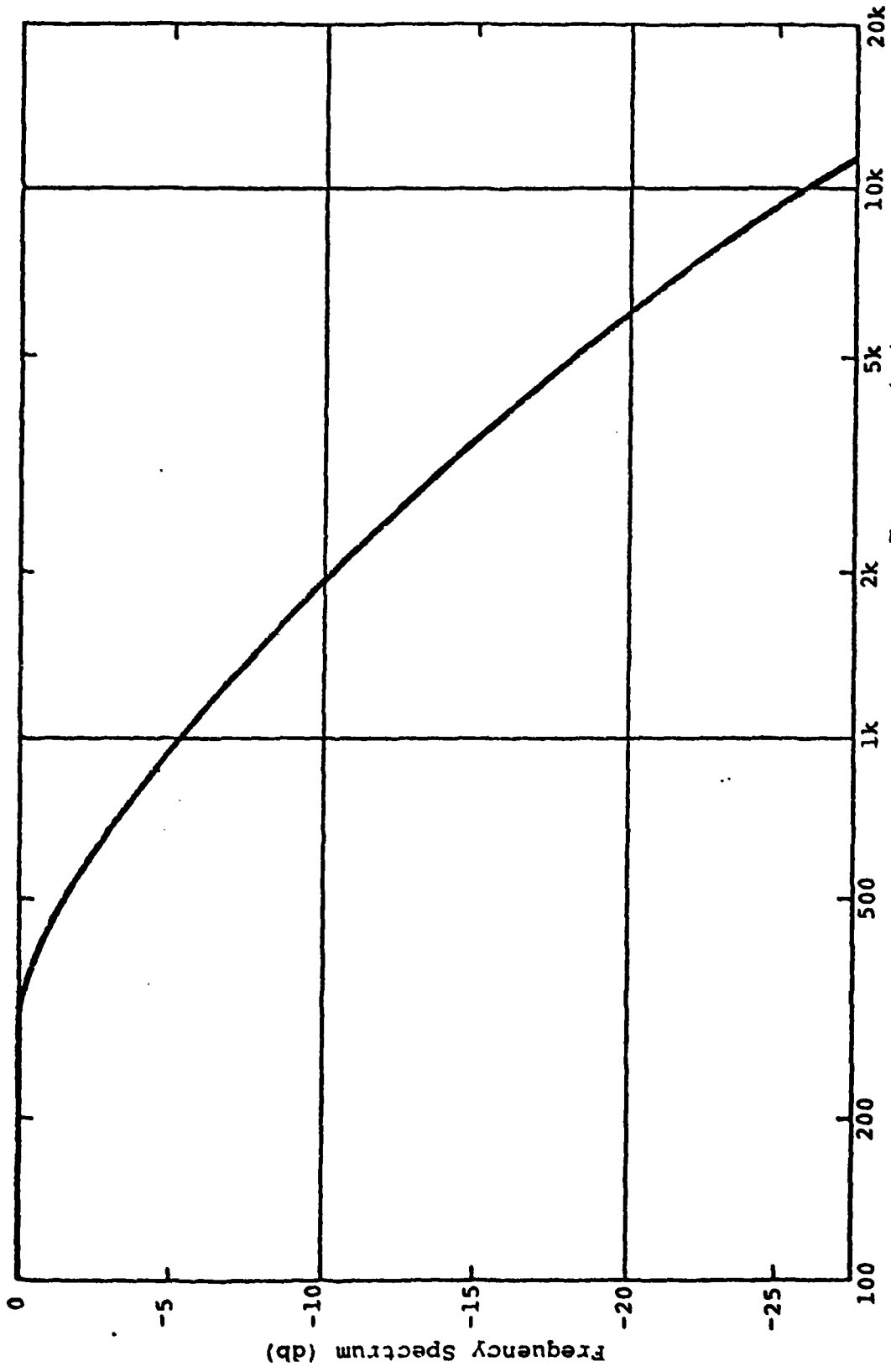


Figure 2: The frequency spectrum produced by the radial fan. (Smoothed Curve)

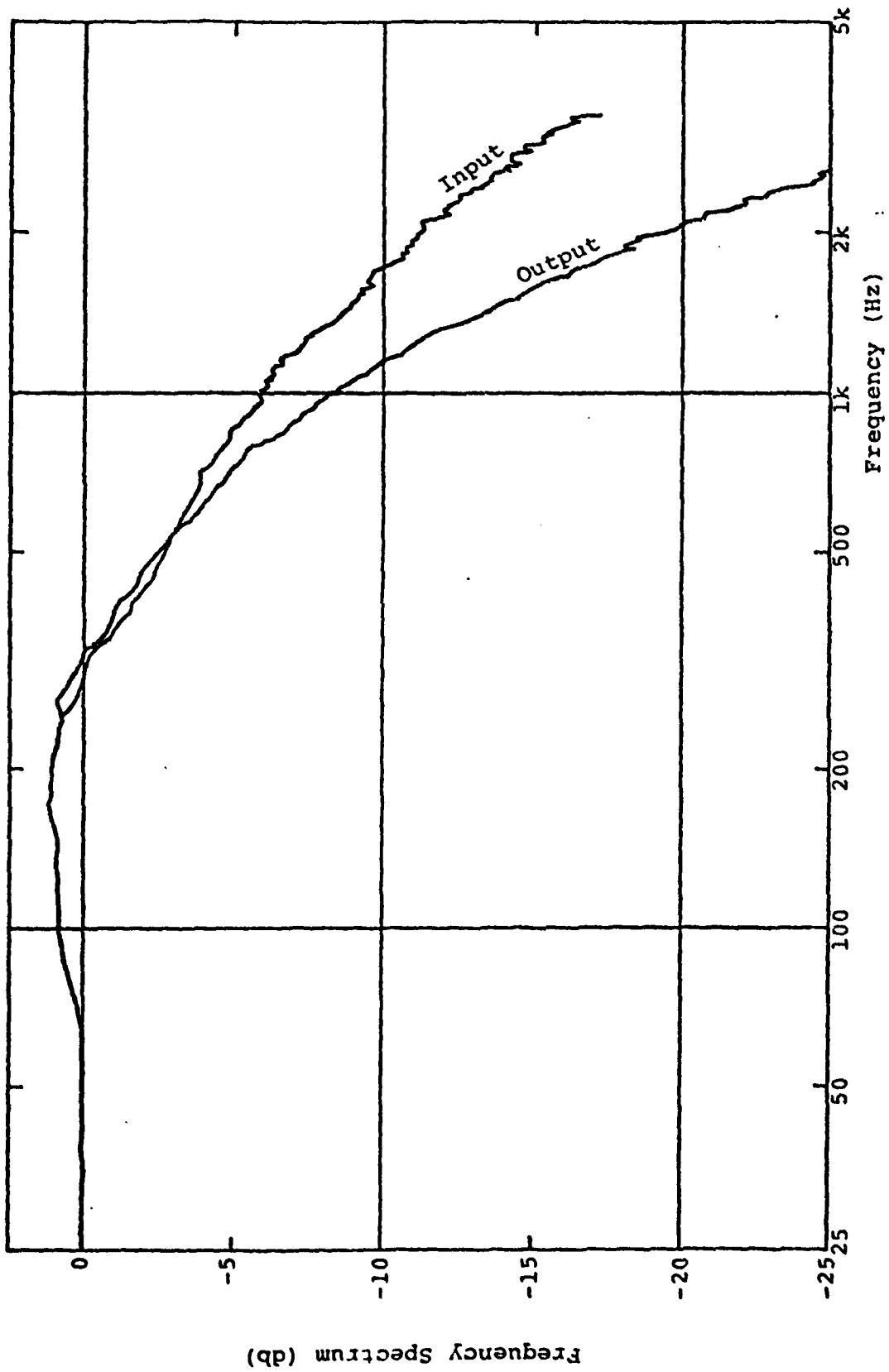


Figure 3: Frequency spectra for sensor 2. The upper curve is the input spectrum and the lower the output spectrum of sensor 2.

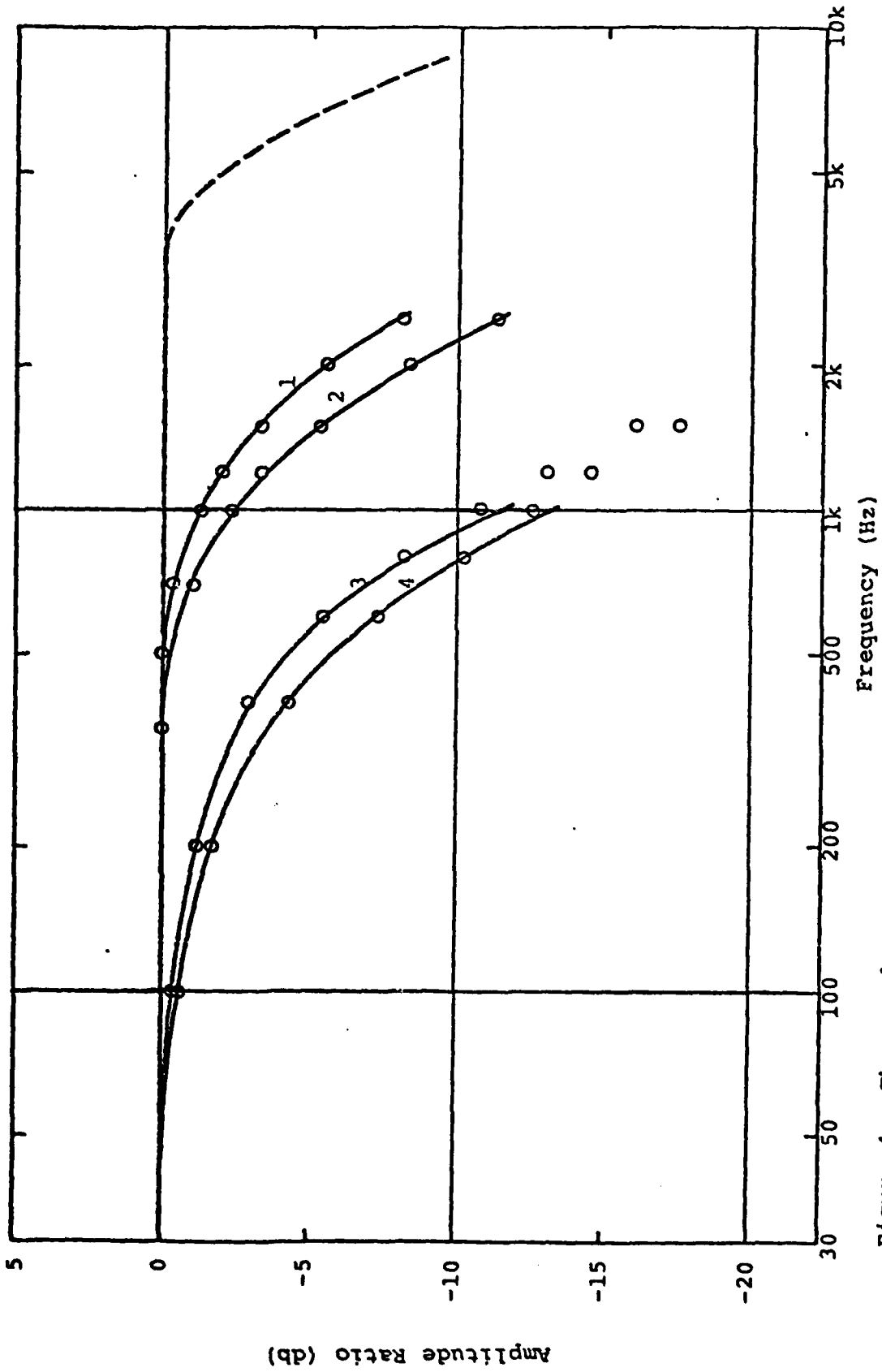


Figure 4: The results of the direct and the indirect tests of frequency response. The dashed curve is the indirectly determined response of the reference sensor. Solid curves 1-4 are the results of the direct tests for sensors 1-4. The circles are the results of the indirect tests for sensors 1-4.

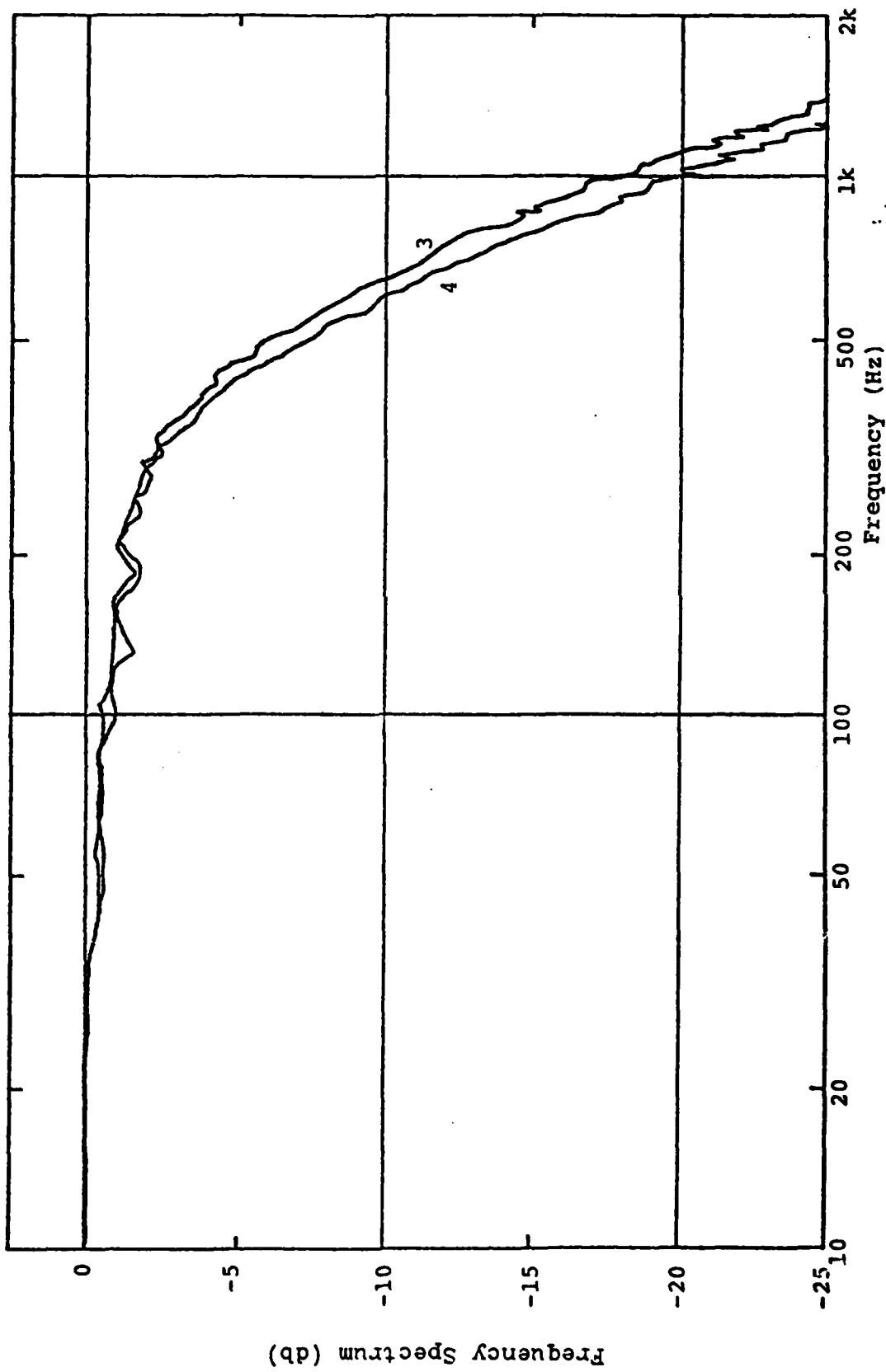


Figure 5: Output spectra of sensor 3 (overheat 1.39) and sensor 4 (overheat 1.39).

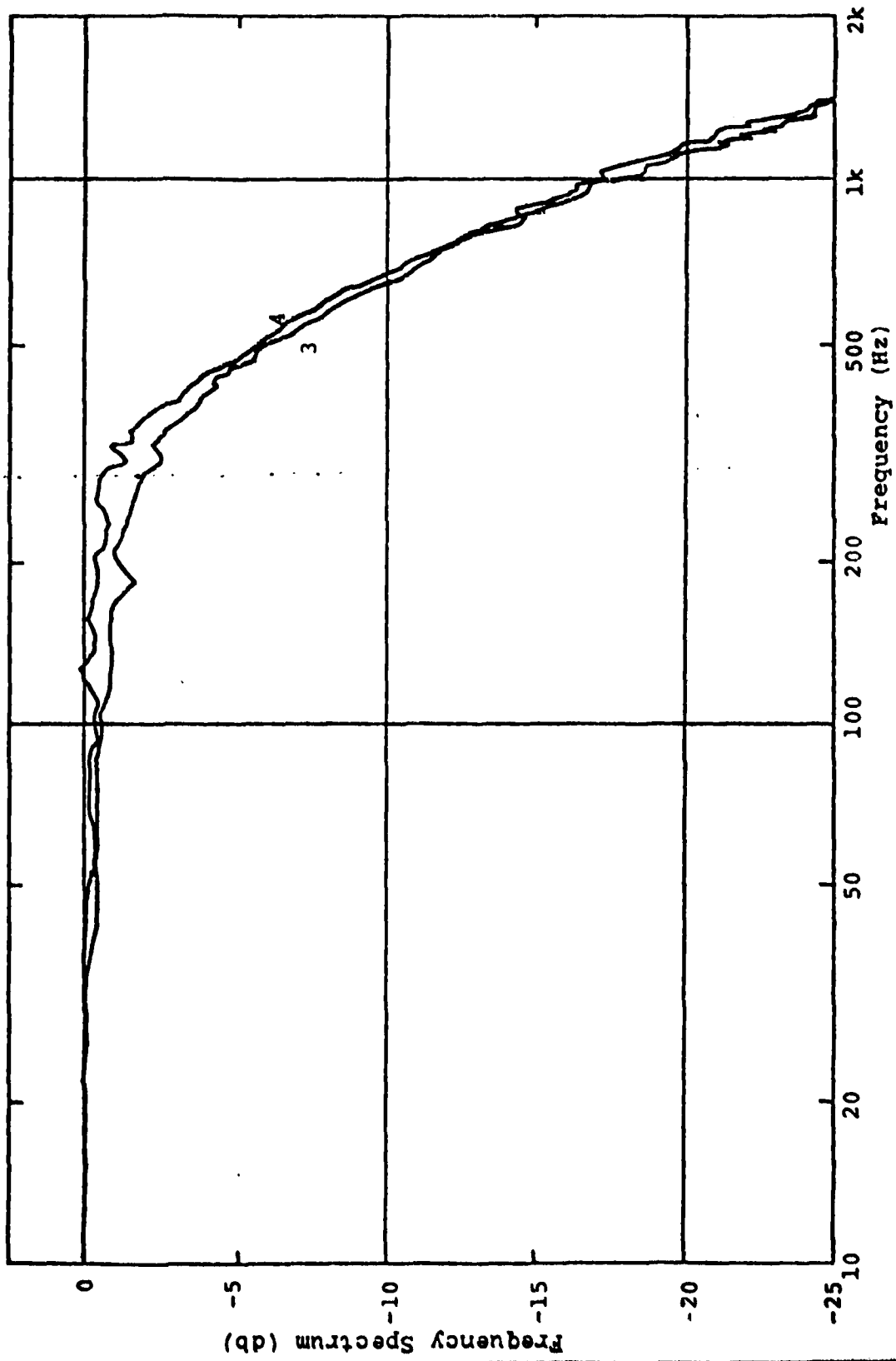


Figure 6: Output spectra of sensor 3 (overheat 1.39) and sensor 4 (overheat 1.44).

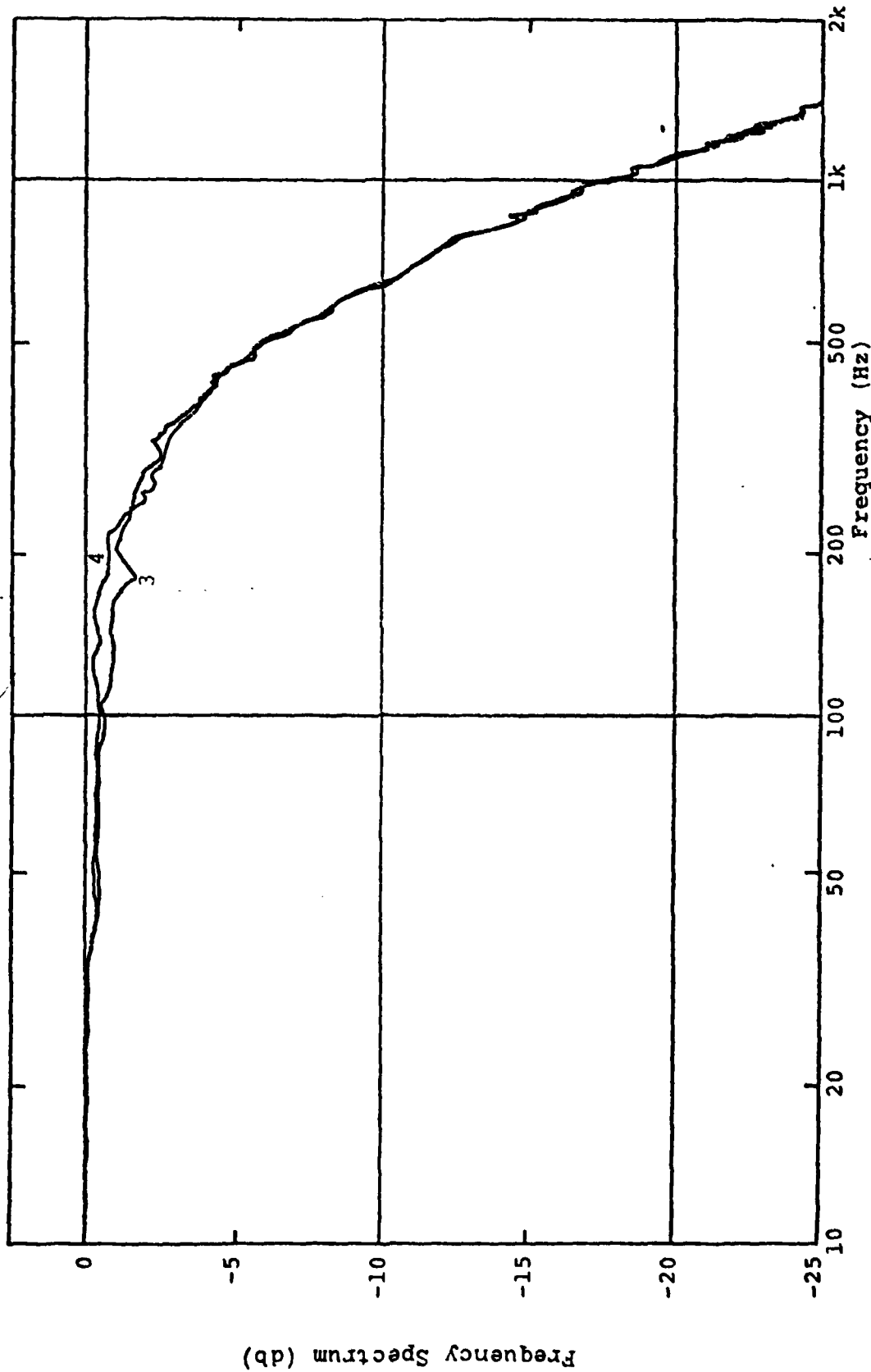


Figure 7: Output spectra for sensor 3 (overheat 1.39) and sensor 4 (overheat 1.42).

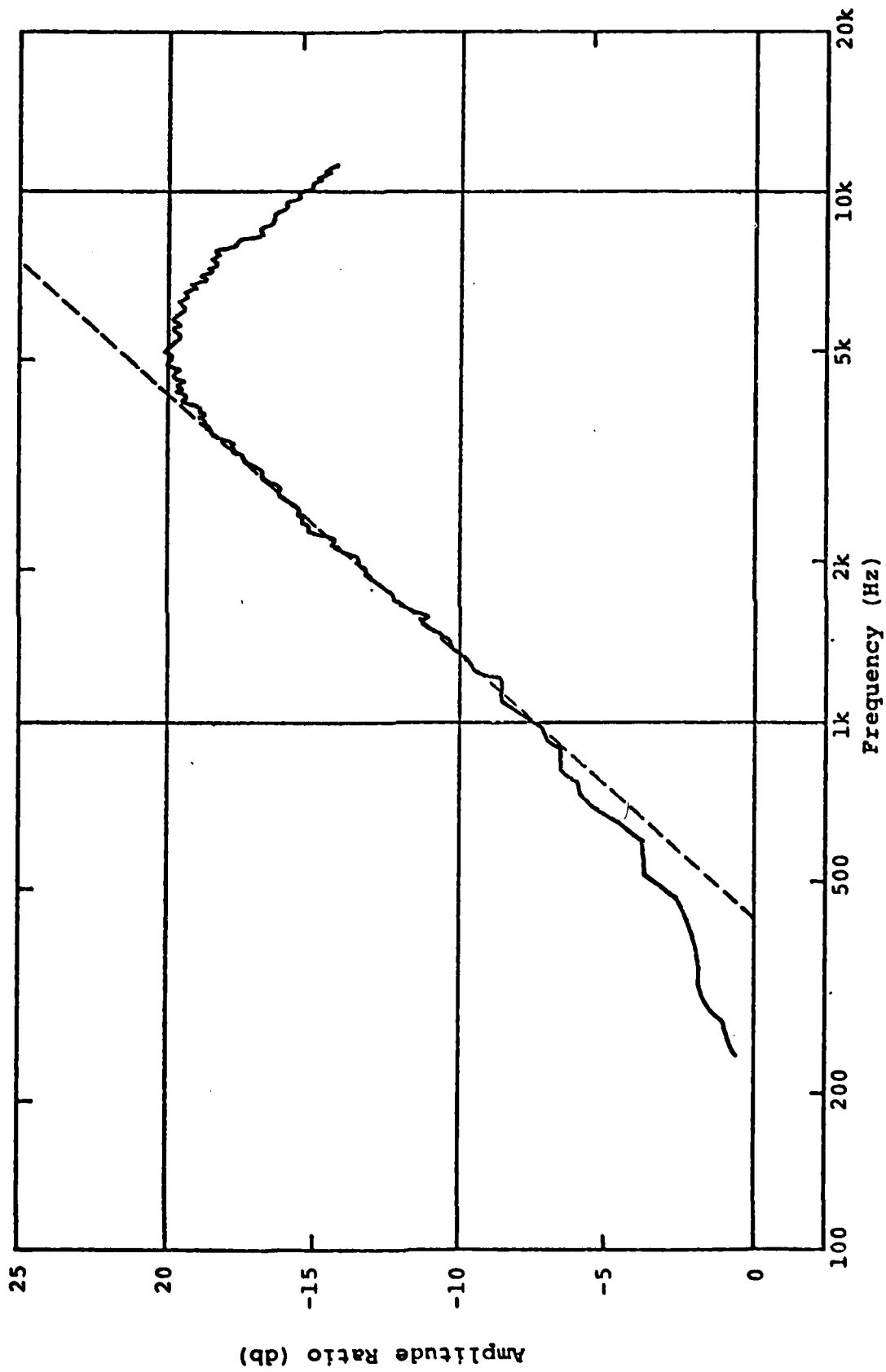


Figure 8: Response of the anemometer with the reference sensor to electrical input (solid line); 20 db/decade asymptote (dashed line).

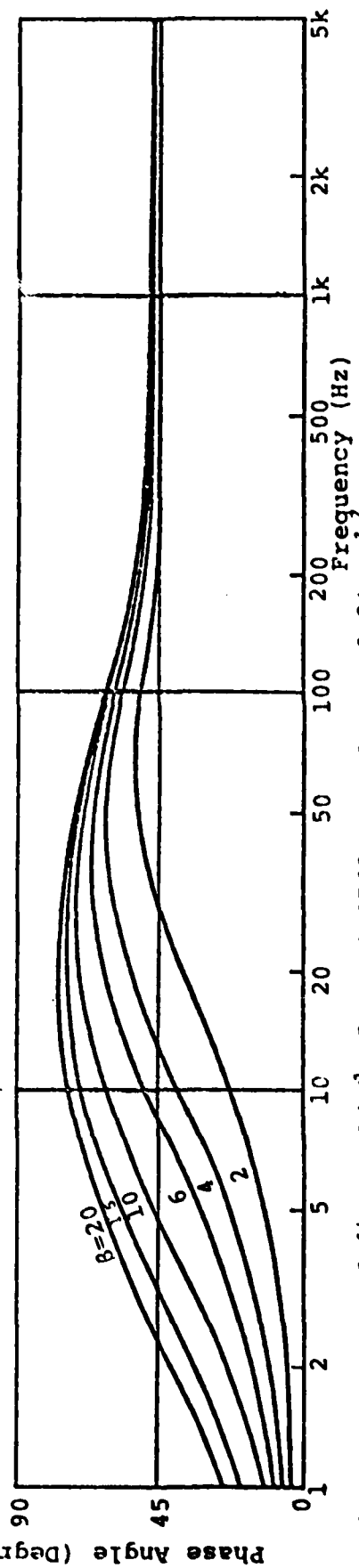
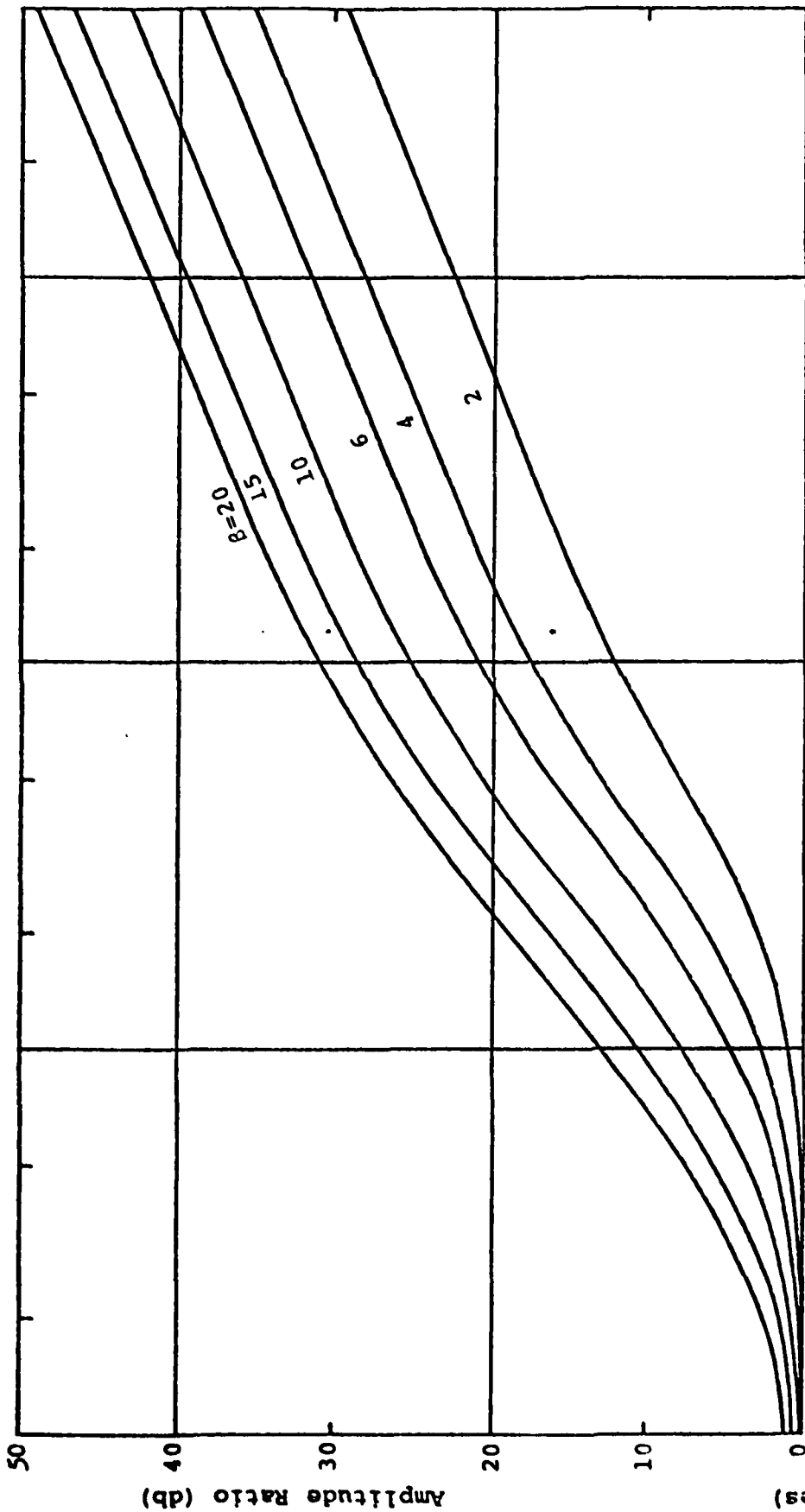


Figure 9: Plot of $|1 + Bxk|$ for $a = 0.0762$ mm and $K_s = 0.84$ mm²/s.

Appendix C



EFFECT OF CHANGING ROTOR PARAMETERS ON ROTOR
WAKE VELOCITIES AT VERY LOW ADVANCE RATIOS

by

Henry R. Velkoff, Professor
Hanan Terkel, Research Assistant
Fu Kuo Shaio, Research Assistant

The Department of Mechanical Engineering
The Ohio State University
Columbus, Ohio U.S.A.

FIFTH EUROPEAN ROTORCRAFT AND POWERED LIFT AIRCRAFT FORUM
SEPTEMBER 4 - 7TH 1979 - AMSTERDAM, THE NETHERLANDS

LIST OF SYMBOLS

b	Number of blades, dimensionless
c	Blade chord, inch
i	Shaft angle, degrees
I_B	Flapping Moment of Inertia, slugs - feet ²
k^2	Constant to express the deviation from Cosine-Law of cylindrical anemometer sensors, dimensionless
V_{eff}	Effective cooling velocity of a sensor, feet/second
V	Magnitude of velocity vector, feet/second
X	Wind tunnel coordinate direction
Y	Wind tunnel coordinate direction
Z	Wind tunnel coordinate direction
μ	Advance ratio, dimensionless
θ	Collective angle, degree
δ	Angle between direction of V and cylindrical sensor

ABSTRACT

Tests were conducted on a two bladed teetering model helicopter rotor and on a two bladed rotor with twisted blades at very low advance ratios. Data on the time-average structure of the rotor wake were taken using a three wire hot-film probe. The findings present data which may be useful in further understanding the nature of the wake at low speed flight of helicopters and may prove useful in the development of models for the rotor wake.

EFFECT OF CHANGING ROTOR PARAMETERS ON ROTOR WAKE VELOCITIES AT VERY LOW ADVANCE RATIOS

H. R. Velkoff, H. Terkel, F. Shaio
The Ohio State University
Columbus, Ohio U.S.A.

1. INTRODUCTION

The need for data on helicopter rotor wakes at low advance ratios has increased because the recent emphasis on low speed nap-of-the-earth flight. To provide data for this region of flight, tests using a model rotor in a wind tunnel have been conducted. The initial data obtained utilized a two bladed model rotor at advance ratios of 0.04 through 0.10 and were reported in a recent paper (1). In those initial tests data were provided at only one value pitch angle, $\theta = 8^\circ$, and shaft tilt, $i = 8^\circ$. The results of those initial tests revealed that the overall rotor flow tended to roll-up into two discrete vortices similar to a low aspect ratio wing. A particularly unique flow characteristic was also observed at the advance ratios of $\mu = 0.08$ and below. This characteristic was the pronounced tendency for the flow to not only form the two vortices, but to also present concentrated regions of enhanced magnitude of the axial component of velocity in the vortex. Such localized regions of high dynamic pressure associated with the vortices could possibly affect the design of empennage for helicopters.

Since data in the low advance ratio region are limited, primarily that of reference 1, Heyson and Katsoff (2), and Bowden and Shockey (3), further tests were planned and undertaken to secure a wider range of data. The data presented here includes tests of a two bladed rotor at a given pitch angle and three tilt angles. A twisted blade rotor was also tested to evaluate the effect of blade twist on rotor wake velocity.

2. EXPERIMENTAL ARRANGEMENT

The tests were conducted in a wind tunnel with a 8 foot by 4 foot test section. The flow turbulence is reduced by means of a 2 to 1 contraction ratio, nested 1/8 inch diameter straws, and three layers of screening. The tunnel with the turbulence reduction system in place provides air velocities up to 75 feet per second. Further details on the wind tunnel can be found in reference 4.

3. ROTOR CHARACTERISTICS

The rotors which were tested are indicated below.

Two Bladed Rotor

Teetering Rotor

Rotor radius	1.25, feet
Blade chord	2.125, inch
Rotor solidity	$bc/\pi R = 0.0902$
Root cutout	$\%R = 11.7$
Blade taper ratio	$= 1$
Coning angle	$= 0^\circ$
Blade aspect ratio	$\frac{r}{c} = 7.06$
Blade twist	$= 0^\circ$
Airfoil section NACA	0012
I_B	$= 0.005583 \text{ slug-feet}^2$

Two Bladed Rotor With Twisted Blades

Teetering Rotor

Rotor radius	1.25, feet
Blade chord	2.1875, inch
Rotor solidity	$bc/\pi R = 0.0928$
Root cutout	$\%R = 12.08$
Blade taper ratio	$= 1$
Coning angle	$= 0^\circ$
Blade twist	$= 8^\circ$ (From 12.08%R to 100%R)
Airfoil section NACA	0012
I_B	$= 0.004260 \text{ slug-feet}^2$

The rotors are driven by a variable speed electric motor. The collective pitch and the shaft angle are adjustable. The rotors are not trimmed but are allowed to flap freely. There is no rotor moment developed in either of the rotors tested. Figure 1 illustrates the general location of the rotor in the cross section of the wind tunnel.

4. FLOW MEASUREMENT

The velocity data obtained are time average data taken with a three-dimensional hot-film probe connected to three DISA 55D05/102C constant temperature anemometer circuits. Details of the hot wire circuitry used and the method of data reduction may be found in reference 1. In summary each hot film probe is calibrated for

the effects of changes in direction. Of specific importance to obtaining data at low tunnel speeds associated with low advance ratios is the fact that the hot-films must operate at very low probe Reynolds numbers. At such conditions the value of k^2 in the directional correction equation

$$V_{eff}^2/V^2 = \sin^2\delta + k^2 \cos^2\delta$$

can vary significantly. Variation in k^2 can lead to errors in the computed spatial angles of the velocity vectors. In these tests calibration of the effect of low Reynolds number on k^2 was accomplished. A typical result for a TSI 1294-60-18 0.006" diameter hot-film probe is shown in Figure 2.

5. TRAVERSE MECHANISM

The hot-film probe was positioned at discreet points throughout the region of the rotor wake, both below and above the rotor. The region traversed was from 0.4 radius above the rotor to 0.8 radius below the rotor, laterally out to 1.2 radius, and 28 inches forward of the rotor centerline and 40 inches aft of the rotor center. The data points were located at 3 inches along rotor axis, 4 inches laterally and 4 inches along the tunnel centerline or tunnel flow direction. A total of 1584 measurement-locations result. However the number of points is reduced since data can not be taken in the vicinity of the rotor plane. Further details on the traversing system may be found in reference 1.

6. ERROR ANALYSIS

An extensive discussion of the errors in velocity and angle measurements and probe location is also presented in reference 1. In general the error in angular measurement is believed to be of the order of 2°, velocity in the order of ± 1 feet per second, tunnel speed of the order of 2%, rotor speed to within 2%, and probe position to within ± 0.25 inches.

7. TEST RESULTS

The test conditions for the two bladed teetering rotor were

Blade tip speed, feet/second	300
Advance ratio	0.06
Collective pitch angle, degrees	8
Rotor shaft tilt, degrees	2,4,8
Coning angle, degrees	0

An additional test was run for a two bladed teetering rotor with twisted blades. The test conditions for this rotor were

Blade tip speed, feet/second	300
Advance ratio	0.06
Collective pitch angle at 75%R, degrees	8
Twist angle, (From 12.08%R to 100%R) degrees	8
Rotor shaft tilt, degrees	8
Coning angle, degrees	0

The data are presented in terms of computer generated vector plots. Components of the total velocity, V , are shown in X-Y, Y-Z, and Z-X planes. The locations of these planes (X-Y, Y-Z, etc.) is depicted in Figure 3. It should be remembered that the data presented are average velocity data, averaged at each point over many revolutions of the rotor, and that the rotors are not trimmed, and do not generate rotor moment.

Data are presented for advance ratio of 0.06, pitch angle of 8 degrees, and shaft angles of 2, 4, 8 degrees. For the shaft angle of 8 degrees, an additional condition is presented with twisted blades. For the last case the twist is two degree for the blade's length and the pitch angle was measured at 75% of the radius.

Figure 4 presents the data for $i = 8^\circ$ for the transverse Y-Z plane. The expected rollup as the flow moves downstream can be observed from the data. Figure 5 for $i = 8^\circ$, depicts the various longitudinal X-Z planes showing the downwash influence of the rotor. Figure 6 for $i = 8^\circ$ and X-Y planes show the flow field when viewed from "above" the rotor and the lateral flow due to rollup can be seen.

For $i = 4^\circ$ Figure 7 presents the transverse Y-Z planes, Figure 8 presents the longitudinal X-Z planes and Figure 9 presents the X-Y planes.

For $i = 2^\circ$ Figure 10 presents the transverse Y-Z planes, Figure 11 presents the longitudinal X-Z planes and Figure 12 presents the X-Y planes.

Figure 13 presents the transverse Y-Z planes for $i = 8^\circ$ and twisted blades. Figure 14 presents the longitudinal X-Z planes and Figure 15 presents the X-Y planes.

8. DISCUSSION OF TEST RESULTS

Examination of the data for $\mu = 0.06$ was shown in the Y-Z planes in Figures 4, 7, 10, 13 reveals a vortex rollup similar to what would be expected behind a low aspect ratio wing. In this particular case the intensity of the vortex developing aft of the advancing side (on the right hand side of the figure) seems to be

greater than the vortex developed aft of the retreating side. Figures 4, 7, 10 which depict shaft angles of 8, 4, 2 respectively. do not show a distinct change in the flow pattern, and one would have to use a more thorough statistical analysis to interpret the influence of shaft angle on the rotor's wake. Figure 13 reveals that the vortex intensity is much greater for the twisted blades but the general shape of two vortices rolling up remains the same.

The flow pattern when viewed from the side of the rotor (X-Z planes) Figures 5, 8, 11, 14 shows an anticipated up flow in the plane outside the rotor tip on the advancing side ($Y/R = 1.33$). Just inside the rotor tip at $Y/R = -0.8$ a strong downwash pattern develops. Closer to the hub at $Y/R = -0.267$ the downwash pattern is still evident. At $Y/R = 0.0$ the downwash pattern is still apparent but reduced in intensity. At the retreating side at $Y/R = 0.53$ a highly concentrated region of downwash is again evident. The flow beyond the tip at $Y/R = 1.33$ is upwards similar to the plane at $Y/R = -1.33$. As with the Y-Z planes, changes in shaft angle do not reveal a significant alteration in the flow pattern (Figures 5, 8, 11). However, the twisted blade creates a larger longitudinal component (X direction) as well as a stronger downwash (Z direction).

The "squirt effect" discussed in reference (1) is revealed in these experiments again. The X-Z planes for the twisted blades at $Y/R = -0.267$ and $Y/R = -0.533$ are actually revealing a funnel like behaviour. The flow coming out of the rotor between $X/R = -0.8$ and $X/R = -1.07$ is squirted aft is concentrated streams.

The view from above the rotor, Figures 6, 9, 12, 15 reveals the anticipated inflows above the trailing vortex structure, $Z/R = 0.2$. At $Z/R = 0.0$ and below the rotor one can see the outflow in the region of the trailing vortex. For these planes, again the change in shaft angle does not show a significant effect on the flow pattern, but the rotor with the twisted blades creates a more distinct flow pattern by having bigger velocity components in the x and y directions.

9. ACKNOWLEDGEMENT

Specific mention must be made for the valuable help of several undergraduate students whose willingness to work long and unusual hours contributed to the success of the data acquisition. They are: R. Cooley, K. Yamarak, R. Cooke, R. Navarro, and T. Parker.

REFERENCES

1. H. R. Velkoff, and D. Horak, Rotor Wake Measurements At Very Low Advance Ratios, 35th Annual Forum of the American Helicopter Society, Paper Nr. 79-6, Washington, D.C., May 1979.
2. H. H. Heyson, and S. Katzoff, Induced Velocities Near A Lifting Rotor With Nonuniform Disc Loading, NASA Rep. 1319, 1957.
3. T. H. Bowden, and G. A. Shockey, A Wind Tunnel Investigation Of The Aerodynamic Environment Of A Full-Scale Helicopter Rotor In Forward Flight, Bell Helicopter Company, USAAVLABS Technical Report 70-35, U. S. Army Aviation Material Laboratories, Fort Eustis, Virginia, July 1970.
4. H. R. Velkoff, D. A. Blaser, and K. M. Jones, Boundary Layer Discontinuity On A Helicopter Rotor Blade In Hovering, AIAA Journal of Aircraft, Vol. 8, No. 2, 1971.

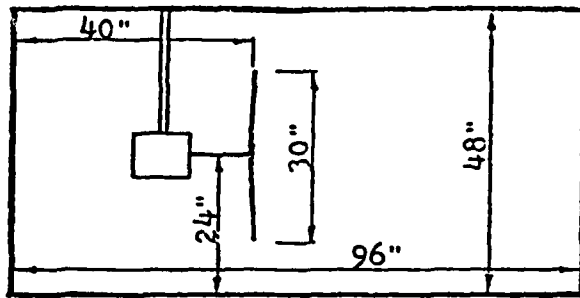


FIGURE 1. Location of the Rotor in the Test Section.

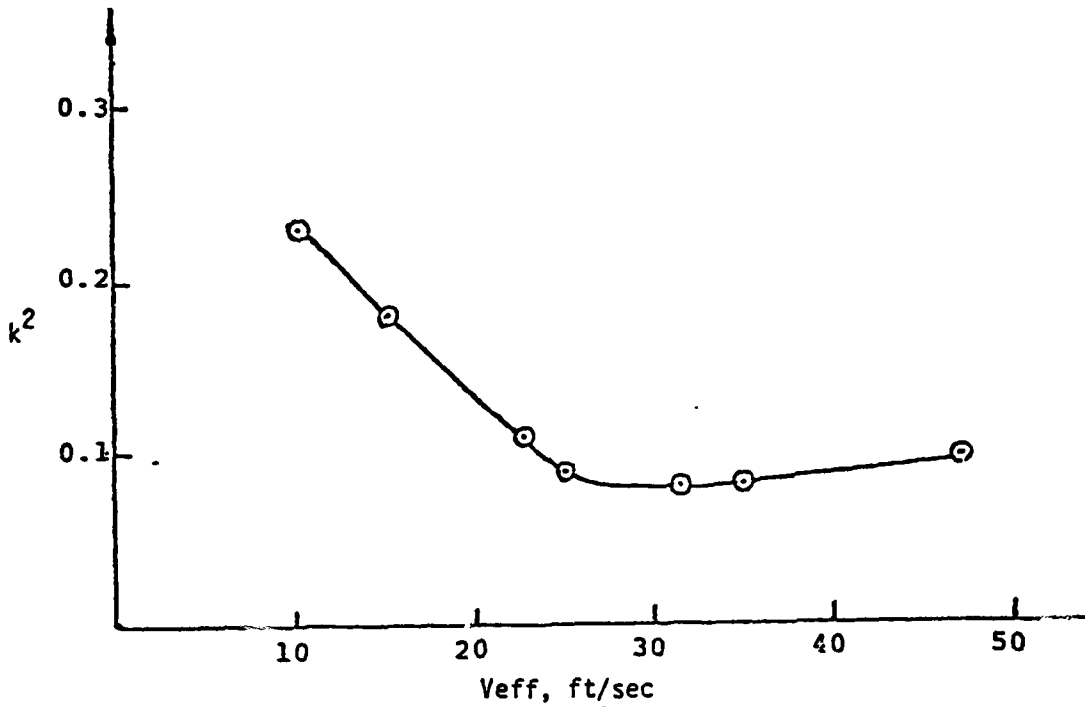


FIGURE 2. Changes of k^2 as a Function of V_{eff}

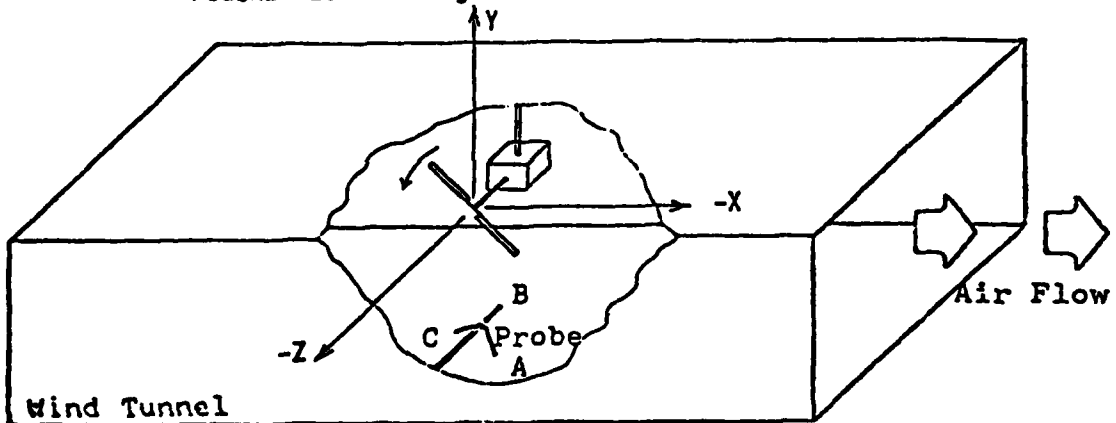


FIGURE 3. The Spatial Orientation of the Hot Film in the Wind Tunnel.

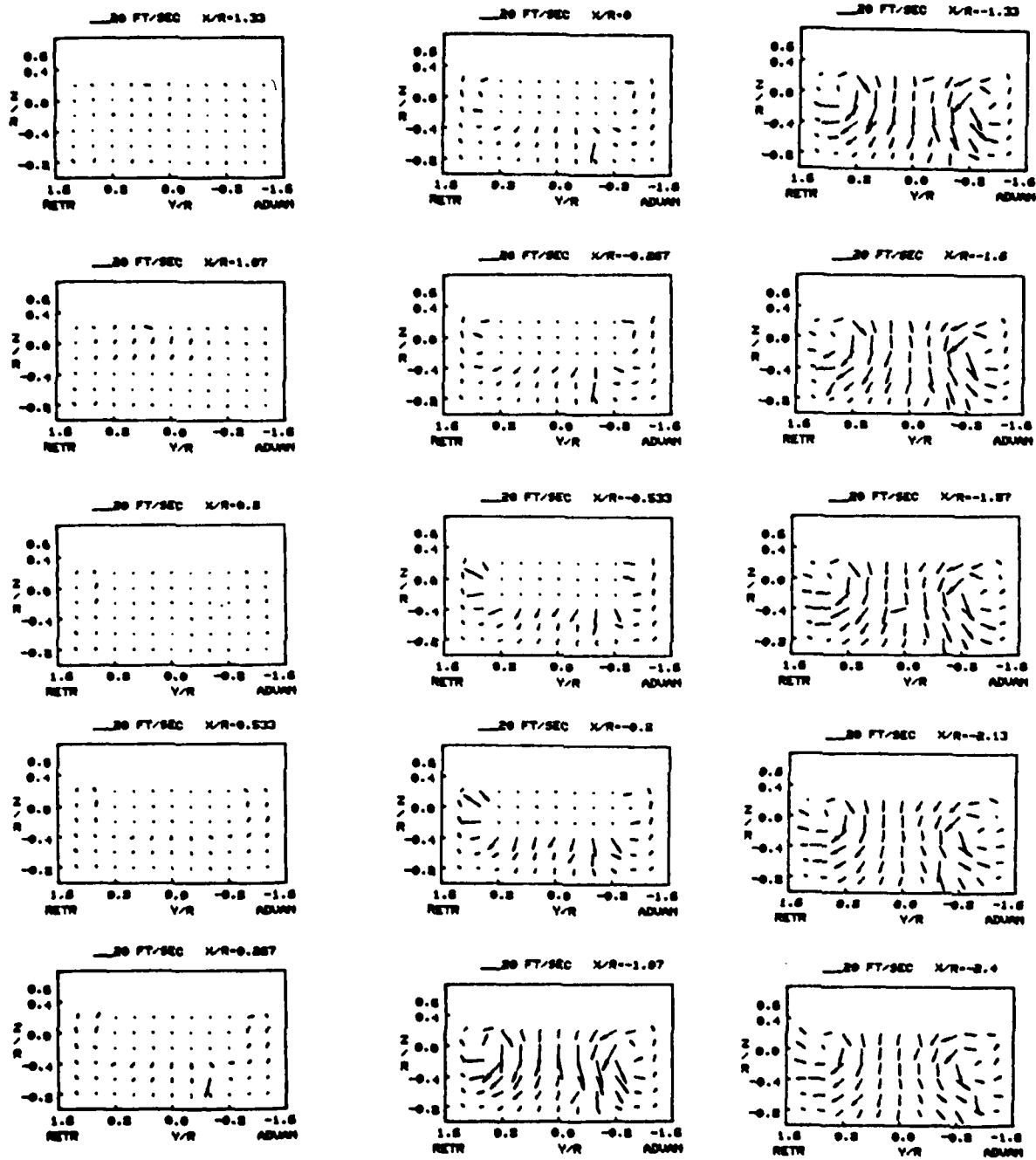


Figure 4.

Velocity vectors in Y-Z plane
 for $\mu=0.06$, $\theta=8^\circ$, and $i=8^\circ$.
 Note that coordinates depict
 probe position only.

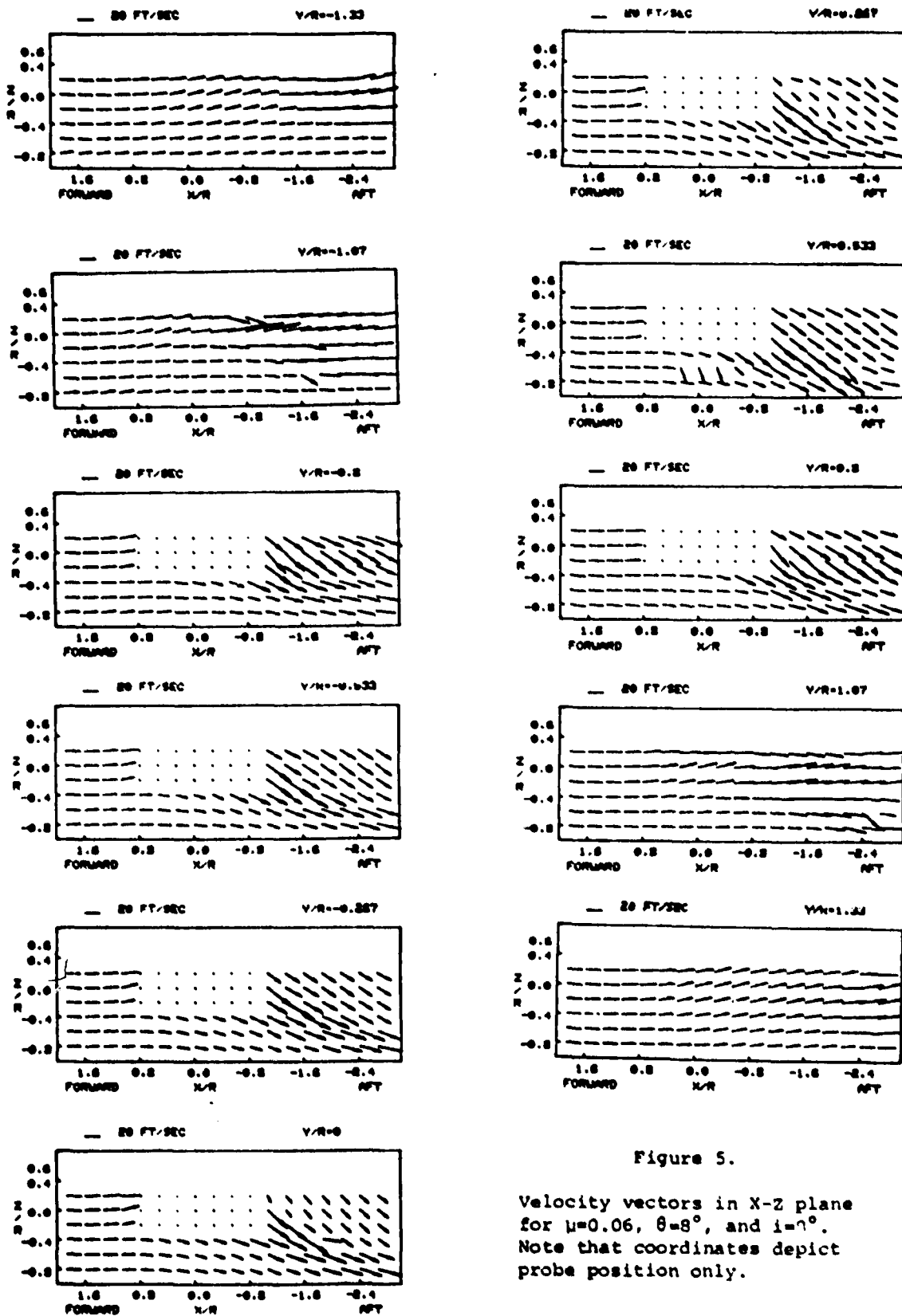


Figure 5.

Velocity vectors in X-Z plane for $\mu=0.06$, $\theta=8^\circ$, and $i=7^\circ$. Note that coordinates depict probe position only.

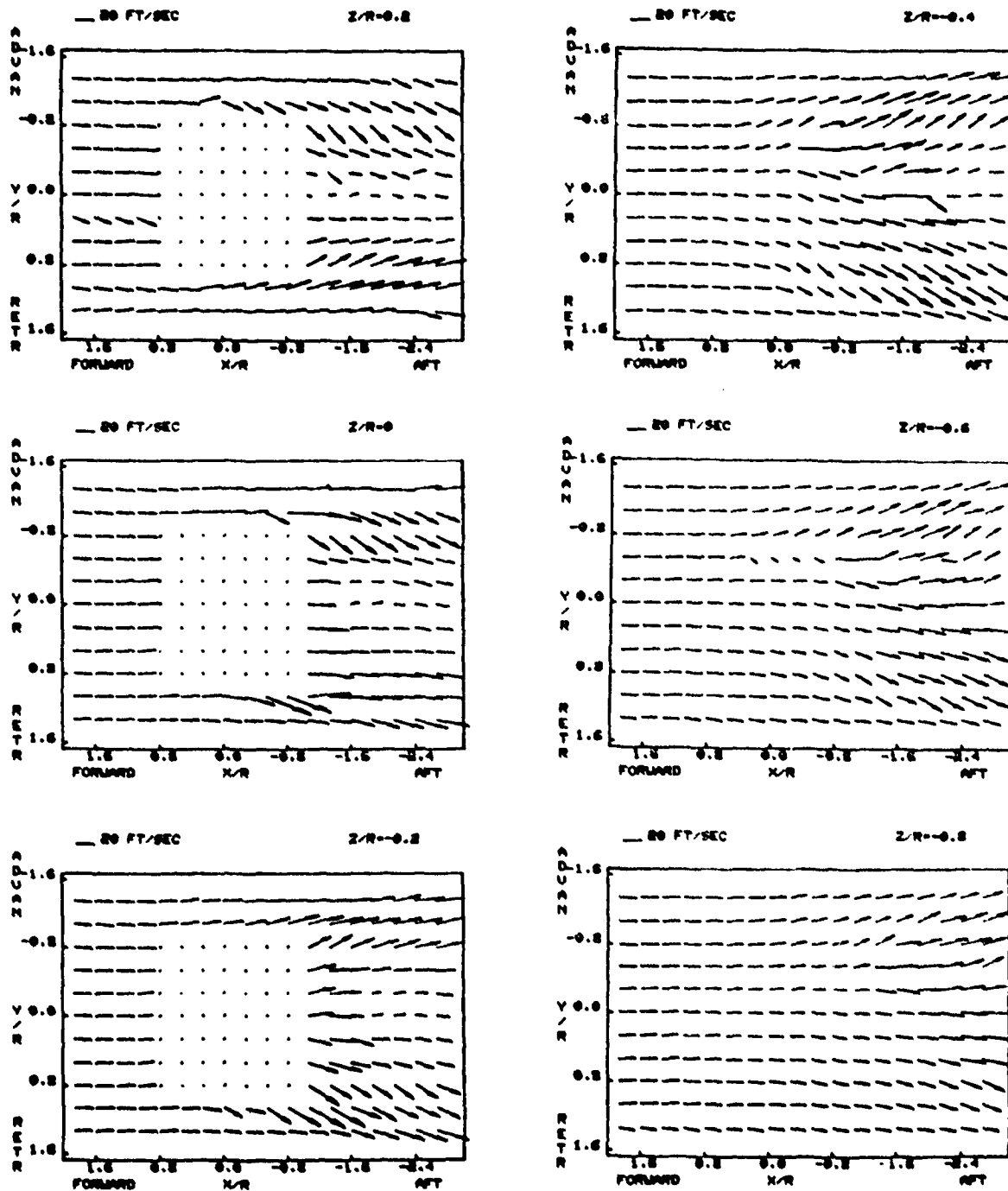


Figure 6.

Velocity vectors in X-Y plane
 for $\mu=0.06$, $\theta=8^\circ$, and $i=8^\circ$.
 Note that coordinates depict
 probe position only.

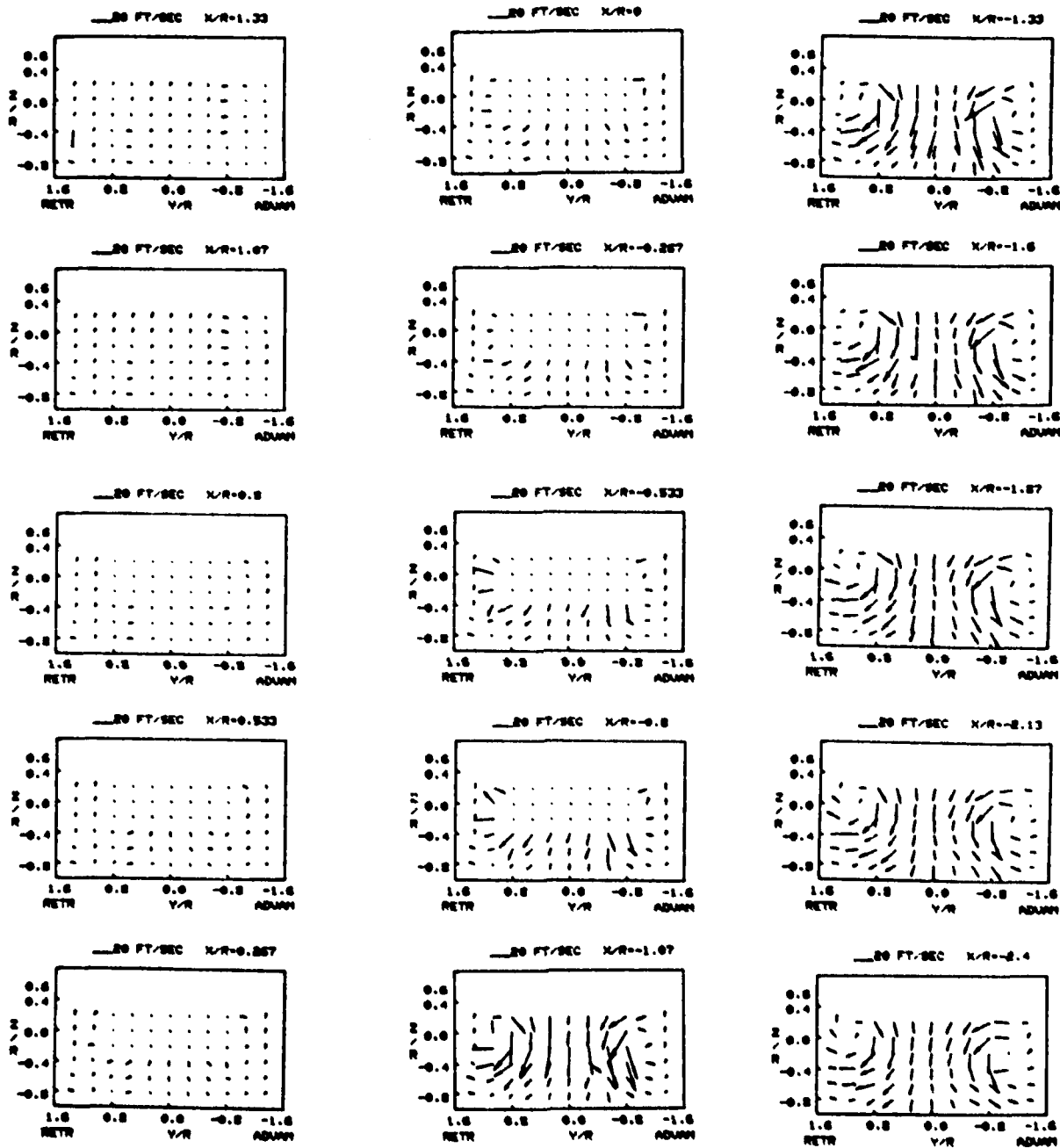


Figure 7.

Velocity vectors in Y-Z plane
 for $\mu=0.06$, $\theta=8^\circ$, and $i=4^\circ$.
 Note that coordinates depict
 probe position only.

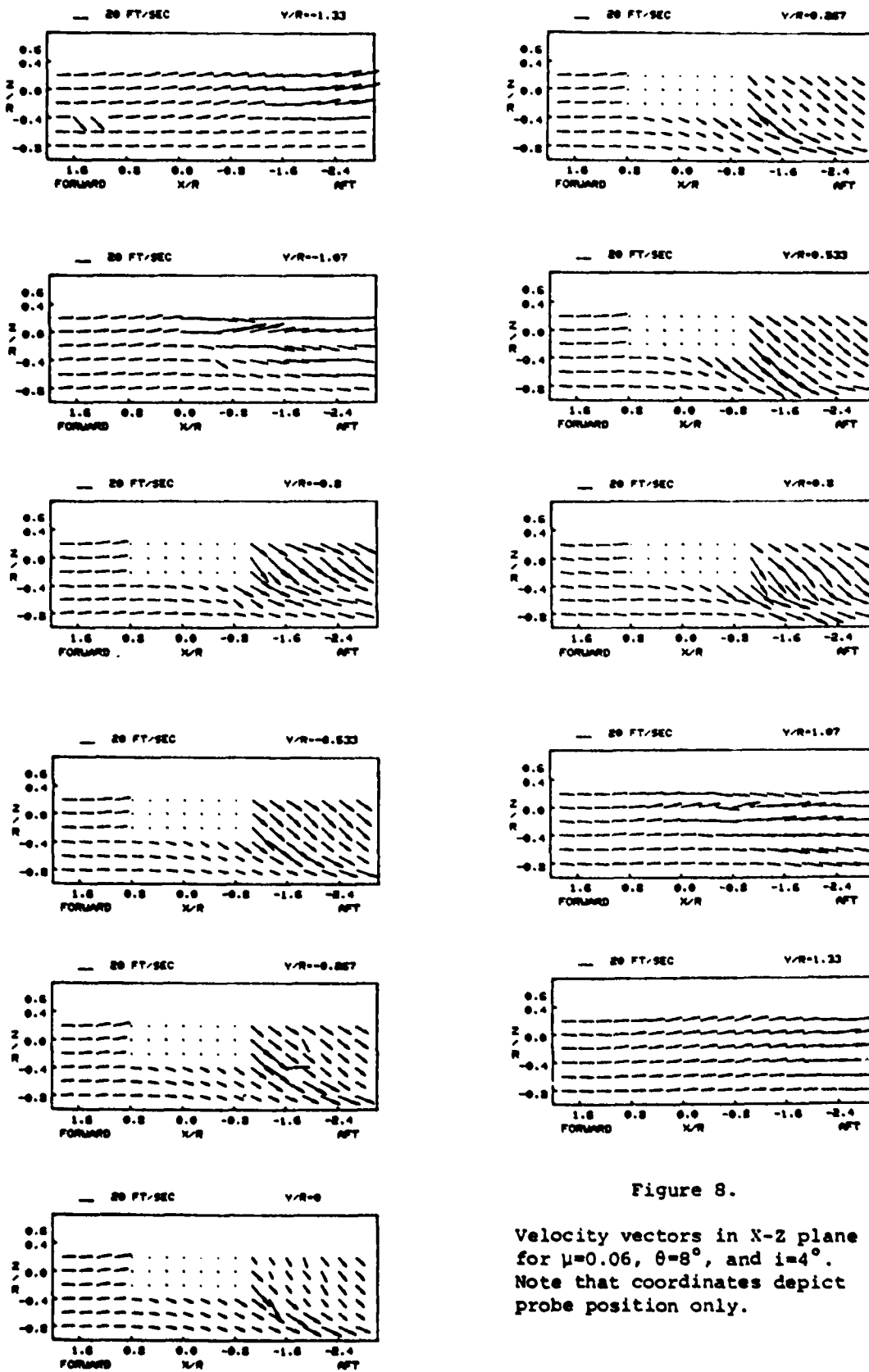


Figure 8.

Velocity vectors in X-Z plane for $\mu=0.06$, $\theta=8^\circ$, and $i=4^\circ$. Note that coordinates depict probe position only.

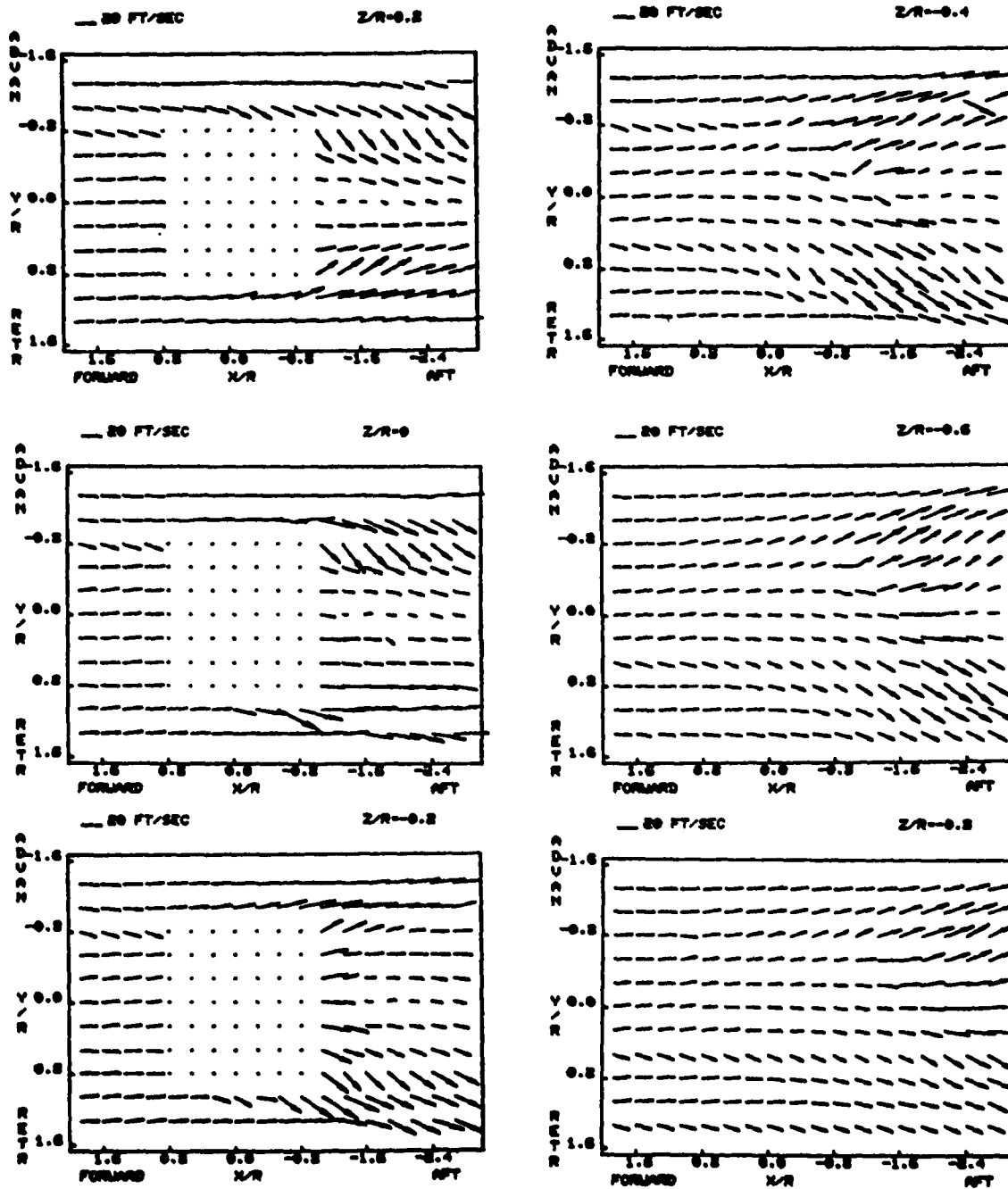


Figure 9.

Velocity vectors in X-Y plane
 for $\mu=0.06$, $\theta=8^\circ$, and $i=4^\circ$.
 Note that coordinates depict
 probe position only.

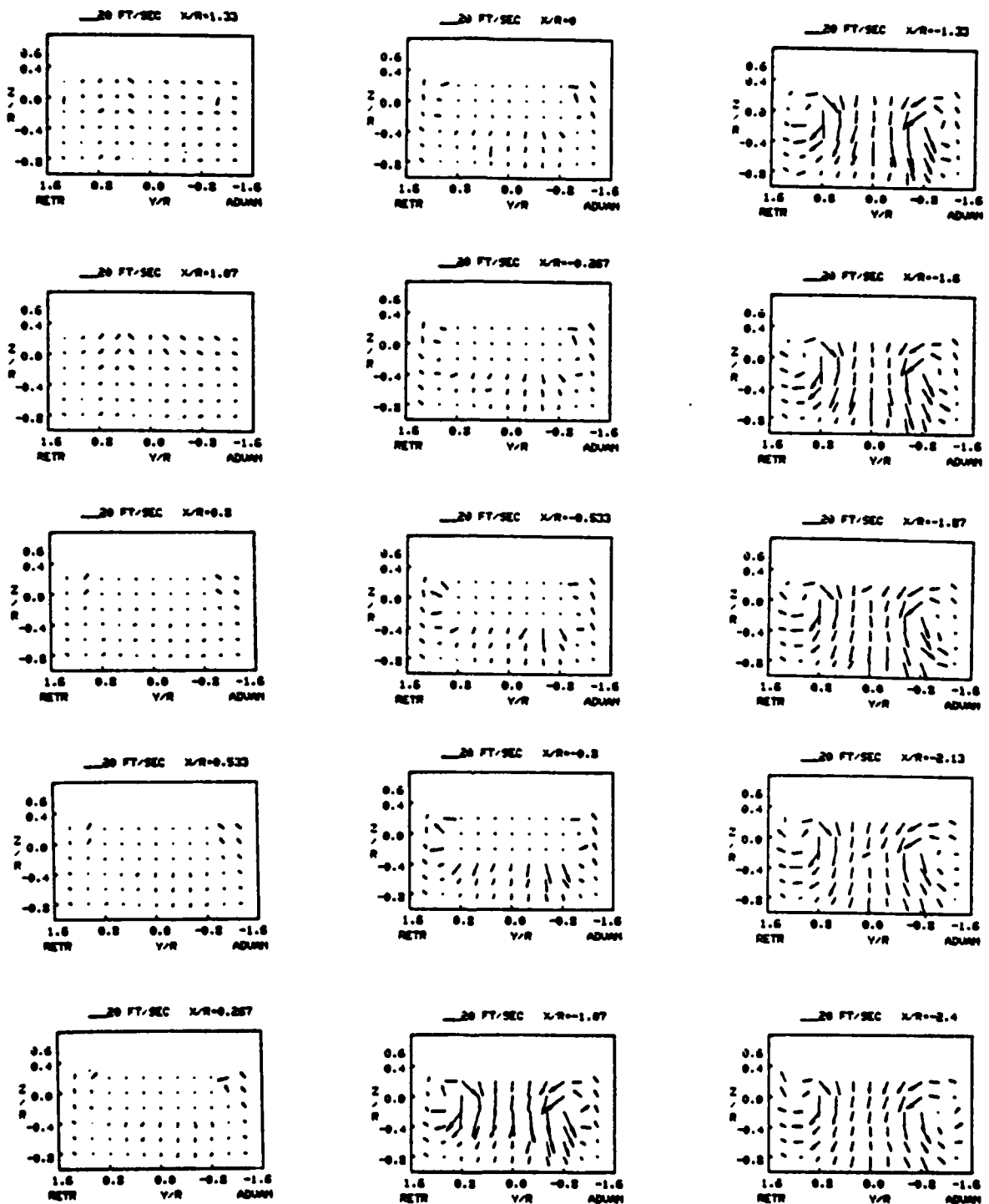


Figure 10.

Velocity vectors in Y-Z plane
 for $\mu=0.06$, $\theta=8^\circ$, and $i=2^\circ$.
 Note that coordinates depict
 probe position only.

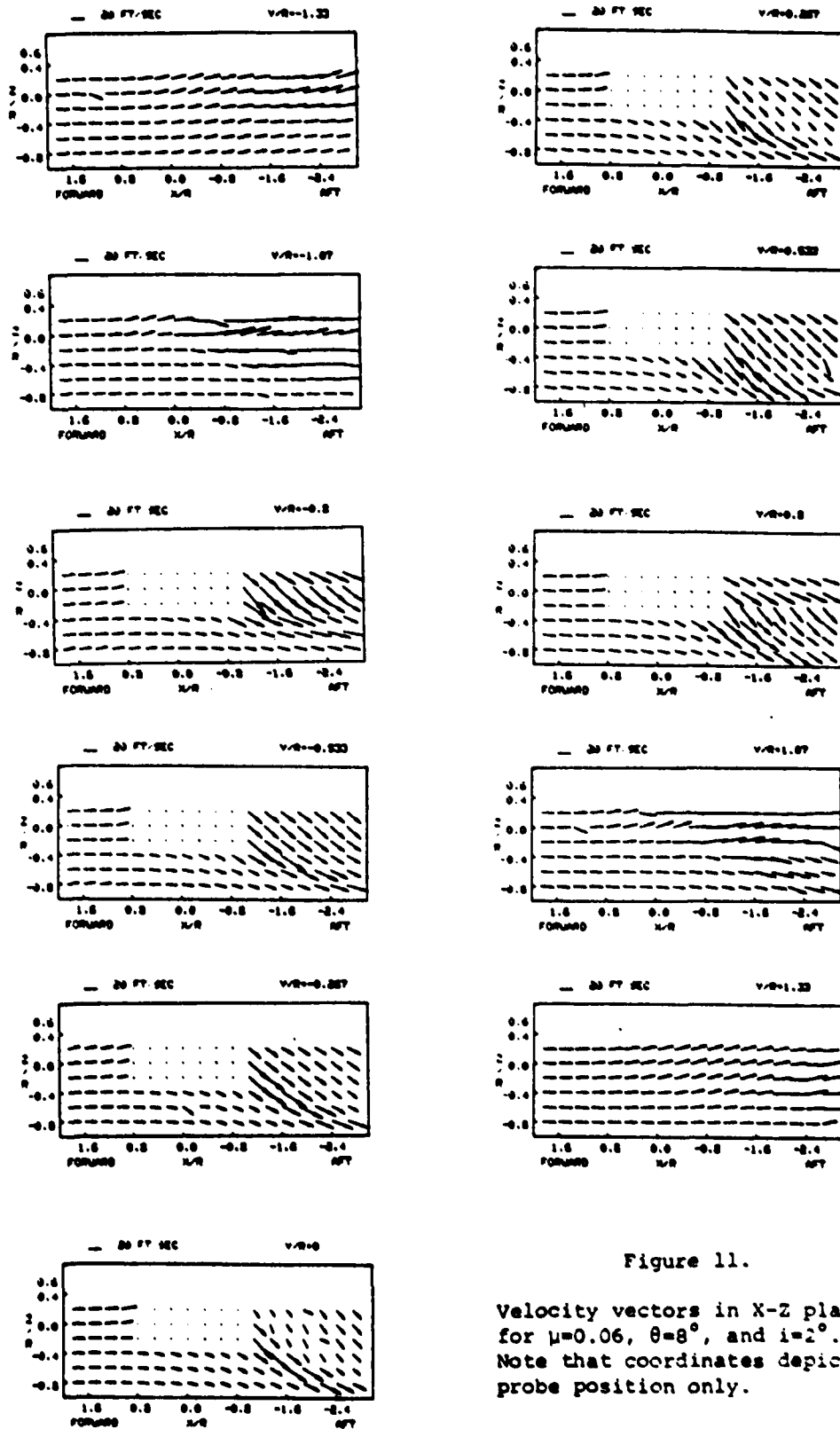


Figure 11.

Velocity vectors in X-Z plane
 for $\mu=0.06$, $\theta=8^\circ$, and $i=2^\circ$.
 Note that coordinates depict
 probe position only.

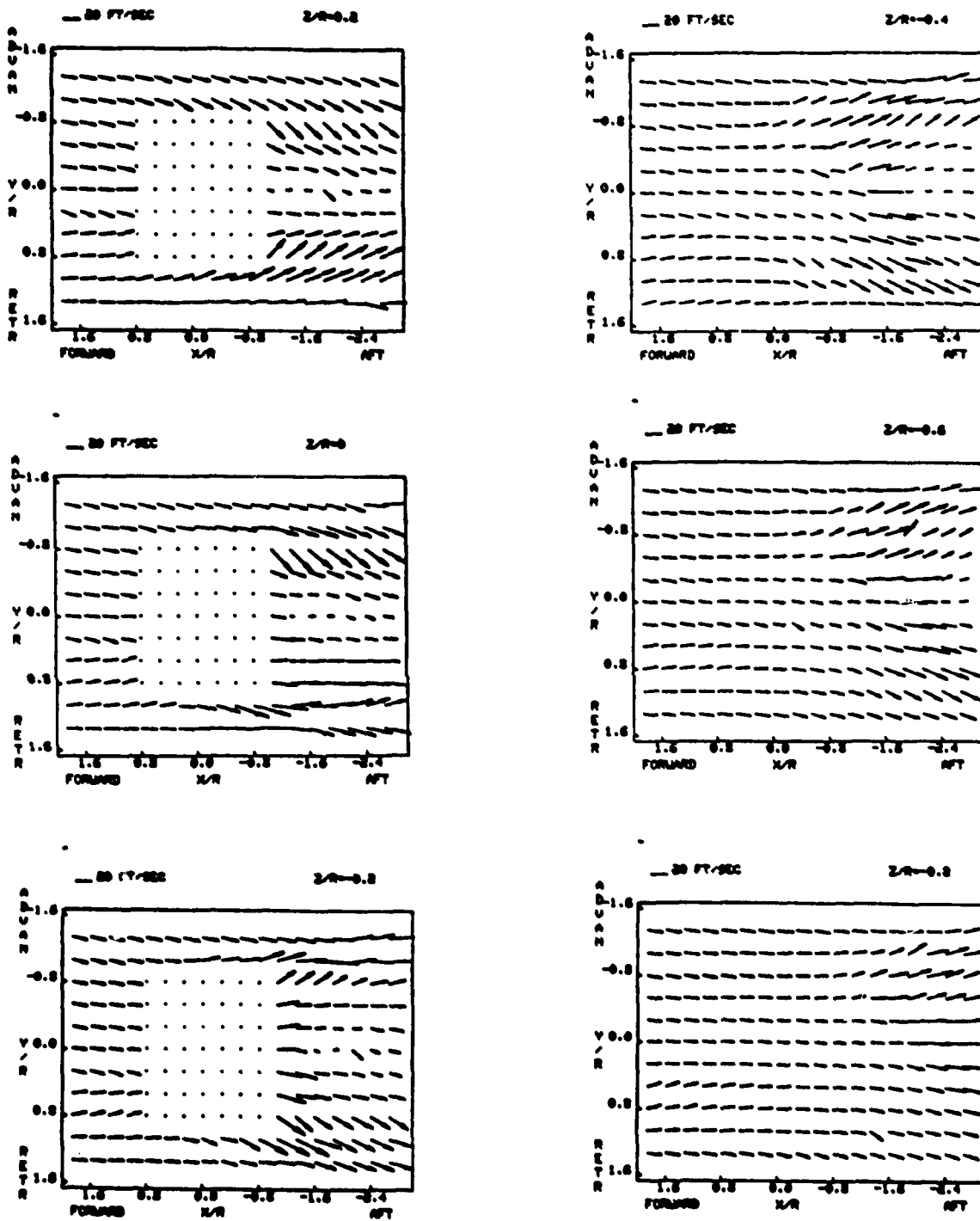


Figure 12.

Velocity vectors in X-Y plane
 for $\mu=0.06$, $\theta=8^\circ$, and $i=2^\circ$.
 Note that coordinates depict
 probe position only.

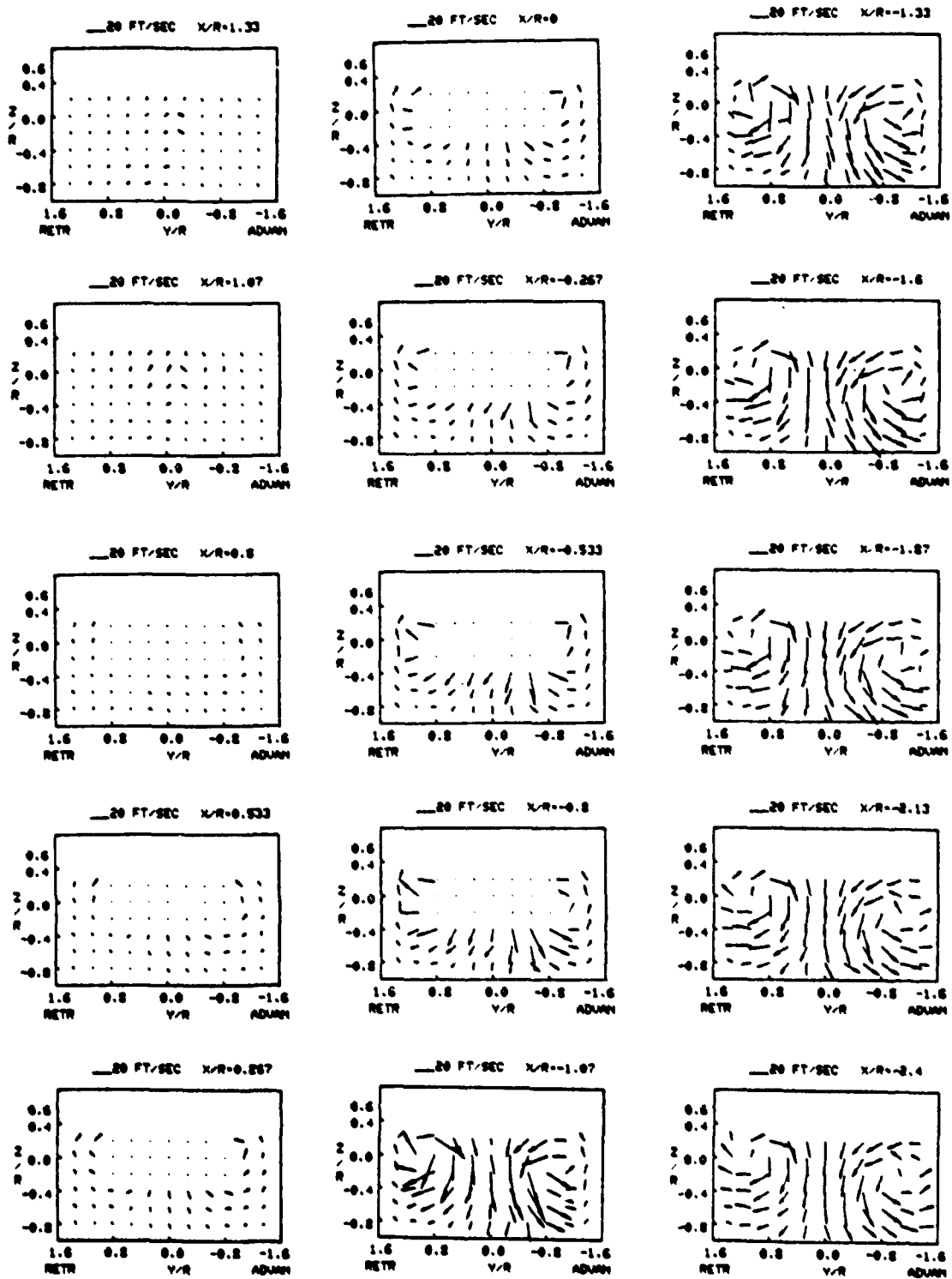


Figure 13.

Velocity vectors in Y-Z plane
 for $\mu=0.06$, $\theta_{75\%R} = 8^\circ$, and
 $i=8^\circ$. Note that coordinates
 depict probe position only.

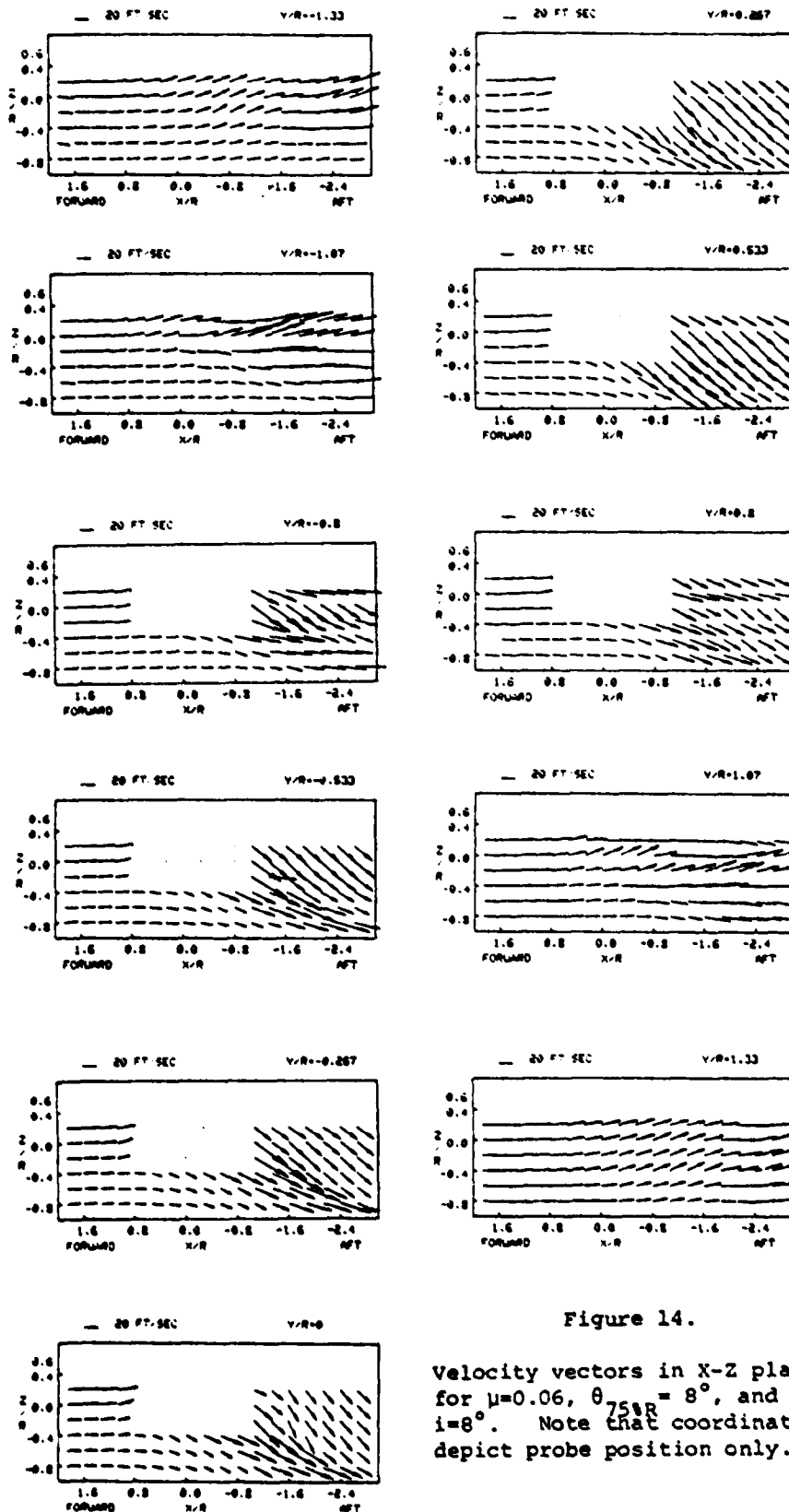


Figure 14.

Velocity vectors in X-Z plane for $\mu=0.06$, $\theta_{75\%R} = 8^\circ$, and $i=8^\circ$. Note that coordinates depict probe position only.

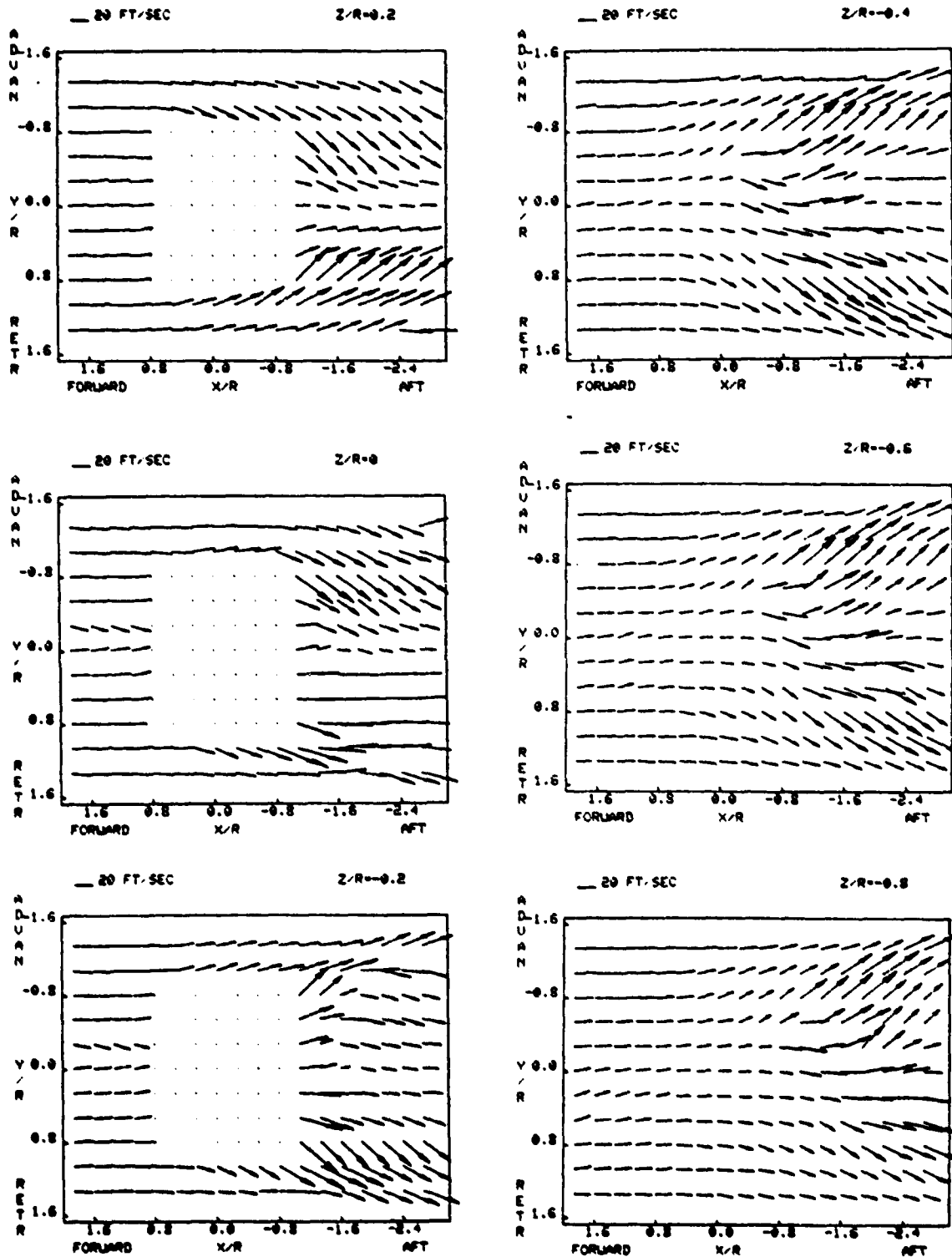


Figure 15.

Velocity vectors in X-Y plane
 for $\mu=0.06$, $\theta_{\text{tip}} = 8^\circ$, and
 $i=8^\circ$. Note that coordinates
 depict probe position only.